

Joar Frækaland
Martin Mork Breivik

Fibre Reinforced Concrete in Load-Carrying Structures

Structural Behaviour and Evaluation of
Calculation Methods

Master's thesis in Civil and Environmental Engineering
Supervisor: Terje Kanstad

June 2023

Joar Frækaland
Martin Mork Breivik

Fibre Reinforced Concrete in Load-Carrying Structures

Structural Behaviour and Evaluation of Calculation Methods

Master's thesis in Civil and Environmental Engineering
Supervisor: Terje Kanstad
June 2023

Norwegian University of Science and Technology
Faculty of Engineering
Department of Structural Engineering





MASTER THESIS 2023

SUBJECT AREA: Concrete Structures	DATE: 10.06.2023	NO. OF PAGES: 75 + 72
--------------------------------------	---------------------	--------------------------

TITLE:

Fibre Reinforced Concrete in Load-Carrying Structures: Structural Behaviour and Evaluation of Calculation Methods

Fiberarmert betong i bærende konstruksjoner:
Konstruksjonens oppførsel og evaluering av beregningsmetoder

BY:

Joar Frækaland

Martin Mork Breivik



SUMMARY:

This thesis examines the use of fibre reinforced concrete in load-bearing structures. A full-scale experimental investigation has been conducted for 16 plate elements, related to the project Fibercon. Prior to this, a comprehensive literature study regarding the potential of fibre reinforced concrete. The objective was to compare different casting methods for horizontal and vertical casted elements. The comparison involved the use of steel- and basalt fibre, with and without the inclusion of rebars. Also, the fibre content and distribution related to the obtained capacity and crack pattern for the elements have been investigated. Moreover, the obtained test results have been compared with the results derived from calculation rules according to EC2 and NB38.

The results are obtained by performing laboratory experiments and calculations. To determine the mechanical properties, the compression test and the three-point bending test are conducted. These properties form the basis for calculations performed on the plate elements. The calculation methodology for fibre reinforced concrete is done according to EC2 and NB38. The moment capacity of the plate elements is performed with both yield line analysis and strip method. Then, the full-scale experiment was conducted as a plate bending test with elements supported on all four sides. From this test, the load-displacement curve and the crack propagation are obtained. To justify variation in test results, the fibre orientation and distribution are determined by inductive test.

The results show a significantly higher capacity for fibre reinforced concrete when conventional reinforcement is included. In general, the highest capacity was achieved for the horizontally casted element due to favourable fibre orientation. However, the elements performed differently depending on fibre type and concrete mixtures. The stable self compacting concrete with steel fibre exhibits the highest capacity for horizontally casted elements. Further, the vibrator compacted concrete exhibits the highest capacity for the vertical casted elements. From the calculations, the orientation factor for walls, only reinforced with fibres, was found to be notably conservative. Also, the crack width calculations according to EC2 provide accurate results in the serviceability limit state compared to NB38.

SUPERVISOR: Terje Kanstad

CARRIED OUT AT: Department of Structural Engineering, NTNU

Preface

This master's thesis is written for the Department of Structural Engineering at the Norwegian Institute of Science and Technology (NTNU) in Trondheim, Norway. The experimental project, Fibercon, was a collaboration between NTNU, SINTEF and several relevant companies within the profession. The master's thesis have been accomplished during 20 weeks in the spring semester of 2023.

Our main motivation was to develop a comprehensive knowledge of fibre reinforced concrete through a combination of experimental and theoretical research. This was a subject that both of us want to dive into because it required skills we did not yet have. We have gained a great educational experience and increased our knowledge in this demanding process.

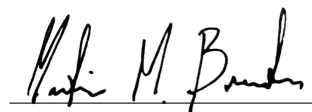
We would like to thank everyone that helped us with this thesis, especially our supervisor Terje Kanstad for sharing his knowledge and guiding us whenever it was needed. Also, we would like to thank the PhD candidate Guillermo Rojas Orts for the collaboration and guidance throughout the spring semester.

Furthermore, we would like to extend our gratitude to Johan Fagervold at The Department of Structural Engineering (KT) for his help with organising and running the tests in the laboratory.

Trondheim, June 2023



Joar Frækaland



Martin Mork Breivik

Abstract

This thesis examines the use of fibre reinforced concrete in load-bearing structures. A full-scale experimental investigation has been conducted for 16 plate elements, related to the project Fibercon. Prior to this, a comprehensive literature study regarding the potential of fibre reinforced concrete. The objective was to compare different casting methods for horizontal and vertical casted elements. The comparison involved the use of steel- and basalt fibre, with and without the inclusion of rebars. Also, the fibre content and distribution related to the obtained capacity and crack pattern for the elements have been investigated. Moreover, the obtained test results have been compared with the results derived from calculation rules according to EC2 and NB38.

The results are obtained by performing laboratory experiments and calculations. To determine the mechanical properties, the compression test and the three-point bending test are conducted. These properties form the basis for calculations performed on the plate elements. The calculation methodology for fibre reinforced concrete is done according to EC2 and NB38. The moment capacity of the plate elements is performed with both yield line analysis and strip method. Then, the full-scale experiment was conducted as a plate bending test with elements supported on all four sides. From this test, the load-displacement curve and the crack propagation are obtained. To justify variation in test results, the fibre orientation and distribution are determined by inductive test.

The results show a significantly higher capacity for fibre reinforced concrete when conventional reinforcement is included. In general, the highest capacity was achieved for the horizontally casted element due to favourable fibre orientation. However, the elements performed differently depending on fibre type and concrete mixtures. The stable self compacting concrete with steel fibre exhibits the highest capacity for horizontally casted elements. Further, the vibrator compacted concrete exhibits the highest capacity for the vertical casted elements. From the calculations, the orientation factor for walls, only reinforced with fibres, was found to be notably conservative. Also, the crack width calculations according to EC2 provide accurate results in the serviceability limit state compared to NB38.

Sammenheng

Denne masteroppgaven undersøker bruken av fiberarmert betong i bærende konstruksjoner. En fullskala forsøksserie er gjennomført for 16 plateelementer relatert til prosjektet Fibercon. I tillegg er det gjennomført et omfattende litteraturstudie om potensialet til fiberarmert betong. Målet var å sammenligne ulike støpemetoder for vertikal- og horisontalstøpte elementer. Samtidig sammenligne bruken av stål- og basaltfiber, både med og uten tradisjonell armering. I tillegg er fibermengde og -fordeling undersøkt, relatert til elementenes kapasitet og riss-mønster. Videre er testresultatene sammenlignet med resultatene fra beregningsregler i henhold til EC2 og NB38.

Resultatene er oppnådd gjennom laborietester og beregninger. For å fastslå de mekaniske egenskapene benyttes trykktesting av betong og trepunkts bøyetest. Disse egenskapene danner grunnlaget for beregninger på elementer. Beregningsmetodikken for fiberarmert betong er utført i henhold til EC2 og NB38. Momentkapasiteten til plateelementene er beregnet ved bruk av bruddlinjeteori og stripemetoden. Det ble gjennomført bøyetest av plater med opplegg på alle sider. Last-deformasjonskurven og riss utviklingen ble registrert fra dette forsøket. For å undersøke bakgrunnen for variasjonen i testresultatet ble fiberorientering og -fordeling bestemt gjennom induktiv testing.

Resultatene viser en betydelig høyere kapasitet for fiberarmert betong når tradisjonell armering er inkludert. Det ble oppnådd høyere kapasitet for horisontalstøpte elementer på grunn av gunstig fiberorientering. Elementene oppførte seg forskjellig avhengig av fibertype og betongblandning. Den stabile, selvkomprimerende betongen med stålfiber oppnådde høyest kapasitet for horisontalstøpte elementer. Videre viser vibrert betong høyest kapasitet for vertikalstøpte elementer. Fra beregningene av vegger med bare fiberarmert betong ble orienteringsfaktoren sett på som for konservativ. Når det gjelder beregning av rissvidde, viser resultatene i bruksgrensetilstand en oversstemmelse med EC2 sammenlignet med NB38.

Table of Contents

List of Figures	x
List of Tables	xii
1 Introduction	1
1.1 Background	1
1.2 Aim and Limitations	1
1.3 Outline of the Thesis	2
2 Theory	3
2.1 Fibre Reinforced Concrete	3
2.2 Fibre Types	3
2.2.1 Steel Fibre	4
2.2.2 Basalt Fibre	4
2.3 Mechanical Properties	5
2.3.1 Compressive Strength	5
2.3.2 Tensile Strength	6
2.4 Cracking	7
2.4.1 Fibre Bridging	7
2.4.2 Combined Aggregate and Fibre Bridging	7
2.5 Fibre Orientation and Distribution	8
2.5.1 Casting Process	9
2.5.2 Shape and Size	10
2.5.3 Obstacles	11
2.5.4 Assessment of Fibre Content and Orientation	11
2.6 Plate Theory	11
2.6.1 Yield Line Theory	11
2.6.2 Strip Method	13
3 Laboratory Experiment	14
3.1 Test Specimens	14
3.1.1 Materials	14
3.1.2 Element Overview	15
3.1.3 Casting Procedure and Storage	16
3.2 Three-Point Bending Test	17
3.3 Plate Bending Test	19
3.4 Inductive Test	21
3.4.1 Cubic Specimens	22
3.4.2 Cylindrical Specimens	22
3.4.3 Calculation of Fibre Content	23

4	Design Methods	26
4.1	Concrete Strength	26
4.2	Residual Strength	26
4.2.1	Residual Tensile Strength According to EC2	28
4.2.2	Residual Tensile Strength According to NB38	29
4.3	Ultimate Limit State	29
4.3.1	Moment Capacity	30
4.3.2	Ultimate Load Using Yield Line Method	33
4.3.3	Ultimate Load Using Strip Method	34
4.4	Serviceability Limit State	34
4.4.1	Calculation of Crack Width According to EC2	35
4.4.2	Calculation of Crack Width According to NB38	37
4.4.3	Calculation of Stress in Reinforcement Bars	37
4.5	Minimum Reinforcement	39
4.5.1	Minimum Reinforcement for SFRC According to EC2	40
4.5.2	Minimum Reinforcement for SFRC According to NB38	40
4.5.3	Lightly Reinforced SFRC Structures	40
5	Laboratory Results	41
5.1	Compression Test	41
5.2	Three-Point Bending Test	41
5.3	Plate Bending Test	44
5.3.1	Load-Displacement	44
5.3.2	Crack Pattern	50
5.4	Inductive Test	54
6	Calculation Results	58
6.1	Ultimate Load	58
6.2	Crack Width Calculation	62
7	Discussion	63
7.1	Experimental Series	63
7.1.1	Experimental Error	63
7.1.2	Comparison of Residual Tensile Strength	64
7.1.3	Comparison of Elements	65
7.2	Comparing of Calculated- and Laboratory Results	68
7.2.1	Ultimate Load	68
7.2.2	Crack Width Calculation	69
7.2.3	Comparing of EC2 and NB38	70
7.3	Fibre Orientation and Distribution	70
8	Conclusions	72

References **74**
Appendix

List of Figures

2.1	Shapes and types of fibres	4
2.2	Behaviour for plain concrete and FRC in compression	5
2.3	Tensile behaviour of different concrete materials	6
2.4	Pull-out of fibre with hooked ends	7
2.5	Description of crack propagation in FRC	8
2.6	Orientation influenced by shear stress	10
2.7	Orientation along boundary	10
2.8	Explanation on upper and lower bound methods	12
3.1	Two types of fibres	15
3.2	Two casting methods	16
3.3	Element casting processes	17
3.4	Typical arrangement for measuring deflection	18
3.5	Setup for three-point bending test	18
3.6	Test setup for the plate bending test	19
3.7	Element 13 in the testing rig	20
3.8	Localization of LVDTs	21
3.9	Impedance analyser	21
3.10	Section used for cubes	22
3.11	Test order on inductive test for cubes	22
3.12	Test order on inductive test for cylinders	23
4.1	Relation between flexural strength and uniaxial strength	29
4.2	Simplified stress and strain distribution for FRC	30
4.3	General stress- and strain distribution for FRC exposed to pure bending	30
4.4	Stress- and strain distribution, with strain in fibres as the limited factor	31
4.5	Assumed yield line pattern	33
4.6	Static system in one direction of the plate	34
4.7	Effective tension area	35
4.8	Stress distribution in SLS at given curvature	38
5.1	Residual flexural tensile strengt from 3PBT	43
5.2	Comparison of the mean residual flexural tensile strength	44
5.3	Illustration of adjusted curve for LVDT A in first plate (ID-1)	45
5.4	Load-displacement curve for small slabs with fibre reinforcement	46
5.5	Load-displacement curve for small walls with fibre reinforcement	47
5.6	Load-displacement curve for small slabs with fibre- and conventional reinforcement	48
5.7	Load-displacement curve for small walls with fibre- and conventional reinforcement	48
5.8	Load-displacement curve for large slabs with fibre- and conventional reinforcement	49
5.9	Crack pattern for the small slabs with fibre reinforcement	51
5.10	Crack pattern for the small walls with fibre reinforcement	52
5.11	Crack pattern for the small slabs with fibre- and conventional reinforcement	53

5.12	Crack pattern for the small walls with fibre- and conventional reinforcement . . .	53
5.13	Crack at the top surface on element 13	54
5.14	Crack pattern for the large walls with fibre- and conventional reinforcement . . .	54
5.15	Fibre content in samples from elements	56
5.16	Isotropy factor in samples from elements	57
6.1	Load-elongation curve	62
7.1	Gap between element and roller support	64
7.2	Comparison of mean residual flexural tensile strength	65
7.3	Comparison of elements	66
7.4	Comparison of mean calculated capacity and experimental capacity	68
7.5	Comparison of characteristic calculated capacity and experimental capacity . . .	69

List of Tables

3.1	Concrete mixture	14
3.2	Product data for the two fibre types	15
3.3	Element overview	16
3.4	Description of test setup	19
3.5	Constant parameters for cylindrical and cubic specimens	24
4.1	Partial factors for SFRC in tension	28
4.2	Yield line length for the different plates	33
5.1	Compressive strength at 91 days	41
5.2	Residual flexural tensile strength	43
5.3	Ultimate load	49
5.4	Crack registration	50
5.5	Fibre content and orientation in cubes	55
5.6	Isotropy factor in the core samples	57
6.1	Ultimate load using mean value according to EC2	58
6.2	Ultimate load using characteristic value according to EC2	59
6.3	Ultimate load using mean value according to NB38	60
6.4	Ultimate load using characteristic value according to NB38	61
6.5	Calculated crack widths for element 11	62
7.1	Average fibre content orientated in x-direction in the beams	71

1 Introduction

This chapter gives a short overview of the fibre's background, research and development in recent years, and application area today. Also, the thesis's aim and limitations are presented, and finally, a short outline of the thesis.

1.1 Background

Fibre reinforced concrete can provide an alternative to conventional reinforcement in concrete structures, especially due to increasing demands for efficiency. Although fibres are primarily limited to steel fibre reinforcement for non-structural applications, such as floors, foundations, toppings and shotcrete. There is a growing need for verification of guidelines concerning the design, execution and inspection of structures reinforced with fibre reinforced concrete.

Extensive research and development in recent years have provided knowledge of the challenges and opportunities associated with the use of fibre reinforcement in concrete structures. Numerous laboratory and field experiments, as well as theoretic analyses, have been conducted on elements with fibre reinforcement. Notably, the use of fibre reinforcement in combination with self compacting concrete has demonstrated significantly enhanced load-bearing capacity compared to similar elements made of conventionally vibrated concrete.

Today, the knowledge has reached a level where fiber reinforced concrete, with or without conventional reinforcement, can provide acceptable load-bearing capacity when the fibres are distributed and orientated as intended. However, achieving this can only be accomplished through good execution and control. Also, the variability in residual tensile strength is often greater for fibres compared to conventional reinforcement. Furthermore, precautions must be taken to prevent weak zones with a low proportion of effective fibres in elements [1].

1.2 Aim and Limitations

The experimental investigation in this thesis is connected to the project Fibercon, which is a collaboration between NTNU, SINTEF and several relevant companies within the profession. As mentioned, an experimental series is carried out and the results are compared to the calculation rules in the new Eurocode 2 for the design of concrete structures (EC2) and publication No. 38 from the Norwegian Concrete Association (NB38). There will also be a comparison of different casting methods for horizontal and vertical casted elements. The comparison involved the use of steel- and basalt fibre, with and without the inclusion of rebars. Also, the fibre content and distribution related to the obtained capacity and crack pattern for the elements have been investigated.

The work has been limited to investigating steel fibre reinforced concrete, both with and without the inclusion of conventional reinforcement. As well as basalt fibre reinforced concrete without conventional reinforcement. Also, investigating the difference between the use of Danish and NS14651 casting methods, specifically, in relation to the use of stable, unstable and vibrated

concrete mixes. Furthermore, the loading conditions investigated have been limited to bending and normal force in a short-term response such that no creep and shrinkage are considered. Regarding the crack width calculations, these are only carried out for elements with a combination of fibre and conventional reinforcement due to regulations in NB38 and EC2. Eventually, there is no possibility to verify the distribution and orientation of basalt fibres in elements, since the inductive test depends on which material properties are picked up by the magnetic field.

The work serves as a valuable resource for recipients such as structural engineers, material testing institutes and standardisation organizations.

1.3 Outline of the Thesis

The thesis starts with a literature study in *Chapter 2* to illustrate the different mechanical properties and behaviours of fibre reinforced concrete. Also, the mechanisms of crack formation and propagation in the concrete are described. Fibre orientation and distribution are also reviewed, also including methods for assessing fibre content and orientation. In addition, some relevant approaches for structural analysis are presented.

The laboratory experiments element overview, with their respective concrete mixes, are presented in *Chapter 3*. Further, test methods for the three-point bending test, plate bending test and inductive test are described. In addition to this, *Chapter 4* gives guidelines for the calculation methodology for fibre reinforced concrete in EC2 and NB38.

Regarding the result, they are separated into two chapters. Specifically, laboratory results and calculation results, for *Chapter 5* and *Chapter 6*, respectively. The results are mainly presented in plots and tables, with a short description of the findings.

In *Chapter 7* the discussion of the laboratory results and the calculated results is presented. Moreover, a comparison of load capacity and crack pattern for the tested elements. A comparison of the calculation rules in EC2 and NB38, while also considering their conformity to test results. Finally, a discussion of the fibre orientation and distribution is given according to their effect on the element's capacity and crack development.

The major conclusion is presented in *Chapter 8*. Also, further work is suggested after the conclusion.

2 Theory

To understand fibre reinforced concrete, it is necessary to provide an overview of theoretical composition. In short, the mechanical properties and behaviours of fibre reinforced concrete are reviewed. In addition, the mechanisms of crack formation and propagation in the concrete are described. Further, the fibre orientation and distribution are investigated, also including methods for assessing fibre content and orientation. Finally, some relevant approaches for structural analysis are presented.

2.1 Fibre Reinforced Concrete

Fibre reinforced concrete (FRC) is a composite material characterized by a cement matrix and discrete fibres. Concrete is significantly strong in compression. However, extremely low tensile strength and tensile capacity. To enhance the tensile strength, fibre reinforcement or conventional reinforcement, or a combination can be applied. Moment- and axial-loaded sections with only fibre reinforcement have lower ductility, compared to conventional reinforcement [2]. Hence, NB38 requires that all constructions with a risk of collapse should contain a minimum of conventional reinforcement [1].

2.2 Fibre Types

There are numerous fibre types available for commercial and experimental use. The most common fibres are listed below [3]:

- Steel fibre reinforced concrete (SFRC)
- Glass fibre reinforced concrete (GFRC)
- Synthetic fibre reinforced concrete (SNFRC)
- Natural fibre reinforced concrete (NFRC)

There is a wide range of fibres, which differ mainly in material, shape, shaped end, and surface treatment. Some of them are straight, others bent and with hooked ends, as shown in Figure 2.1. Fibres with hooked ends have higher tensile strength, because it provide mechanical anchorage (bonding) within the cementitious matrix. Hence, it is recommended to use deformed fibres, such as hooked ends fibres [4]. Another factor which influences the effectiveness of the fibre reinforcement is the fibre aspect ratio. The fibre aspect ratio, defined as the ratio of the fibre length to fibre diameter, provides an indication of the stiffness of the fibre [5]. By increasing the fibre volume fraction in the concrete, the absorbed fracture energy and tensile strength are increased. The choice of fibre type is related to the required effect. Often used to reduce crack widths, while others are used to reduce plastic shrinkage cracking or to avoid spalling of concrete in the event of fire [6].

Material	Shape	Shaped end		Cross - section shape
Steel	Straight	Hooked ends 3D	Button ends	Round shaped
Polypropylen	Hooked			Rectangular shaped
Nylon		4D	Deformed ends	
Glass	Crimped (wave shaped)			Irregular shaped
...	Defromed shaped	5D		

Figure 2.1: Shapes and types of fibres [7]

2.2.1 Steel Fibre

Steel fibre reinforced concrete (SRFC) is the most commonly-used fibre. In general, produced from carbon steel and stainless steel. Recommended length for fibres is 30-60 mm , and the length/diameter ratio between 50-80. The steel fibres yield point is recommended to be higher than $1000 N/mm^2$. Favourable properties of this type is high modulus of elasticity, high strength, high ductility and good durability in the alkaline environment of the concrete. In Norway, definitions, specifications and conformity for steel fibres in concrete are given in NS-EN 14889-1 [8]. Five types of steel fibres are classified into groups, in accordance with the basic material used for the production of the fibres [9]:

- Type I, cold-drawn wire
- Type II, cut-sheet
- Type III, melt-extracted
- Type IV, mill cut
- Type V, modified cold-drawn wire

2.2.2 Basalt Fibre

Basalt fibre reinforced concrete (BFRC) is derived from basalt rock, a natural material that is found in volcanic rocks originated from frozen lava. The basic characteristics of these inorganic fibres are high thermal resistance, high corrosion resistance, resistance to acids, high strength, good thermal stability and low cost. Typically applied in heat shields, composite reinforcement, and thermal and acoustic barriers [10].

Basalt fibres are obtained using basalt gravel melted and drawn at $1450-1500\text{ }^{\circ}C$, which results in basalt fibres of similar chemical compositions. A significant economic alternative to higher-temperature-resistant fibres, due to their ability to resist low temperatures, about $-200\text{ }^{\circ}C$, up to high temperatures in the range of $700-800\text{ }^{\circ}C$ [11]. This induces the fibres to have good resistance to chemical attack and good durability in seawater environment [12].

2.3 Mechanical Properties

Concrete quality is normally expressed by the compressive strength which can be easily found by testing. In contrast, the tensile strength is often neglected due to low strength. For this reason, it is common to design concrete structures such that the concrete withstand the compressive force, whereas the tension force is carried by the reinforcement. By adding fibre reinforcement to the concrete, both the compressive- and tensile strength is generally unaffected for moderate concentrations ($<1\%$) of fibres, and cannot expect to fully replace conventional reinforcement. However, other properties can be influenced favourably.

2.3.1 Compressive Strength

The compressive strength of concrete is generally good independent of reinforced or not. To increase the strength, a high concentration of fibres is required. For moderate/low fibre volume the change in compressive strength is normally small, if any at all. However, it becomes more ductile. Concrete is essentially a brittle material, hence, the fibres contribute to increasing safety level, as illustrated in Figure 2.2. The failure mechanism in compression is related to tension failure, where cracks propagates parallel to the compressive load, and tensile stress occur perpendicular to the cracks. In such a failure mechanism the main effect of fibres is to reduce crack growth. A detailed description of the crack mechanism can be found in chapter 2.4 [13].

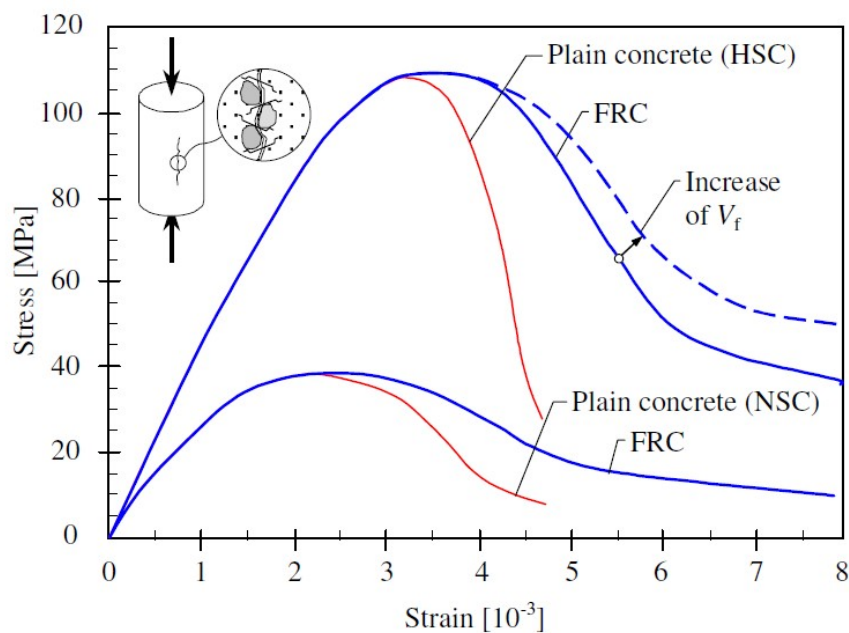


Figure 2.2: Behaviour for plain concrete and fibre reinforced concrete in compression [13]

2.3.2 Tensile Strength

The tensile behaviour of concrete can be classified as either strain-softening or strain-hardening. Plain concrete is characterized as a strain-softening material which implies that the tensile strength reaches the peak when the concrete cracks, and then the stress decreases. For FRC it is possible to achieve strain-hardening, where multiple cracks occur as the load increases, subsequently to the first crack. This can be achieved by a high concentration of fibres, also called high-performance fibre reinforced concrete (HPFRC). However, for moderate concentration (<1%) of fibres, FRC exhibits strain-softening behaviour like plain concrete with a more ductile post cracking behaviour, as shown in Figure 2.3 [13].

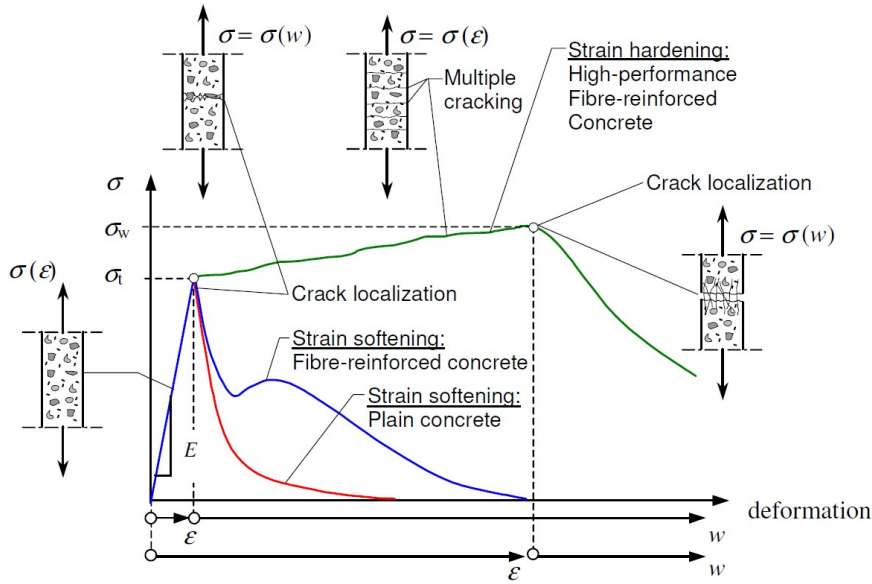


Figure 2.3: Tensile behaviour of different concrete materials [13]

Fibres are considered to be mechanically neutral until the crack localization starts, then the effect of fibres becomes important, especially for counteracting macrocrack propagation [14]. The post cracking strength is described by the residual tensile strength. To design FRC structures the residual tensile strength and ductility class must be determined. These can be obtained by different test methods. According to the EC2 and NB38 the residual tensile strength should be obtained by a three-point bending test. In chapter 3.2 and 4.2 the test setup and calculation methodology for residual strength is described in detail.

The desirable failure mechanism for FRC is fibre pull-out. This way, a more ductile behaviour is achieved before failure. Fibres are then first debonding from the concrete, and then pulled out as the crack width increases. For deformed fibres, more energy is required to straighten them out and eliminate anchorage of the fibres, this is shown in Figure 2.4. To achieve fibre pull-out as the dominating failure mechanism the combination of fibre and concrete is important. Too high adhesion between fibres and concrete can result in fibre rupture, hence a more brittle failure mechanism, nevertheless high enough to ensure sufficient residual tensile strength [6].

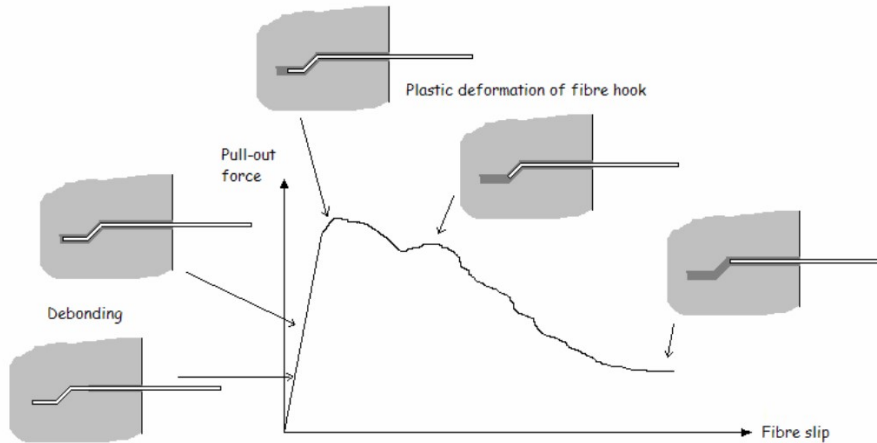


Figure 2.4: Pull-out of fibre with hooked ends [6]

2.4 Cracking

The mitigation of cracking during the serviceability limit state is one of the main reasons for the use of FRC. Crack control is a crucial factor affecting the durability of structures and is an advantage of FRC compared to conventional reinforcement [14]. Cracks in concrete structures can lead to several issues, such as reduced structural integrity, decreased service life, water penetration and subsequent reinforcement corrosion, leading to concrete peeling. Hence, crack control in concrete structures is essential to ensure long-term durability and serviceability.

2.4.1 Fibre Bridging

When a crack is formed due to stress within the cementitious matrix, the relative displacements between two opposing crack sides activate the fibre bridging mechanism, simultaneously with the gradual loss of concrete cohesion. The activated fibres transfer stresses between the two crack sides and delay further expansion of the crack. This induces a stress distribution over a larger volume, which results in formation of new cracks in other regions. Hence, FRC can absorb more energy and the behaviour becomes more ductile. The fibre bridging continues until all fibres across the crack are completely pulled out or ruptured. The number of cracks formed within the cementitious matrix and the overall mechanical response depends on the fibre bridging effect. However, the fibre bridging effect is governed by the mechanical properties of fibres and concrete matrix [15].

2.4.2 Combined Aggregate and Fibre Bridging

For FRC there will be a combined effect of aggregate and fibre bridging, as shown in Figure 2.5 where four distinct zones can be identified. A traction-free zone, which occurs due to large crack openings, a bridging zone, where stress is transferred by fibres and aggregate bridging, a zone with macrocrack growth, and eventually a zone with microcracking.

The fracture process is initiated by the presence of pre-existing microcracks exist within the concrete, which arise from internal restraint caused by the aggregate, shrinkage and thermal deformations. These microcracks are introduced even before any external stresses are applied. When stresses are applied, microcracks will start to grow, initially at the interface between the cement paste and the concrete aggregates (A), eventually the microcracks propagate into the mortar (B). At the peak stress (C), the microcracks continue to propagate in an unstable manner, leading to crack localization and the eventual propagation of macrocracks through the specimen, resulting in stress-drop (D). Depending on the characteristics of the fibre, the stress curve will slowly decrease proportionally to increasing crack opening until it becomes zero (E). For deformed fibres, e.g. end-hooked fibres, the curve may induce an ascending part where the stress increases as the fibre is deformed during the fibre pull-out, but eventually decrease until it becomes zero [13].

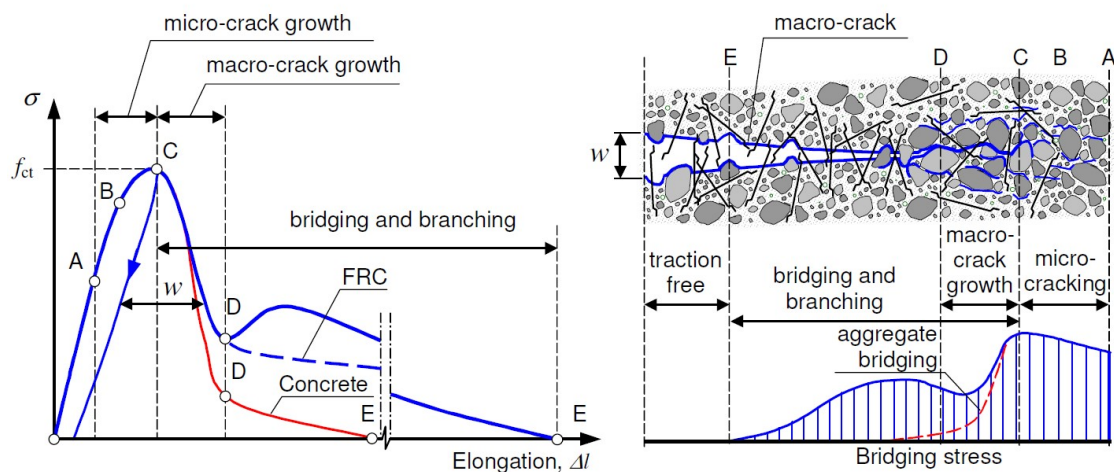


Figure 2.5: Description of crack propagation in FRC [13]

The crack propagation for plain concrete exhibits a larger stress-drop (D), as shown by the red curve in Figure 2.5. Aggregate bridging has a major influence on crack bridging and crack branching. Hence, the crack propagation depends on the aggregates and their bond to the matrix. It can be expected that the stress-crack opening relationship for plain concrete should depend primarily on the characteristics of aggregates.

2.5 Fibre Orientation and Distribution

Orientation and distribution of fibres have a big influence on the post-crack tensile strength. Ideally, it is desirable that the fibres are orientated perpendicular to the cracks and thereby create a bridge for the stresses to pass the cracks. How the fibres are distributed and orientated is highly dependent on the casting process, concrete mix, shape and size of the element and obstacles like conventional reinforcement and cutouts [6].

2.5.1 Casting Process

A number of studies have shown that the fibres tend to orientate perpendicular to the flow direction when the concrete is poured [1]. How the fibres are distributed and orientated is highly dependent on the workability of the fresh concrete.

Vibrator compacted concrete (VCC) can have poor flowability, hence, the concrete requires vibration to ensure even distribution and eliminates potential air pockets. This process can have a negative impact on the orientation and distribution of fibres depending on compacting method and duration. When using a vibration table, the fibres tend to be planar orientated, resulting in an anisotropic property. The influence is time dependent, and it is shown that vibration for a short time will not have a significant effect, however, this requires good workability of the concrete to ensure sufficient compaction. For larger structures, this can be impractical, and an immersion vibrator may be the only alternative. An immersion vibrator is usually not recommended, especially around critical zones, as it can cause weak spots where fibres are moved away from the vibrator [6, 1].

To avoid vibration, self compacting concrete (SCC) is preferred. When using SCC with fibres, stable concrete is required to reduce the chances of segregation and uneven distribution of the fibres. If concrete segregates, the distribution over the height can be uneven where steel fibres, which have higher density, are likely to have a larger fraction of fibre in the lower part. Contrary, fibres with low density are likely to have a higher fraction in the upper part [6].

Due to the flowability of SCC, the fibres are able to orient during the flow. While the concrete is flowing, shear stress between the concrete and formwork will influence the distribution and orientation. The roughness of the mould surface has an impact on the flow velocity, where the flow velocity close to the mould is slower compared to the top layer. This can result in uneven orientation over the height, as illustrated in Figure 2.6. This effect, for slabs casted on slip surfaces, is overruled by the horizontal shear, resulting in a consistent orientation due to an almost constant flow velocity over the height. The horizontal shear acts perpendicular to the flow direction whereas shear induced fibre orientation causes an orientation perpendicular to the flow direction. For a rough surface, the flow velocity varies more over the height, where the lower part gets a more isotropic orientation, and unidirectional in the upper part [16].

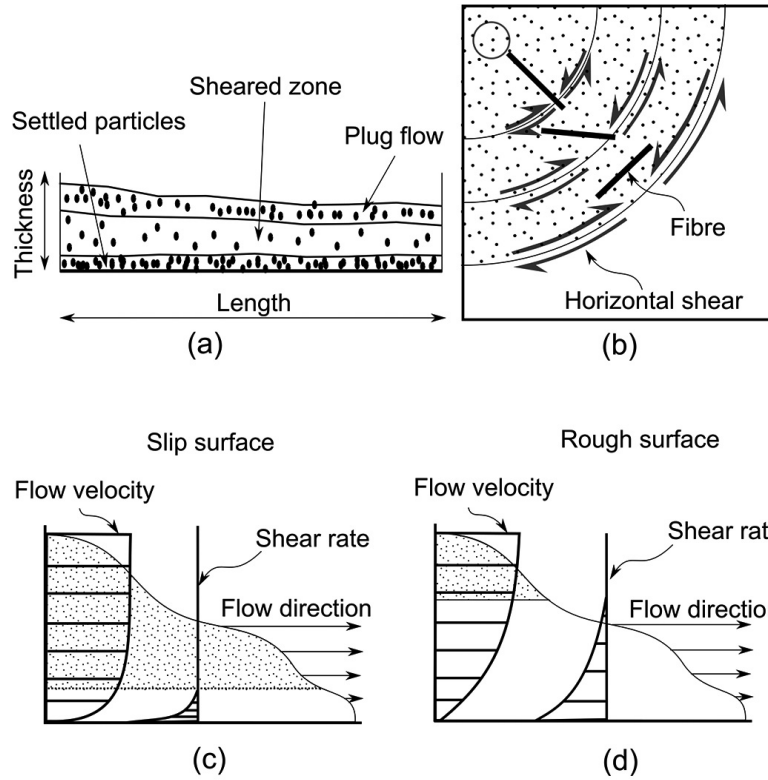


Figure 2.6: Orientation influenced by shear stress [16]

2.5.2 Shape and Size

Along the boundaries of a structure, the fibres tend to orientate parallel to the formwork due to physical constraints illustrated in Figure 2.7 [1]. Hence, the orientation for slender elements can be highly dominated by this wall effect. For beams and columns, the fibre orientation will be dominated in the longitudinal direction and thereby have a uni-directed orientation. This effect will also influence thin plates and walls where the fibres tend to be plane orientated. Otherwise, for solid concrete elements, the wall effect is limited and a three-dimensional and isotropic orientation may be achieved.

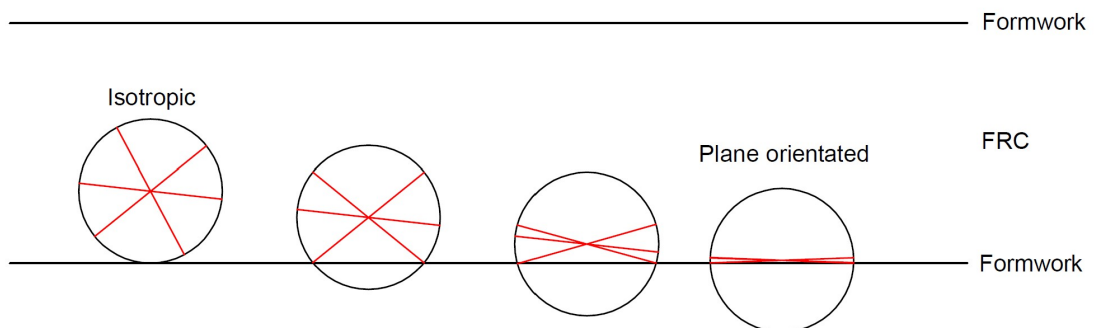


Figure 2.7: Orientation along boundary. To the left, the fibres are free to orientate in any direction and obtain an isotropic property. As the "bubble" gets closer to the boundary the fibres are forced into plane orientation [1].

2.5.3 Obstacles

A combination with reinforcement bars is used for most load-bearing structures with fibre reinforcement. These rebars create obstacles that influence the concrete flow, hence, this may affect the distribution and orientation of the fibres. The effect of rebars in slabs can be compared with FRC casted on rough surfaces where the flow velocity decreases. Obstacles like rebars can also affect the distribution by causing fibre blockage resulting in an accumulation of fibres [16]. To reduce the risk of blockage, both EC2 and NB38 recommend that the spacing between rebars should be at least twice the length of the fibres.

2.5.4 Assessment of Fibre Content and Orientation

The inductive method proposed by Torrents et al. [17] and improved by Cavalaro et al. [18] represents a non-destructive approach. The method relies on the assessment of the inductance change induced by the interaction between a magnetic field and a sample of SFRC. It is capable to estimate both the fibre content and the fibre orientation in SFRC samples, without causing any structural damage to the specimen under examination. The method presents a high accuracy and allows for assessing the characterization of each specimen in a short time [19]. The procedure for the test is presented in chapter 3.4.

2.6 Plate Theory

To determine concrete structures behaviour and resistance, structural analysis is required. From such analysis, among other things, one can gather information about the forces, moments, stresses and strain acting in a cross section. With respect to the design codes, the resistance is often given as forces and moments. Hence, the analysis should express the current forces and moments produced in the desired cross section. For concrete slabs supported on all four sides, the moments and forces will be carried in two directions, acting as a two-way slab. For such slabs, several methods have been established with varying efficiency and accuracy. The yield line method and strip method are two well known and simple methods, which represent the upper and lower bound, respectively [20].

2.6.1 Yield Line Theory

Yield line theory is based on assumed failure mechanisms compatible with the boundary conditions and plastic properties of under-reinforced slabs. The assumed failure mechanism is defined by a pattern of yield lines when the reinforcement has yielded. Also, the location of the corresponding load and boundary conditions influence the most critical yield line pattern [20]. The well-founded method is used in ULS and is characterized as a simple and economical method for the design of reinforced concrete slabs, such as flat slabs.

The virtual work method is the most common way of applying yield line theory. A fundamental principle is that work done externally and internally must balance. In other words, this means that the external work done by the load deforming the structure equals the internal work done by plane segments rotating along the yield lines. Thus, when a slab is loaded to failure, yield lines occur at the most stressed areas and develop into continuous plastic hinges. These plastic hinges develop into a mechanism forming a yield line pattern and it might be necessary to investigate several yield line patterns when calculating. The objective of investigating yield line patterns is to find the one pattern that gives the critical moment or the lowest load capacity, as this represents the most critical pattern [21].

The method represents an upper bound approach with respect to the load carrying capacity of slabs. Hence, the method gives an ultimate load for a given slab that is either correct or too high, as shown in Figure 2.8.

Normally the mathematically correct solution is within 10 % of the result from the yield line analysis. Hence, it is common to include a 10 % margin on the design moment to be on the safe side. With regard to this margin, an upper bound method can be applied. In addition, the slabs might experience compressive membrane action and strain hardening of reinforcement, which will increase the capacity. Even if the calculation is unsafe, the mentioned effect combined with the 10 % margin tends to make the calculation safe. However, there is a substantial disadvantage with this method, that it is not suitable for SLS calculations, like crack widths and deflections since it assumes a failure mechanism.

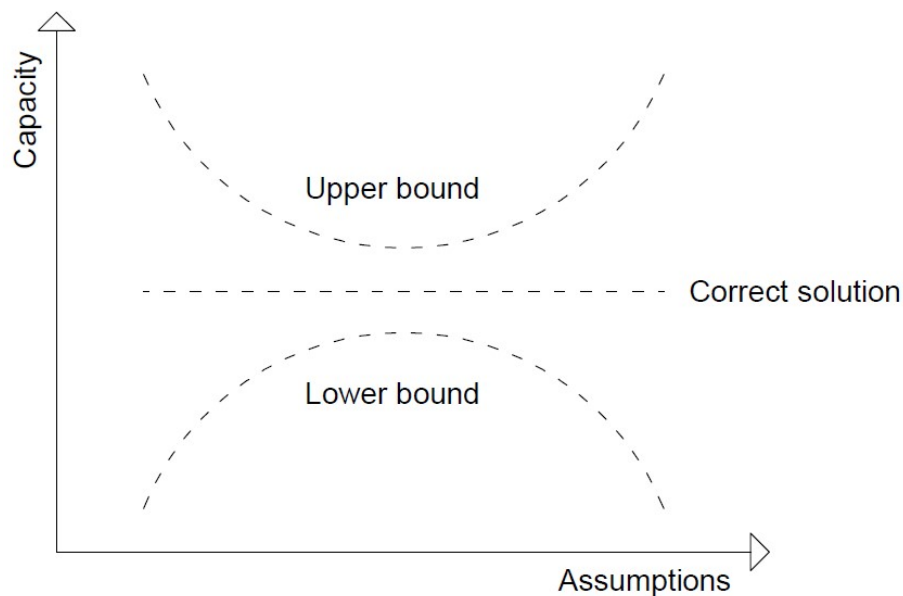


Figure 2.8: Explanation on upper and lower bound methods

2.6.2 Strip Method

The strip method is a lower bound design method for reinforced concrete two-way slabs. Regarding the method, the load is carried entirely by bending in the x- and y-directions, hence, the slab can be visualized as being composed of two systems of strips running in the x- and y-direction. Then, to explain the lower bound method more clearly, it gives a ultimate load for a slab lower than the correct value [20].

The equilibrium equation for a plate element is derived as follow:

$$\frac{\partial^2 m_x}{\partial x^2} + 2 \cdot \frac{\partial^2 m_{xy}}{\partial x \partial y} + \frac{\partial^2 m_y}{\partial y^2} = -q \quad (2.1)$$

Here, m_x and m_y are bending moments in x- and y-direction, respectively, m_{xy} is torsion moment and q is uniformly distributed load.

Based on the lower bound theory, a design solution can be considered valid if it fulfills the condition where any combination of m_x , m_y and m_{xy} satisfies Eq. (2.1) at all points in the slab. In addition, the boundary conditions must be fulfilled and the moment capacity in the respective directions is not exceeded. For the strip method, the torsion moment is set to $m_{xy} = 0$. This means that the load is carried entirely by bending in x- and y- directions, as mentioned.

Furthermore, Eq. (2.1) can be replaced by two equations that represent strip action, where the torsion is neglected:

$$\frac{\partial^2 m_x}{\partial x^2} = -\gamma q \quad (2.2)$$

and

$$\frac{\partial^2 m_y}{\partial y^2} = -(1 - \gamma)q \quad (2.3)$$

where γ is a factor chosen by the designer, and represents the load distribution in x- and y-direction, $0 \leq \gamma \leq 1.0$. The value of γ may vary throughout the slab without affecting the validity. Note that if $\gamma = 1$ all the load is carried by bending in one direction, either x- or y-direction, respectively.

3 Laboratory Experiment

This chapter provides an overview of the materials and elements used in the study. Also, the casting procedure and storage conditions are implemented. Furthermore, it presents all the laboratory tests conducted in the experimental investigation, such as the three-point bending test, plate bending test and inductive test. Regarding the compressive strength of test specimens, SINTEF has carried out these tests according to guidelines in NS-EN 12390-3:2019 [22].

3.1 Test Specimens

Prior to the upcoming tests, an overview of the concrete mixtures and plate elements is presented. The elements are casted as slabs and walls with various casting procedures. In addition, standardized beam- and cylinder specimens are casted to determine the strength properties of each concrete mixture.

3.1.1 Materials

The experiment was supposed to have five concrete mixtures. However, batch 4 got cancelled since batch 3 was expected to give approximately similar results. Three of the mixtures were produced as self compacting concrete (SCC) and two as vibrator compacted concrete (VCC). Details about the different mixtures and their concrete strength class and type, fibre type and amount are shown in Table 3.1. The composition of the concrete mixture is a class A, low carbon concrete, with a high proportion of fly ash. A full overview of the concrete recipe is shown in appendix B.1. Regarding the amount of steel fibres compared to basalt fibres, the difference in kilogram per cubic meter is significant. However, the volume of the fibres is approximately similar to each other.

Table 3.1: Concrete mixture

Concrete mixture	Concrete class	Concrete type	Fiber type	Fiber amount [kg/m ³]	Fiber amount [%]
Batch 1	B45/M40	SCC Stable	Steel DE 60/0.9 N	35	0.45
Batch 2	B45/M40	SCC Unstable	Steel DE 60/0.9 N	35	0.45
Batch 3	B45/M40	SCC Stable	Basalt Minibar 55	10	0.48
Batch 4	N/R	N/R	N/R	N/R	N/R
Batch 5	B45/M40	VCC	Steel DE 60/0.9 N	35	0.45

Two types of fibres were used, Steel fibre DE 60/0.9 N and Basalt fibre Minibar 55, as shown in Figure 3.1a and 3.1b. The steel fibre is a wired fibre with a round cross-section and hooked ends. On the other hand, Basalt fibre is a drawn, continuous fibre without hooked ends. Product data is given in Table 3.2.



Figure 3.1: Two types of fibres

Table 3.2: Product data for the two fibre types

Fibre type	Steel DE 60/0.9 N	Basalt Minibar 55
Material	Steel	Basalt
Length, L [mm]	60	55
Diameter, d [mm]	0.9	0.65
Ratio, (L/d)	67	85
Density [kg/m^3]	7840	2100
E-modulus [MPa]	210 000	45 000
Tensile strength [MPa]	1150	1000

3.1.2 Element Overview

In order to determine the residual tensile strength and compressive strength, seven beams and three cylinders for each batch were casted. The beam specimen is a concrete prism with a width and height of both 150 mm and lengths varying from 600 to 700 mm. With regard to the cylinders, the height is 300 mm with a diameter of 150 mm.

The full-scale laboratory experiment consists of a total of 16 elements that shall be tested. Element 1-10 includes only fibre reinforcement and 11-16 has a combination of fibre- and conventional reinforcement. For the slabs, elements 11, 12, 15 and 16, conventional reinforcement is included at the bottom side with a cover of 25 mm. For the walls, element 13 and 14, conventional reinforcement are included at both the bottom- and top-side with a cover of 15 mm. Details about the design, batch and reinforcement are shown in Table 3.3. In addition, appendix A.1 gives a full overview of all the test specimens.

Table 3.3: Element overview

Element ID	Dimension [m]	Thickness [mm]	Batch	Conventional reinforcement
1	1.3 x 1.3	150	1	N/R
2	1.3 x 1.3	150	3	N/R
3	1.3 x 1.3	150	2	N/R
4	1.3 x 1.3	150	1	N/R
5	1.2 x 1.2	150	1	N/R
6	1.2 x 1.2	150	2	N/R
7	1.2 x 1.2	150	5	N/R
8	1.2 x 1.2	150	3	N/R
9	1.2 x 1.2	150	1	N/R
10	1.2 x 1.2	150	5	N/R
11	1.3 x 1.3	150	1	ø10c250
12	1.3 x 1.3	150	2	ø10c250
13	1.2 x 1.2	150	1	ø10c250
14	1.2 x 1.2	150	2	ø10c250
15	2.0 x 2.0	180	1	ø10c250
16	2.0 x 2.0	150	1	ø10c250

3.1.3 Casting Procedure and Storage

The beam specimens are casted from two different methods, as illustrated in Figure 3.2. For the casting method stated in NS14651, the concrete was filled and vibrated in three layers. Regarding the Danish casting method, the concrete was poured through a funnel from one side until the formwork was filled. For batches 1, 2 and 3 the specimen was self compacting, meaning topped up and levelled off without external vibration. Batch 5 on the contrary, had compaction carried out by external vibration. There are seven beam specimens of each batch 1, 2 and 3, casted according to Danish casting method. In addition, Batch 5 includes seven specimens carried out by the Danish casting method and seven specimens carried out by the casting method stated in NS14651. After casting, the beam specimens were stored for 14 days in indoor conditions. Then placed in a water bath until testing 89 days after casting. A similar process for storage applies to cylinder specimens.

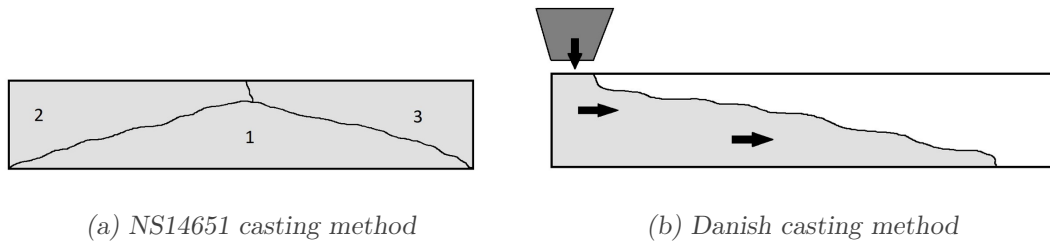


Figure 3.2: Two casting methods

The elements are casted with four different methods, as illustrated in Figure 3.3. For slabs, which were horizontally casted, the concrete was poured from one corner of the formwork until the height of the formwork was covered. In contrast, the walls were vertically casted. Thus, the concrete was poured from one side and the hose was lifted as the formwork was filled. Regarding elements 15 and 16, they are horizontally casted with two different methods. Concrete was poured from the top corner of the formwork for element 15. However, the casting was gradually moved towards the opposite corner to obtain optimal concrete spreading. For element 16 the concrete was poured with a constant flow from one side to another until the formwork was covered.

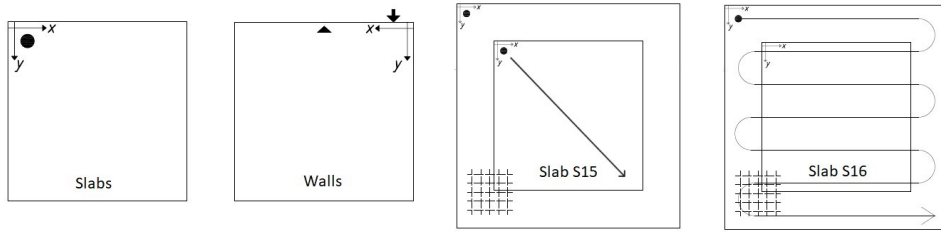


Figure 3.3: Element casting processes

After casting, the elements were stored outside for 81 days in winter conditions and covered with tarpaulin. Then transported to laboratories for the Department of Structural Engineering at NTNU where the elements were stored for 50 days in indoor conditions, to enhance the curing process, before testing. All the elements were also painted white on the bottom surface to ease the crack location during and after testing.

3.2 Three-Point Bending Test

SINTEF carried out the three-point bending test (3PBT) 90 days after casting, according to NS-EN 14651. The European standard specifies a method of measuring the flexural tensile strength of metallic fibre concrete on moulded test specimens. The residual flexural tensile strength values are determined from the load at certain crack mouth opening displacements (CMOD). However, the test only measured load and deflection. Hence, CMOD is derived from Eq. (4.8). The test method can be applied according to the standard for other types of fibres besides steel fibres. This is significant since this study employs both steel- and basalt fibres.

The setup was installed with a linear variable differential transformer (LVDT) to measure vertical displacement at the centre of the beam, as shown in Figure 3.4. Also, including two supporting rollers and one loading roller, both types of circular cross section with a diameter of 30 mm capable of rotating freely around their axis. The distance between the centre of the supporting rollers, i.e. the span length, should be 500 mm. Hence, a minimum length of 550 mm is required for the beam. The mould should be filled up to approximately 90 % of the height of the test specimen. Regarding the fibre length, neither the steel fibre nor the basalt fibre exceeds the maximum limitation of 60 mm [23].

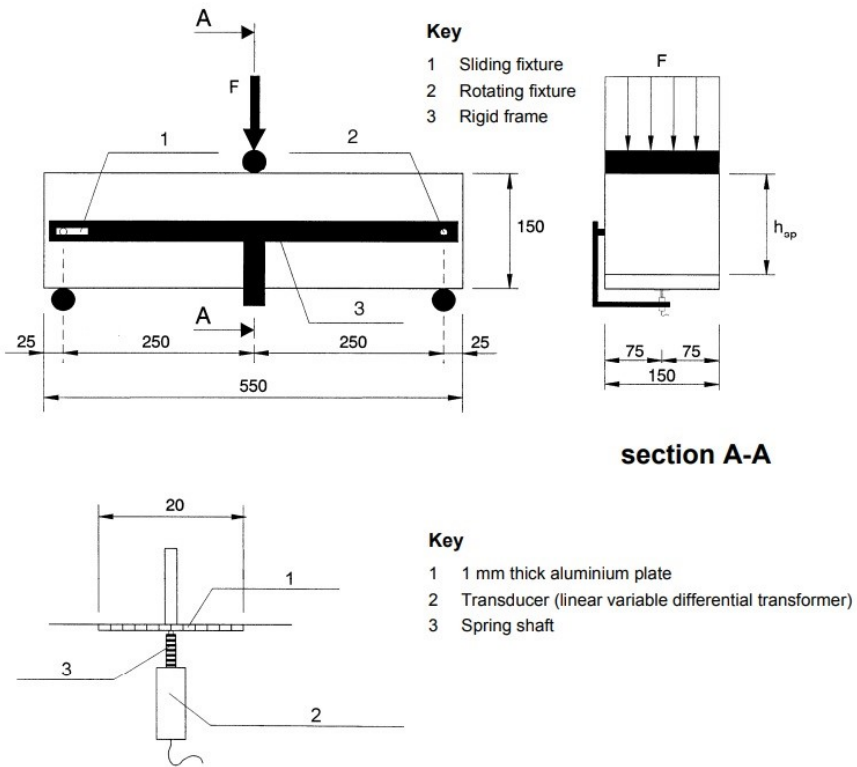


Figure 3.4: Typical arrangement for measuring deflection [23]

The notch is made by wet sawing the beam. The width is equal to 5 mm and the depth of the notch is 25 mm. Cracking of the concrete will always happen at mid-span due to the notch where the cross section is smaller, hence, larger bending stresses will occur. For the LVDT to be placed at the centre over the notch, it requires a thin plate fixed to the top of the transducer. The machine was operated so that CMOD increased at a constant rate of 0.2 mm/min, until reaching a CMOD value of 4 mm. Figure 3.5 shows a photo of the beam placed in the rig for the 3PBT.

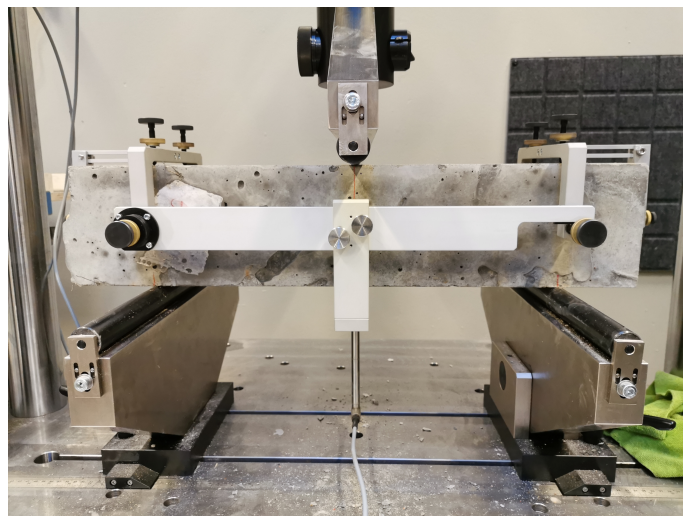


Figure 3.5: Setup for three-point bending test

3.3 Plate Bending Test

The full-scale experimental program consists of 16 elements, and a complete description of the elements and their parameters are summarised in Table 3.3. The objective of the plate bending test is to examine how the FRC, with or without conventional reinforcement, influences the capacity, displacement and cracking, with respect to the batches and casting methods.

The test was carried out as a bending test with four point loads representing an even distributed load, with a distance between the loads that varies based on the element size. The test setup is illustrated in Figure 3.6, in addition to dimensions in Table 3.4.

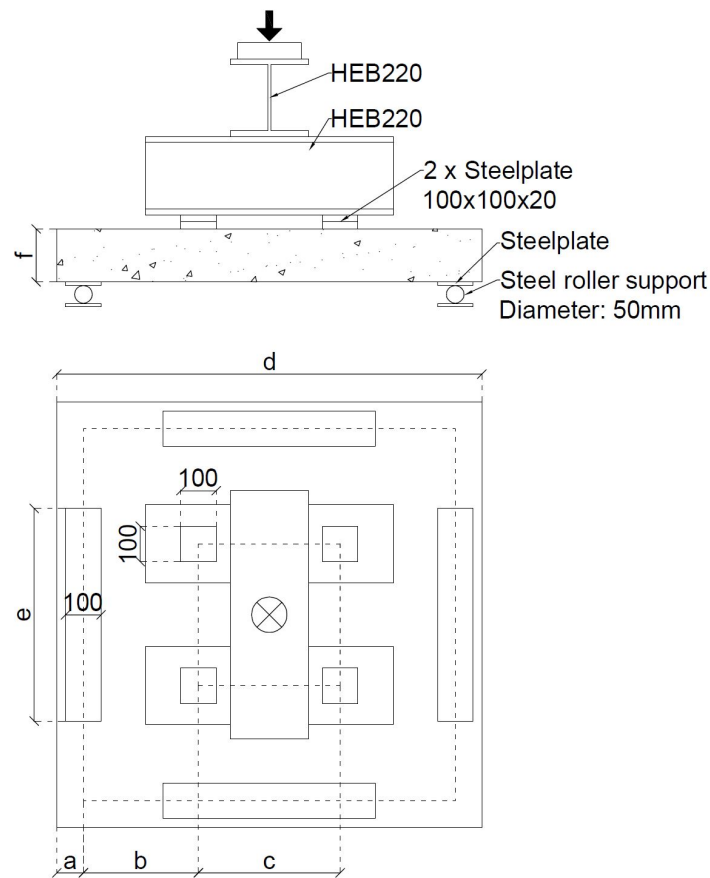


Figure 3.6: Test setup for the plate bending test

Table 3.4: Description of test setup

Element ID	a [mm]	b [mm]	c [mm]	d [mm]	e [mm]	f [mm]
1-4 & 11-12	125	275	500	1300	600	150
5-10 & 13-14	75	325	400	1200	600	150
15	100	450	900	2000	1000	180
16	100	450	900	2000	1000	150

As shown in the test setup the support is located on each side of the element. Thus, elements are working as two-way slabs. The plates were simply supported with steel rollers that allow horizontal translation and rotation about the roller's length axis, preventing axial forces from appearing. Regarding the load from the jack, steel beams in two layers are distributing the load into steel plates. In addition to steel plates, plywood is placed between the concrete and the steel plates to mitigate irregularities in the top surface. The steel beams will give the element an additional loading of 260 kg (2.6 kN) and 340 kg (3.4 kN), for elements 1-14 and 15-16, respectively. This is due to the number of beams that are required to distribute the load from the jack. Respectively, three for elements 1-14 and four for elements 15 and 16. Figure 3.7 shows a photo of element 13 after being installed in the testing rig.

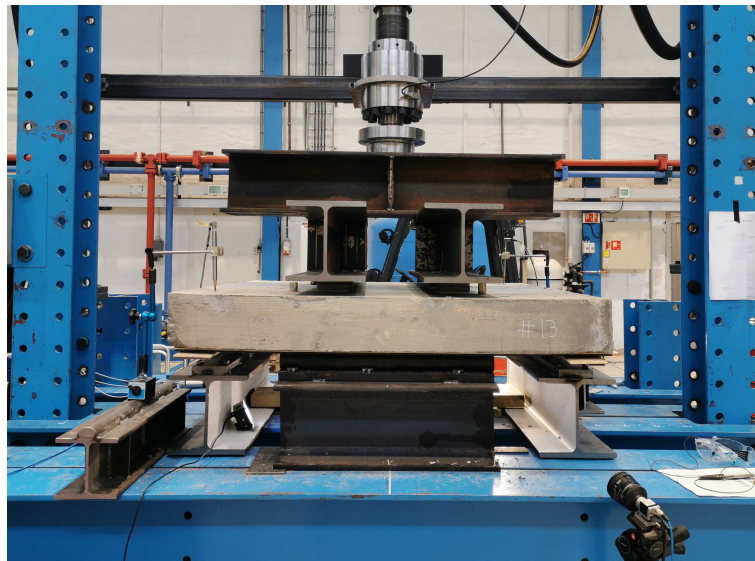


Figure 3.7: Element 13 in the testing rig

An essential aspect of the bending test is finding the ultimate load for each element. The tests were conducted with deflection control at a crosshead speed of approx. 1.0 mm/min . All the elements were installed with LVDTs to measure vertical displacement and horizontal elongation in different areas of the elements. Figure 3.8 shows where the LVDTs were located. Related to the localization of the LVDTs, most of them were installed in the centre at the bottom side due to the expected displacement. However, LVDTs are also located at two corners on the top side to account for the corner efficiency. Complementary to these, two more LVDTs are installed closer to the support at the bottom side and two more at the centre at the top side for elements 15 and 16. Regarding the horizontal LVDTs to measure crack openings, they are located according to the expected yield line pattern. Another essential device for the test was the camera to ease the crack detection on the bottom side of the element. Two cameras were placed on each side of the test rig and provided one picture every third or fifth second, for elements 1-14 and elements 15 and 16, respectively. Hence, the first cracks and their further spreading can be analysed in relation to the load. Subsequently to the test, the smaller secondary cracks are drawn on the element to clarify the crack pattern.

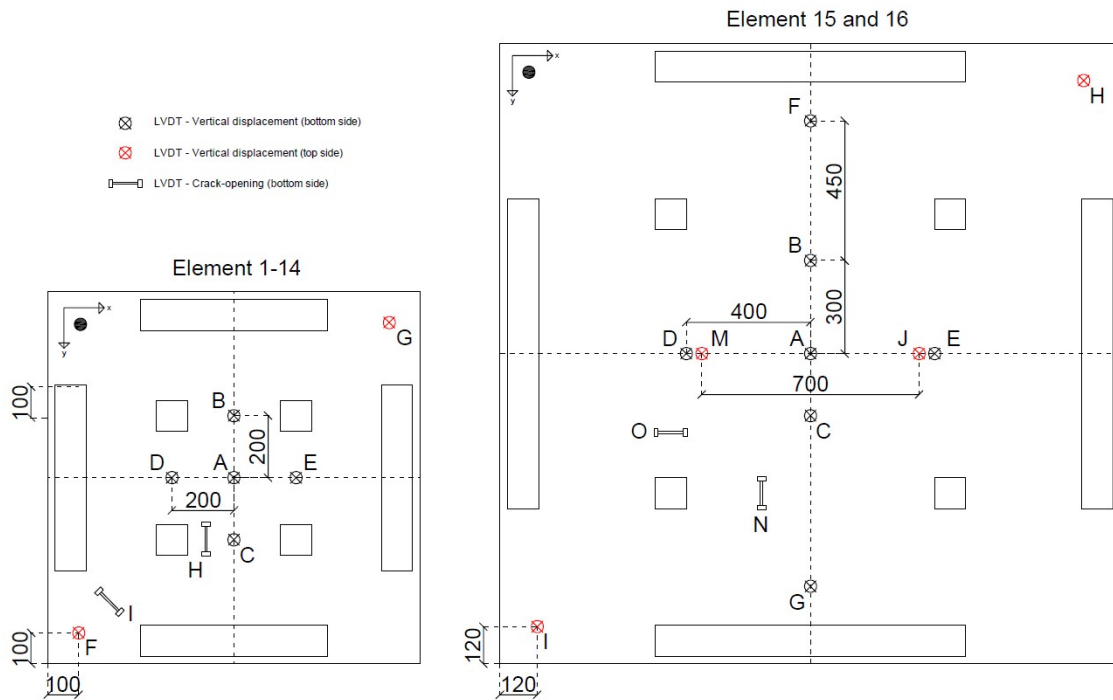


Figure 3.8: Localization of LVDTs

3.4 Inductive Test

The objective of the inductive test is to analyse how the different casting methods and batch types influence the fibre content and distribution within and between the elements. This also applies to the beam specimens. Regarding the test, it uses an impedance analyser, as shown in Figure 3.9, which produces an electrical flow through a circular coil, thus inducing a magnetic field around it. Different inductance variation (L_i) is measured after placing the sample into the coil in different positions.

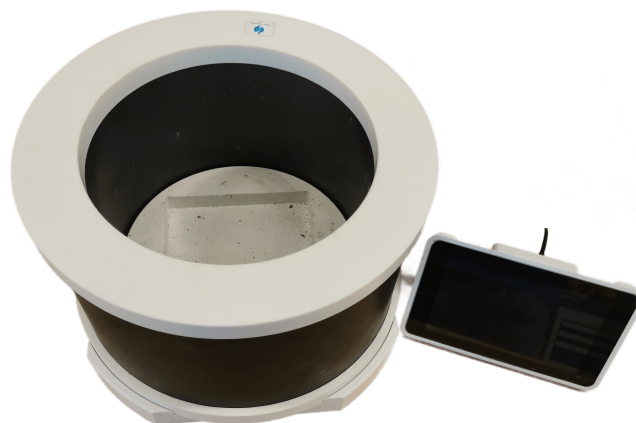


Figure 3.9: Impedance analyser

3.4.1 Cubic Specimens

The inductive test for cubic specimens consists of 16 cubes, sawn off from the beam specimens for batches 1, 2, 5D and 5S. An important consideration is that the cube's first cut was at a distance of 25 mm from the crack, located in the centre of the beam specimen. These cubes contain SFRC and have the possibility to be investigated. On the other hand, batch 3 consists of BFRC and cannot be investigated for fibre content and orientation with this method. As shown in Figure 3.10, two cubes from the same beam specimen were examined. Therefore, the axis is important to maintain the cube's orientation and position. Another essential point pertains to the selection of the two beam specimens from each batch for examination. Specifically, these specimens were chosen based on their residual flexural tensile strength at $CMOD_3 = 2.5 \text{ mm}$, with the beam exhibiting the highest and lowest value.

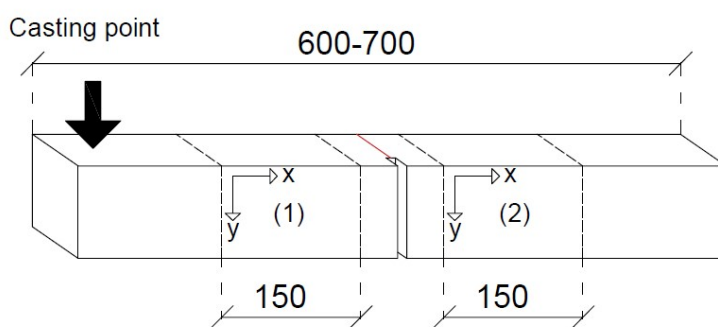


Figure 3.10: Section used for cubes

The inductance change should be measured in the three directions (X, Y and Z) perpendicular to the face of the specimen. Then, the summed inductance in the three axes is linearly related to the fibre content. The three directions for the test are shown in Figure 3.11.

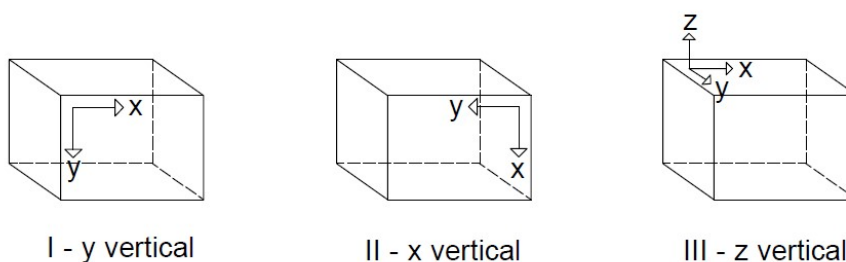


Figure 3.11: Test order on inductive test for cubes

3.4.2 Cylindrical Specimens

The cylindrical specimens underwent an inductive testing procedure subsequent to the completion of the plate bending test, whereby SINTEF performed core drilling. Inductive testing was performed for elements 1, 5, 9, 13 and 14. In appendix A.2, the precise locations of core drilling for each individual cylindrical specimen are shown.

The inductance change should be measured in the four directions (Z, 0°, 45° and 90°), where the summed inductance in axis Z, 0° and 90° is linearly related to the fibre content. Compared to cubes, cylindrical specimens have an extra measure at 45°. The advantage of this is the opportunity to mathematically calculate the orientation in any direction and propose a level of isotropy. The four directions for the test are shown in Figure 3.12. Also, note that the arrow indicates the orientation of the cylinder, specifically denoting the negative Y-direction of the plate element.

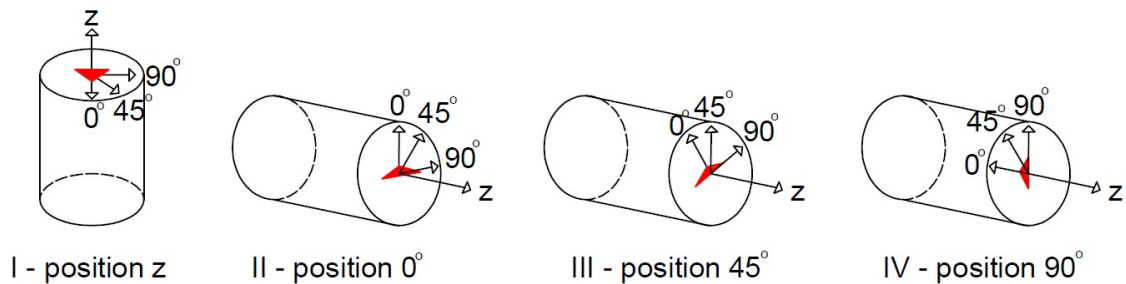


Figure 3.12: Test order on inductive test for cylinders

3.4.3 Calculation of Fibre Content

Before presenting the analysis results, it is necessary to introduce the following equations which were developed by Cavalaro et al.[18] for cubic and cylindrical specimens. First, the content of fibre could be estimated through Eq. (3.1):

$$C_f = \beta \cdot \sum_{x,y,z} \frac{L_i}{B_{V,i}} = \beta \cdot L_e \quad (3.1)$$

Where:

β is the proportionality constant.

L_e is the sum of the ratio between the inductive change measured in each axis and the corresponding constant $B_{V,i}$ from Table 3.5.

Prior to the testing, some specimens had been tested and crushed to find the fibre content. With these results, linear regression is used to express the proportionality constant, β . In addition, a correction of the linear curve was added to the function for fibre content to ensure a linear relation between L_e and C_f . The final expression for fibre content was then expressed as:

$$C_f = 7020.65 \cdot L_e - 1.5556 \quad (3.2)$$

Then, the orientation number in a generally shaped specimen with dispersed fibres is obtained as:

$$\eta_i = \vartheta \cdot \sqrt{\frac{L_i \cdot (1 + 2 \cdot \gamma) - L_e \cdot B_{V,i} \cdot \gamma}{L_e \cdot B_{V,i} \cdot (1 - \gamma)}} - \mu \quad (3.3)$$

Where:

- ϑ is a parameter to account for the non-homogeneity of the magnetic field that is not considered in the analytical ductions, as given in Table 3.5.
- γ is a shape factor, for cubic and cylindrical specimens used in the experiment this factor is determined to a value of 0.05.
- μ is a correction parameter to compensate for the overestimation of fibres per axis, as given in Table 3.5.

Finally, the fibre contribution is calculated as followed:

$$C_i = \frac{\eta_i}{\sum_{i=x,y,z} \eta_i} \quad (3.4)$$

Table 3.5 summarizes the parameters for the assessment of the fibre content and orientation in any cylindrical or cubic specimens. For the cylindrical specimens the axis X and Y coincide with 0° and 90°, respectively.

Table 3.5: Constant parameters for cylindrical and cubic specimens

Shape	Size [mm]	Parameter				
		$B_{V,x}$	$B_{V,y}$	$B_{V,z}$	μ	ϑ
Cylindrical	ϕ 150 x 150	1789	1789	1809	0.085	1.03
Cubic	150 x 150 x 150	2342	2342	2342	0.100	1.03

Further calculations only adapt to cylindrical specimens which have the additional measurement at 45°, where the goal is to determine the level of isotropy through the isotropy factor Ω . The inductive change in any direction in the XY plane can be expressed through superposition of the isotropic and anisotropic parts as:

$$L_\theta = L_{iso} + L_{ani} \cdot [\gamma + (1 - \gamma) \cdot \cos^2(\theta + \theta_{max})] \quad (3.5)$$

Where:

$$L_{ani} = \frac{1}{1 - \gamma} \cdot \sqrt{(L_{0^\circ} - L_{90^\circ})^2 + (L_{0^\circ} + L_{90^\circ} - 2 \cdot L_{45^\circ})^2} \quad (3.6)$$

$$L_{iso} = \frac{L_{0^\circ} + L_{90^\circ} - L_{ani} \cdot (1 + \gamma)}{2} \quad (3.7)$$

The direction with maximum inductance can be calculated according to Eq. (3.8). This angle can be either positive or negative, hence, θ_{max} should be checked according to Eq. (3.5) with $\theta = 45^\circ$ and compared against the measured inductive change L_{45° . The one of the two calculated θ_{max} that coincide with L_{45° is the correct one.

$$\theta_{max} = \pm \frac{1}{2} \cdot \arccos \left[\frac{L_{0^\circ} - L_{90^\circ}}{L_{ani} \cdot (1 - \gamma)} \right] \quad (3.8)$$

The angle with the lowest inductance is perpendicular to θ_{max} .

$$\theta_{min} = \theta_{max} - 90^\circ \quad (3.9)$$

From Eq. (3.5), the maximum and minimum inductance can be found and simplified as:

$$L_{max} = L_{iso} + L_{ani} \quad (3.10)$$

$$L_{min} = L_{iso} + \gamma \cdot L_{ani} \quad (3.11)$$

As for the maximum and minimum inductance, the maximum and minimum orientation number should be separated by 90° and calculated as:

$$\eta_{max} = 1.03 \cdot \sqrt{\frac{L_{max} \cdot (1 + \gamma) - \left(L_{min} + L_z \cdot \frac{B_{V,x}}{B_{V,z}} \right) \cdot \gamma}{\left(L_{max} + L_{min} + L_z \cdot \frac{B_{V,x}}{B_{V,z}} \right) \cdot (1 - \gamma)}} - 0.085 \quad (3.12)$$

$$\eta_{min} = 1.03 \cdot \sqrt{\frac{L_{min} \cdot (1 + \gamma) - \left(L_{max} + L_z \cdot \frac{B_{V,x}}{B_{V,z}} \right) \cdot \gamma}{\left(L_{max} + L_{min} + L_z \cdot \frac{B_{V,x}}{B_{V,z}} \right) \cdot (1 - \gamma)}} - 0.085 \quad (3.13)$$

Finally, the isotropy factor can be calculated as the ratio between the maximum and minimum orientation number. For a perfectly isotropic orientation, η_{max} and η_{min} is equal such that $\Omega = 1$. Otherwise, if the fibres are orientated in the same direction, η_{min} goes toward zero resulting in $\Omega \approx 0$.

$$\Omega = \frac{\eta_{min}}{\eta_{max}} \quad (3.14)$$

4 Design Methods

With a series of laboratory experiments carried out, the results are compared against the regulations for designing FRC. The new Eurocode for concrete structures contains an annex L for calculating FRC structures. Together with the Norwegian guidelines given in NB38, these forms the basis for the calculation methodology for FRC.

4.1 Concrete Strength

Calculation of concrete properties is determined from EC2, using the average compressive strength derived from the results of the compressive test, which gives the basis for further calculations.

According to EC2 the characteristic compressive strength, mean- and characteristic tensile strength is calculated as followed:

$$f_{ck} = f_{cm} - 8MPa \quad (4.1)$$

$$f_{ctm} = \begin{cases} 0.3 \cdot f_{ck}^{\frac{2}{3}} & \text{for } f_{ck} \leq 50 MPa \\ 1.1 \cdot f_{ck}^{\frac{1}{3}} & \text{for } f_{ck} > 50 MPa \end{cases} \quad (4.2)$$

$$f_{ctk;0.05} = 0.7 \cdot f_{ctm} \quad (4.3)$$

The modulus of elasticity may be approximated as:

$$E_{cm} = k_E \cdot f_{cm}^{\frac{1}{3}} \quad (4.4)$$

For concrete with sandstone aggregate k_E can be determined as:

$$k_E = 0.7 \cdot 9500 \quad (4.5)$$

4.2 Residual Strength

To design FRC the residual flexural tensile strength of the fibres needs to be determined. This material parameter is determined by a standardized test, where test specimens undergo a three-point bending test as described in chapter 3.2. From this test, the limit of proportionality and the post-cracking residual flexural tensile strength at four different stages of crack propagation can be expressed. By assuming a linear stress distribution over the height, the stress in the most tensioned fibre can be calculated from the machine load as:

$$f_{R,i} = \frac{6 \cdot M_{R,i}}{b \cdot h^2} \quad (4.6)$$

Where the moment for a simply supported beam with a point load at mid span is:

$$M_{R,i} = \frac{F_{R,i} \cdot L}{4} \quad (4.7)$$

The limit of proportionality expresses the stress for the first crack or at 0.05 mm crack mouth opening for strain-hardening behaviour. The four different values post-cracking should be obtained at specific crack widths. These CMOD should be measured at 0.5 mm, 1.5 mm, 2.5 mm and 3.5 mm. However, since it is easier to measure deflection δ rather than such small crack widths, NS-EN 14651 expresses the relationship between CMOD and deflection as [23]:

$$CMOD = \frac{\delta - 0.04}{0.85} \quad (4.8)$$

Furthermore, the characteristic values are determined with 0.05 percentile as:

$$f_{R,ik} = f_{R,im} - k \cdot s \quad (4.9)$$

Where:

$f_{R,im}$ is the mean residual flexural tensile strength at $CMOD_i$ based on all test specimens from the same batch.

k is a factor corresponding with a confidence level of $\alpha = 0.05$, dependent on the number of test specimens. When the test follows the procedure in NS-EN 14651, NB38 recommends $k = 1.7$ for six samples.

s is the standard deviation of the samples given as:

$$s = \sqrt{\frac{\sum (f_{R,i} - f_{R,im})^2}{n - 1}} \quad (4.10)$$

Where n is the number of samples.

The three-point bending test can result in low characteristic strength due to large statistical scatter. A major reason for the large scatter comes from the small specimen size. In addition, the nature of the fibre concrete material itself. However, it is well documented that such a large scatter does not occur for larger specimens. To ensure a safe and robust design, the characteristic residual flexural tensile strength should not exceed 60 % of the mean value. However, this does not apply to the limit of proportionality.

$$f_{R,1k} \leq 0.6 \cdot f_{R,1m} \quad (\text{serviceability limit state}) \quad (4.11)$$

$$f_{R,3k} \leq 0.6 \cdot f_{R,3m} \quad (\text{ultimate limit state}) \quad (4.12)$$

Further, some differences separate NB38 and EC2 in the calculation of the residual tensile strength. In the following calculation, only the strength at $CMOD_1 = 0.5 \text{ mm}$ and $CMOD_3 = 2.5 \text{ mm}$ is determined since $f_{R,1k}$ corresponds to SLS and $f_{R,3k}$ corresponds to ULS.

4.2.1 Residual Tensile Strength According to EC2

For design according to EC2, this should be satisfied:

$$\frac{f_{R,1k}}{f_{ctk;0.05}} \geq 0.5 \quad (4.13)$$

The effective residual tensile strength is derived by scaling the residual flexural tensile strength to a rigid-plastic model and accounting for fibre orientation and element size. The factor 0.33 in ULS is derived by assuming a concentrated compressive force in the top fibre, while for SLS the factor 0.37 represents a tension height equal to 0.9h.

$$f_{Fts,eff} = \kappa_0 \cdot \kappa_G \cdot 0.37 \cdot f_{R,1k} \quad (\text{Serviceability limit state}) \quad (4.14)$$

$$f_{Ftu,eff} = \kappa_0 \cdot \kappa_G \cdot 0.33 \cdot f_{R,3k} \quad (\text{Ultimate limit state}) \quad (4.15)$$

Where:

κ_0 is a factor accounting for variation in fibre orientation. $\kappa_0 = 1.0$ corresponds to a similar fibre orientation as the beam specimens.

κ_G is a function accounting for the structural volume of the failure mode.

$$\kappa_G = 1.0 + A_{ct} \cdot 0.5 \leq 1.5 \quad (4.16)$$

Where $A_{ct} [m^2]$ is the area of the tension zone in the actual failure mode.

Introducing the partial safety factors for SFRC presented in Table 4.1, the design residual tensile strength is:

$$f_{Ftsd} = f_{Fts,eff} / \gamma_{SF} \quad (4.17)$$

$$f_{Ftud} = f_{Ftu,eff} / \gamma_{SF} \quad (4.18)$$

For SFRC in tension the partial factors in Table 4.1 should be used. For SFRC in compression the partial factor for concrete γ_c applies.

Table 4.1: Partial factors for SFRC in tension

Design situations- Limit states	γ_{SF}
Persistent and transient design situations	1.50
Accidental design situations	1.20
Serviceability limit state	1.00

4.2.2 Residual Tensile Strength According to NB38

To convert the residual flexural tensile strength to uniaxial residual tensile strength NB38 uses a scaling factor as in EC2. The characteristic residual flexural tensile strength is based on linear elastic stress distribution, while the characteristic residual tensile strength must be transformed to constant stresses, as shown in Figure 4.1. In contrast to EC2, NB38 assume a tension height of $0.9h$ in ULS ($f_{R,3k}$), while in SLS ($f_{R,1k}$) the height is assumed to be $0.66h$. The characteristic residual tensile strength is then:

$$f_{Ftsk} = 0.45 \cdot f_{R,1k} \quad (4.19)$$

$$f_{Ftuk} = 0.37 \cdot f_{R,3k} \quad (4.20)$$

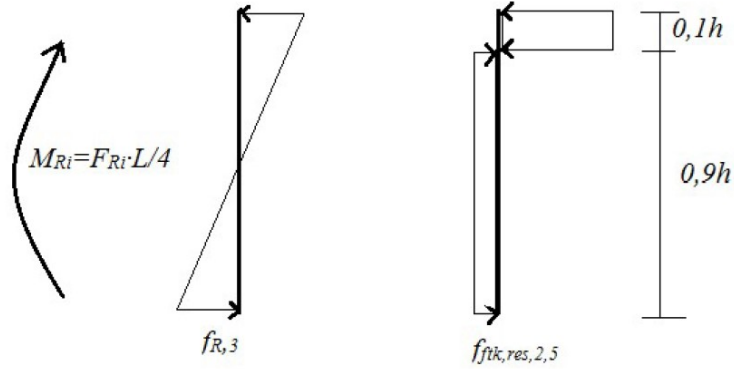


Figure 4.1: Relation between flexural strength and uniaxial strength [1]

As the method described in EC2, the effective residual tensile strength accounts for the fibre orientation with the factor κ_0 . However, NB38 does not have any geometrical factor like EC2.

$$f_{Fts,eff} = \kappa_0 \cdot f_{Ftsk} \quad (4.21)$$

$$f_{Ftu,eff} = \kappa_0 \cdot f_{Ftuk} \quad (4.22)$$

The final design residual tensile strength is found by using the partial factors as done in Eq. (4.17) and (4.18).

4.3 Ultimate Limit State

For design situations in ULS, the fibres contribute with a residual tensile strength determined from the $CMOD_3 = 2.5 \text{ mm}$, with a partial safety factor, $\gamma_{SF} = 1.5$. However, to compare the calculated ultimate load and the results from the laboratory test, the calculation is performed with both mean and characteristic values and no partial safety factors for the fibre reinforcement nor the concrete.

4.3.1 Moment Capacity

To calculate the estimated ultimate load, only the bending moment has been determined, i.e. shear capacity has not been checked. To calculate the moment capacity, NB38 proposes a simplified method for FRC with a design residual tensile strength in ULS below 2.5 N/mm^2 . With this method the residual tensile strength can be assumed to contribute over $0.8h$, as shown in Figure 4.2, giving an internal lever arm equal to half the height. Moment capacity is then:

$$M_{Rd} = 0.4 \cdot f_{Ftud} \cdot b \cdot h^2 \quad (4.23)$$

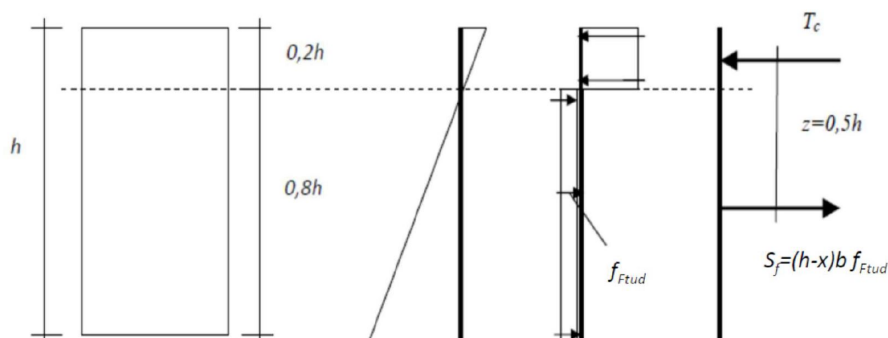


Figure 4.2: Simplified stress- and strain distribution for FRC [1].

A more general, but also more advanced method can be used to calculate the moment capacity. Figure 4.3 shows the strain and stress distribution where the height of the compression zone is the only unknown parameter. This parameter is found using axial equilibrium. However, note that the effective height of the compression zone is only $0.8x$. This method can include additional conventional reinforcement both in the bottom and upper layers. However, the reinforcement close to the neutral axis may not exhibit yielding, hence, an iterative process can be used to calculate the strain and stress in these rebars.

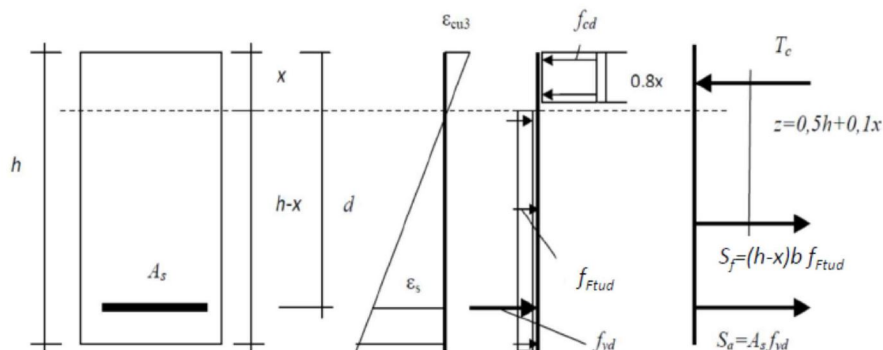


Figure 4.3: General stress- and strain distribution for FRC exposed to pure bending [1].

For lightly reinforced structures the strain in the most tensioned fibre may be too large. According to NB38 the strain on the tension side should not exceed $3/h$ ‰, while EC2 limits the strain to $\varepsilon_{Ftud} = 20$ ‰.

If the strain in the tension reinforcement becomes the limited factor, the compression in the concrete may not be fully utilized and exhibits strain lower than ε_{cu} . A method from fib Bulletin 90 [24] takes this into account by adjusting the concrete compression zone and the resultant with the factors k_1 and k_2 , as shown in Figure 4.4. To establish equilibrium for the section, the concrete strain followed by the neutral axis is found by iterating over different strain values until the cross section reaches axial equilibrium.

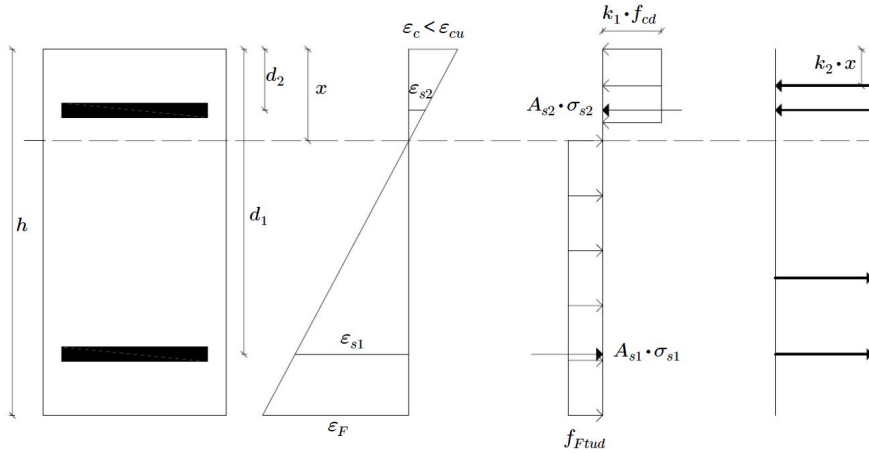


Figure 4.4: Stress- and strain distribution, with strain in fibres as the limited factor

The factor k_1 decreases the concrete stress due to the reduced strain. The maximum value of 0.8 corresponds to an ordinary design, as shown in Figure 4.3. Factor k_2 influences the location of the resultant of the concrete compressive force.

$$k_1 = \begin{cases} \varepsilon_c \cdot \left(0.5 - \frac{1}{12} \cdot \varepsilon_c\right) & \text{for } \varepsilon_c \leq 2 \text{ ‰} \\ 1 - \frac{2}{3 \cdot \varepsilon_c} & \text{for } 2 \text{ ‰} \leq \varepsilon_c \leq 3.5 \text{ ‰} \end{cases} \quad (4.24)$$

$$k_2 = \begin{cases} \frac{8 - \varepsilon_c}{4 \cdot (6 - \varepsilon_c)} & \text{for } \varepsilon_c \leq 2 \text{ ‰} \\ \frac{\varepsilon_c \cdot (3 \cdot \varepsilon_c - 4) + 2}{2 \cdot \varepsilon_c \cdot (3 \cdot \varepsilon_c - 2)} & \text{for } 2 \text{ ‰} \leq \varepsilon_c \leq 3.5 \text{ ‰} \end{cases} \quad (4.25)$$

Normally the height of the compression zone is expressed as $x = \alpha \cdot d$, where d is the distance from the top surface to the tensile reinforcement bars. However, for FRC, the strain in the most tensioned fibre reaches the strain limit before the rebars and limits the calculation. Hence, it is more convenient to express x as a function of the element height.

$$x = \alpha \cdot h \quad (4.26)$$

Where:

$$\alpha = \frac{\varepsilon_c}{\varepsilon_c + \varepsilon_F} \quad (4.27)$$

Resultant force is then:

$$F_c = k_1 \cdot f_{cd} \cdot b \cdot x \quad (4.28)$$

$$F_F = f_{Ftud} \cdot (h - x) \quad (4.29)$$

$$F_{s1} = f_{yk} \cdot A_{s1} \quad (4.30)$$

$$F_{s2} = \sigma_{s2} \cdot A_{s2} \quad (4.31)$$

The stress in the top reinforcement can be calculated using Eq. (4.32). Depending on the height of the compression zone, note that σ_{s2} becomes negative if d_2 is greater than x .

$$\sigma_{s2} = \varepsilon_{s2} \cdot E_s = \left((x - d_2) \cdot \frac{\varepsilon_c}{x} \right) \cdot E_s \quad (4.32)$$

The moment capacity can then be calculated as:

$$M_{Rd} = F_c \cdot (x - k_2 \cdot x) + F_{s2} \cdot (x - d_2) + F_{s1} \cdot (d_1 - x) + F_F \cdot \left(\frac{h - x}{2} \right) \quad (4.33)$$

Using the calculated moment capacity, the ultimate load can be found using yield line or strip methods.

4.3.2 Ultimate Load Using Yield Line Method

Based on the test setup, the yield line pattern was assumed to occur as Figure 4.5 illustrates with dimensions as described in Table 4.2.

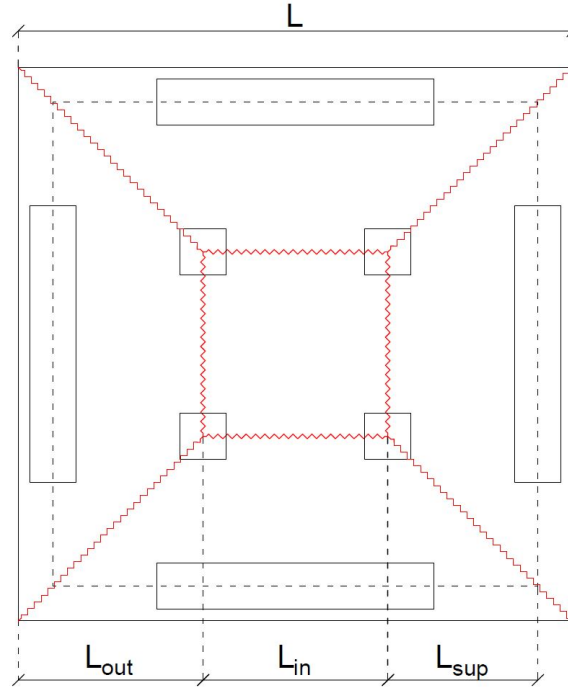


Figure 4.5: Assumed yield line pattern along the red lines

Table 4.2: Yield line length for the different plates

Element ID	L [mm]	L_{out} [mm]	L_{in} [mm]	L_{sup} [mm]
1-4 & 11-12	1300	400	500	275
5-10 & 13-14	1200	400	400	325
15 & 16	2000	550	900	450

From this geometry, the ultimate load can be calculated according to yield line theory, where the internal and external work can be expressed as:

$$W_{ext} = P \cdot w \quad (4.34)$$

$$W_{int} = m_{Rd} \cdot \theta \cdot L \quad (4.35)$$

Where:

$$\theta = \frac{w}{L} \quad (4.36)$$

As the external work should be equal to the internal work, P can be calculated as:

$$P = \frac{m_{Rd} \cdot \theta \cdot L}{w} \quad (4.37)$$

For the yield line pattern in Figure 4.5, the final ultimate load equals:

$$P_{ULS} = 4 \cdot m_{Rd} \cdot \frac{L_{in}}{L_{sup}} + 8 \cdot m_{Rd} \cdot \frac{L_{out}}{L_{sup}} \quad (4.38)$$

4.3.3 Ultimate Load Using Strip Method

Calculation using the strip method distributes the load in two directions, as described in chapter 2.6.2. Since the plates are squares and symmetric about both axis, it is reasonable to assume a 50 % distribution in each direction, giving $\gamma = 0.5$. The static system for one direction is shown in Figure 4.6.

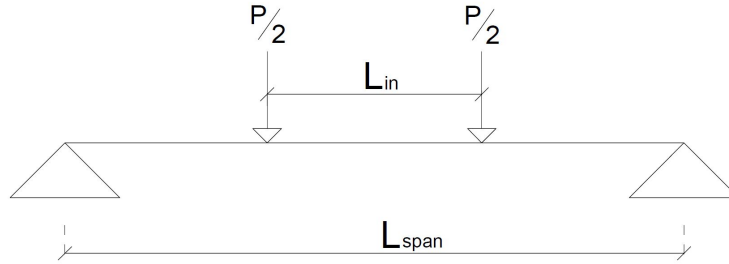


Figure 4.6: Static system in one direction of the plate

Ultimate load is found when the acting moment, as shown in Eq. (4.39), is equal to the moment capacity of the element.

$$M_{Ed} = \frac{\gamma \cdot P}{4} \cdot (L_{span} - L_{in}) \quad (4.39)$$

$$P_{ULS} = \frac{4 \cdot M_{Rd}}{(L_{span} - L_{in}) \cdot \gamma} \quad (4.40)$$

4.4 Serviceability Limit State

For design situations in SLS, the fibres contribute with a residual tensile strength determined from the $CMOD_1 = 0.5 \text{ mm}$, with a partial safety factor, $\gamma_{SF} = 1.0$. However, to compare the calculated crack width and the results from the laboratory test, the calculation is performed with both mean and characteristic values and no partial safety factors for the fibre reinforcement nor the concrete. Regarding the calculation of crack width, there is a slight difference between EC2 and NB38. Also, it should be mentioned that the following calculations only apply to a combination of FRC and conventional reinforcement.

4.4.1 Calculation of Crack Width According to EC2

The calculated crack width $w_{k,cal,F}$ should be considered as a nominal value for the crack width at the plate surface, to be compared with the crack width measured in the plate bending test. Crack width may be determined as:

$$w_{k,cal,F} = k_w \cdot k_{1/r} \cdot s_{r,m,cal,F} (\varepsilon_{sm} - \varepsilon_{cm}) \quad (4.41)$$

Where:

k_w is a factor converting the mean crack width into a calculated crack width.
(k_w equal 1.7 and 1.3, for Eq. (4.43a) and (4.43b), respectively)

$k_{1/r}$ is a coefficient to account for the increase of crack width due to curvature. For the most tensioned fibre this can be defined, in accordance with Figure 4.7, as:

$$k_{1/r} = \frac{h - x}{h - a_{y,i} - x} \quad (4.42a)$$

For the least tensioned fibre of a member, with both faces in tension, the effect of the curvature is favourable and can be defined as:

$$k_{1/r} = \frac{|x|}{a_{y,s} + |x|} \quad (4.42b)$$

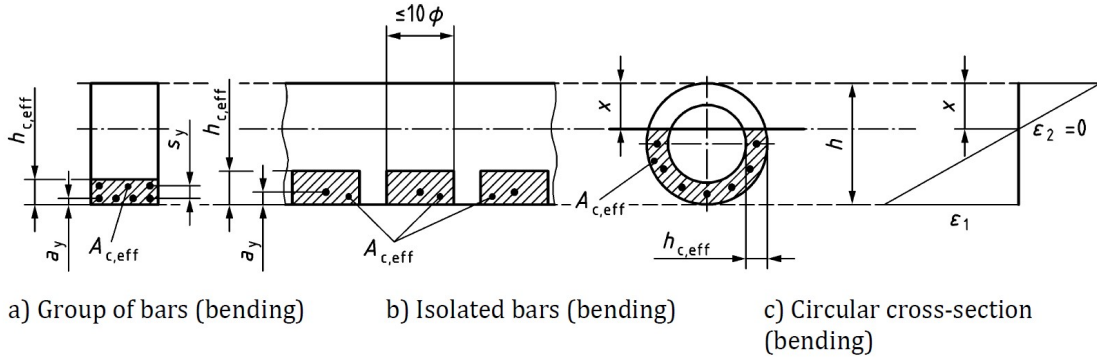


Figure 4.7: Effective tension area [25]

The mean crack spacing $s_{r,m,cal,F}$ is calculated when all cracks have formed, or not. For members with steel fibres and longitudinal bars, subjected to bending, the calculation depends on the spacing s of bonded reinforcement and bar diameter ϕ :

$$\text{For } s \leq 10\phi \quad s_{r,m,cal,F} = 1,5 \cdot c + \frac{k_{fl} \cdot k_b}{7,2} \cdot \frac{\phi}{\rho_{s,eff}} \cdot (1 - \alpha_f) \quad (4.43a)$$

$$\text{For } s > 10\phi \quad s_{r,m,cal,F} = h - x \quad (4.43b)$$

Where:

c is the concrete cover of the bar. For corner bars, the maximum value of the cover applies.

$$k_b = \begin{cases} 1.2 & \text{for poor bond conditions} \\ 0.9 & \text{for good bond conditions} \end{cases}$$

$\rho_{s,eff}$ is the ratio $A_s/A_{c,eff}$

Figure 4.7 shows the effective tension area for isolated bars. For rectangular cross section subjected to pure bending, a coefficient regarding the type of loading is essential:

$$k_{fl} = \frac{h - h_{c,eff}}{h} \quad (4.44)$$

Where:

$h_{c,eff}$ is the height of the effective concrete area around reinforcement for a single layer of bars:

$$h_{c,eff} = \min \left\{ c + 5\phi ; 10\phi ; 3.5c ; h - x ; \frac{h}{2} \right\} \quad (4.45)$$

The last parameter to calculate is the coefficient α_f :

$$\alpha_f = \frac{f_{Fts,eff}}{f_{ctm}} \leq 1.0 \quad (4.46)$$

For plates subjected to direct loads and stabilized cracking, where end restraint dominates, the difference in strain may be determined as:

$$\varepsilon_{sm} - \varepsilon_{cm} = \frac{\sigma_s - k_t \frac{f_{ct,eff}}{\rho_{s,eff}} (1 + \alpha_e \rho_{s,eff})}{E_s} \geq (1 - k_t) \frac{\sigma_s}{E_s} \quad (4.47)$$

Where:

$f_{ct,eff}$ is the mean value of the tensile strength of the concrete effective at the time when the cracks may first be expected to occur:

$$f_{ct,eff} = f_{ctm}$$

α_e is the ratio E_s/E_{cm}

k_t is a coefficient dependent on the duration and nature of the load.
($k_t = 0.6$ for short term loading)

σ_s is the stress in the tension reinforcement closest to the tensioned concrete surface assuming a cracked section. The stress is calculated by the procedure in chapter 4.4.3.

4.4.2 Calculation of Crack Width According to NB38

For crack width calculations derived from NB38, fib Model code 2010 [2] has been essential. In general, the crack width may be determined as:

$$w_{k,cal,F} = s_{r,max,cal,F} \cdot (\epsilon_{sm} - \epsilon_{cm}) \quad (4.48)$$

The max crack spacing $s_{r,max,cal,F}$, at a stabilized crack pattern in the area next to the crack when the first crack is induced, is calculated as:

$$s_{r,max,cal,F} = (2c + 0.35k_b \cdot \frac{\phi}{\rho_{s,eff}}) \cdot (1 - \frac{f_{Fts,eff}}{f_{ctm}}) \quad (4.49)$$

Where:

$$k_b = \begin{cases} 1.6 & \text{for poor bond conditions} \\ 0.8 & \text{for good bond conditions} \end{cases}$$

For plates subjected to direct loads and stabilized cracking, where end restraint dominates, $\epsilon_{sm} - \epsilon_{cm}$ may be determined as followed:

$$\epsilon_{sm} - \epsilon_{cm} = \frac{\sigma_s - k_t \frac{f_{ctm}}{\rho_{c,eff}} (1 + \alpha_e \rho_{s,eff})}{E_s} \geq (1 - k_t) \frac{\sigma_s}{E_s} \quad (4.50)$$

Where:

σ_s is the stress in the tension reinforcement closest to the tensioned concrete surface assuming a cracked section. The stress is calculated by the procedure in chapter 4.4.3.

4.4.3 Calculation of Stress in Reinforcement Bars

The stress in the reinforcement rebars is related to the load, hence, it can be expressed as a function of the curvature for a specimen exposed to pure bending. In SLS the compression field of the concrete can be expressed as linear varying stress and constant residual tensile stress in the tension field, as illustrated in Figure 4.8.

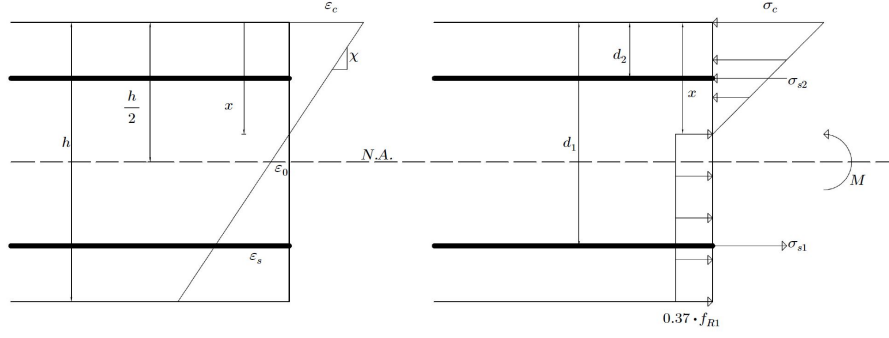


Figure 4.8: Stress distribution in SLS at given curvature

As illustrated in the figure above, the strain is zero at the distance x from the top. By implementing the curvature, the strain at the centre of the cross section can be expressed as:

$$\varepsilon_x = 0 = \varepsilon_0 - (x - h/2) \cdot \chi \quad \rightarrow \quad \varepsilon_0 = (x - h/2) \cdot \chi \quad (4.51)$$

Where:

ε_0 is the strain at the centre of the cross section.

χ is the curvature.

Further, the stress can be derived from Hook's law, $\sigma = \varepsilon \cdot E$:

$$\sigma_c = \varepsilon_c \cdot E_c \quad \rightarrow \quad \varepsilon_c = \varepsilon_0 + h/2 \cdot \chi \quad (4.52)$$

$$\sigma_{s1} = \varepsilon_{s1} \cdot E_s \quad \rightarrow \quad \varepsilon_{s1} = \varepsilon_0 - (d_1 - h/2) \cdot \chi \quad (4.53)$$

$$\sigma_{s2} = \varepsilon_{s2} \cdot E_s \quad \rightarrow \quad \varepsilon_{s2} = \varepsilon_0 + (h/2 - d_2) \cdot \chi \quad (4.54)$$

With the stress derived as a function of the curvature, the unknown height of the compression zone, x , can be found by the equilibrium equation for axial force:

$$\sum N = x \cdot \frac{1}{2} \cdot b \cdot \sigma_c + A_{s2} \cdot \sigma_{s2} - A_{s1} \cdot \sigma_{s1} - (h - x) \cdot b \cdot 0.37 \cdot f_{R1} = 0 \quad (4.55)$$

When the height of the compression zone is found, the stress in the tension reinforcement closest to the tensioned concrete surface, σ_s , is found by Eq. (4.53). Furthermore, the moment at the given curvature can be verified by:

$$M = x \cdot \frac{1}{2} \cdot b \cdot \sigma_c \cdot x \cdot \frac{2}{3} + A_{s2} \cdot \sigma_{s2} \cdot (x - d_2) + A_{s1} \cdot \sigma_{s1} \cdot (d_1 - x) + \frac{(h - x)^2}{2} \cdot b \cdot 0.37 \cdot f_{R1} \quad (4.56)$$

4.5 Minimum Reinforcement

According to the guidelines provided by EC2 and NB38, it recommends that all structures have a minimum amount of conventional reinforcement. The minimum reinforcement for slabs applies for both the x- and y-axis. The new EC2 gives several reasons for the requirement to be provided:

- ensure distributed cracking and to handle forces from restrained deformations which were not considered explicitly in the design.
- ensure sufficient deformation capacity to contribute to structural robustness by allowing alternative load paths.
- avoid failure due to unpredicted cracking.
- ensure constructability.

In structures reinforced with steel fibres exposed to bending, with or without axial force, minimum reinforced should be provided, such that:

$$M_{R,min}(N_{Ed,min}) \geq M_{cr}(N_{Ed,min}) \quad (4.57)$$

Where:

$M_{R,min}$ is the bending strength of the section with $A_{s,min}$.

M_{cr} is the cracking moment of the section.

The cracking moment may be calculated assuming a linear distribution of normal stresses over the cross-section, where the maximum tensile stress is given as the concrete tensile strength f_{ctm} . The influence of the reinforcement may be neglected when calculating the cracking moment M_{cr} :

$$M_{cr} = \frac{1}{6} \cdot bh^2 \cdot f_{ctm} \quad (4.58)$$

Regarding the bending moment of the section, the effect of conventional reinforcement may be included. Furthermore, the effects of the fibres are included by the effective residual tensile strength $f_{Ftu,eff}$:

$$M_{R,min} = f_{yk} \cdot A_{s,min} \cdot z + 0.4f_{Ftu,eff} \cdot b \cdot h^2 \quad (4.59)$$

To please Eq. (4.57), minimum reinforcement is derived from Eq. (4.59) and rewritten as:

$$A_{s,min} = \frac{M_{cr} - 0.4f_{Ftu,eff} \cdot b \cdot h^2}{f_{yk} \cdot z} \quad (4.60)$$

However, minimum reinforcement is determined from the highest value according to the general Eq. (4.60) and the Eq. (4.61) from EC2 or Eq. (4.62) from NB38.

4.5.1 Minimum Reinforcement for SFRC According to EC2

The required minimum reinforcement of the cross section under consideration may be determined for pure bending as followed:

$$A_{s,min} = \frac{0.2 \cdot k_h \cdot f_{ct,eff} \cdot A_c}{f_{yk}} \quad (4.61)$$

Where:

k_h is a coefficient which allows for the effect of non-uniform self-equilibrating stresses, which leads to a reduction of the apparent tensile strength:

$$k_h = 0.8 - 0.6(\min\{b; h\} - 0.3) \quad 0.5 \leq k_h \leq 0.8$$

A_c is the full area of the part of the section under consideration.

f_{yk} is the characteristic value of yield strength of reinforcement.

4.5.2 Minimum Reinforcement for SFRC According to NB38

For cross sections, subjected to bending, the main reinforcement and continuous reinforcement shall correspond to:

$$A_{s,min} = \max \begin{cases} 0.26 \cdot \frac{(f_{ctm} - 2.15 \cdot f_{Ftu,eff})}{f_{yk}} \cdot b_t \cdot d \\ 0.13 \cdot \frac{f_{ctm}}{f_{yk}} \cdot b_t \cdot d \end{cases} \quad (4.62)$$

Given that:

$$\frac{f_{ctm}}{f_{yk}} \geq 0.005 \quad (4.63)$$

4.5.3 Lightly Reinforced SFRC Structures

For SFRC members without longitudinal bars, and structural hardening behaviour under bending with or without axial compression, the mean crack spacing can be determined as defined in Eq. (4.43b).

5 Laboratory Results

This chapter presents the results obtained from all the laboratory testing, such as the three-point bending test, plate bending test and inductive test. Also, the compression test which was tested by SINTEF. The results are mainly presented in tables, plots and bar plots.

5.1 Compression Test

The results obtained from the compression test are shown in Table 5.1 wherein the indicated value signifies the average compressive strength of the concrete after 91 days. The results for batch 5 were considered invalid due to the poor casting of the specimens. Therefore, similar properties obtained for batch 1 were employed for calculation regarding batch 5.

Table 5.1: Compressive strength at 91 days

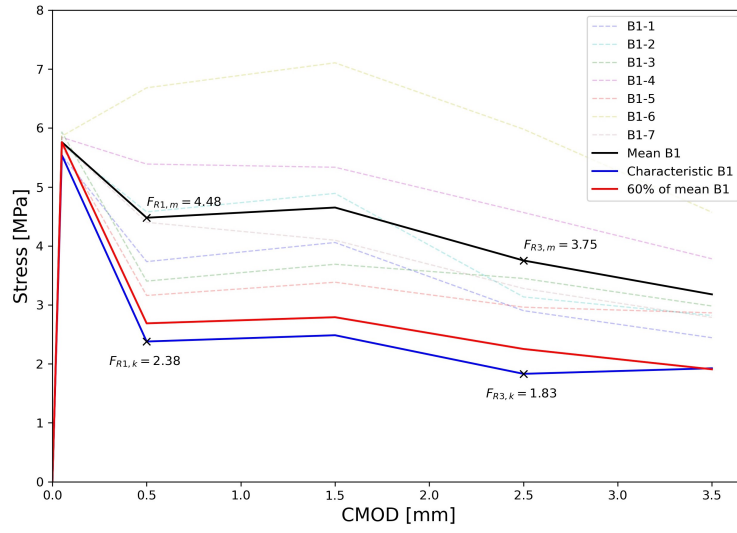
Concrete mixture	f_{cm} [MPa]	CV [%]
Batch 1	68.35	1.61
Batch 2	72.50	0.13
Batch 3	67.76	1.04
Batch 5	-	-

With respect to the low fibre amount, a comparison of compression strength between SFRC and BFRC should not give any significant difference according to the literature presented in chapter 2.3.1, even for a similar concrete mixture. As may be seen in Table 5.1, the different batches did not lead to any significant difference in the compressive strength. However, note that Batch 2 exhibits the highest compressive strength, despite the unstable concrete.

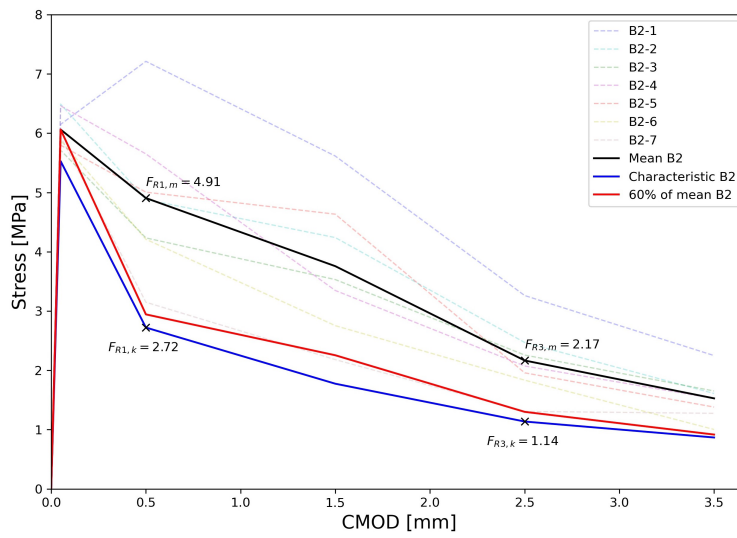
Furthermore, the actual compressive strength for the B45 concrete was found to be significantly higher than the assumed f_{cm} value of 53 MPa after 28 days. This was expected, as the low carbon concrete has an increasing strength between 28 and 91 days. To elaborate, plots for each batch are presented in appendix B.2.

5.2 Three-Point Bending Test

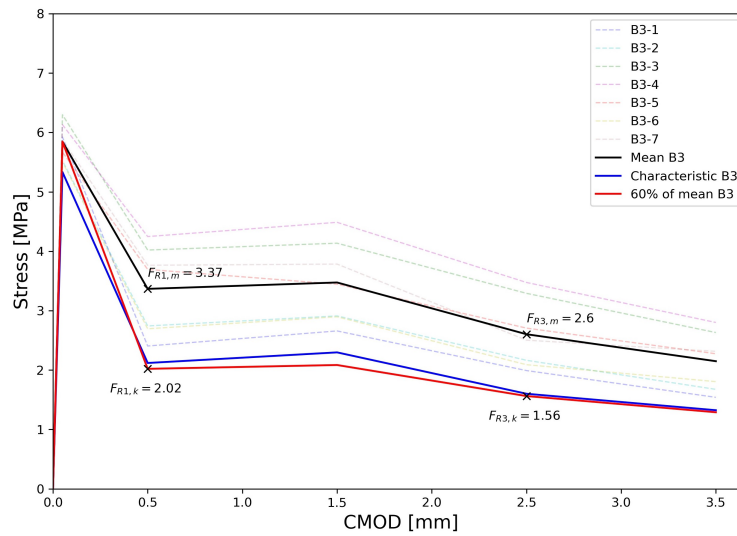
Within the three-point bending test according to chapter 3.2, seven beam specimens were examined for each of the batches. However, one beam from batch 5D was considered invalid due to incomplete test execution. In addition, another beam from batch 5S was not tested due to poor casting. Plots of the residual flexural tensile strength, calculated from formulas in chapter 4.2, are presented in Figure 5.1. To summarise, the mean and the characteristic value for f_{R1} and f_{R3} are given in Table 5.2. Additionally, a bar plot of the mean residual flexural tensile strength is shown in Figure 5.2.



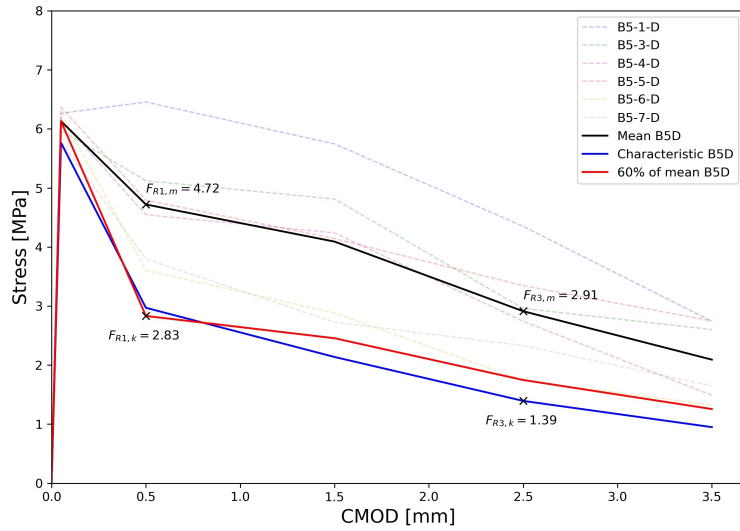
(a) Batch 1



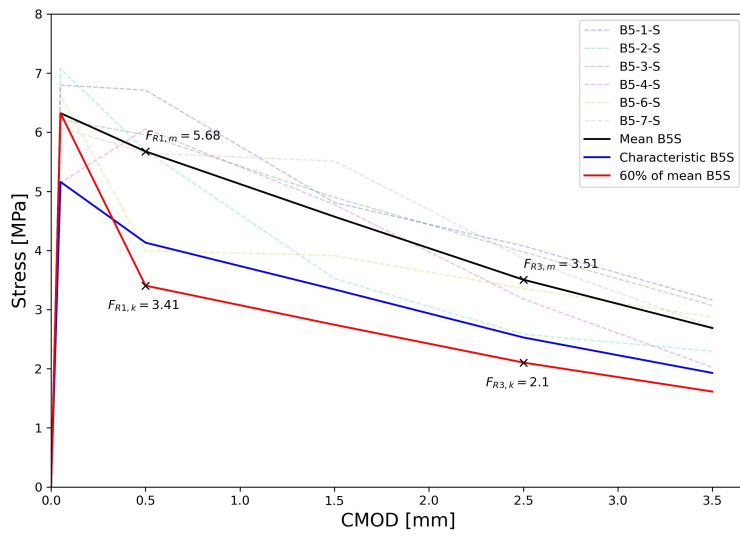
(b) Batch 2



(c) Batch 3



(d) Batch 5D



(e) Batch 5S

Figure 5.1: Residual flexural tensile strengt from 3PBT

Table 5.2: Residual flexural tensile strength [MPa]

Batch	f_{R1}			f_{R3}		
	Mean	Char	CV [%]	Mean	Char	CV [%]
Batch 1	4.48	2.38	28	3.75	1.83	30
Batch 2	4.91	2.72	26	2.17	1.14	28
Batch 3	3.37	2.02	22	2.60	1.56	23
Batch 5D	4.72	2.83	22	2.91	1.39	31
Batch 5S	5.68	3.41	16	3.51	2.10	16

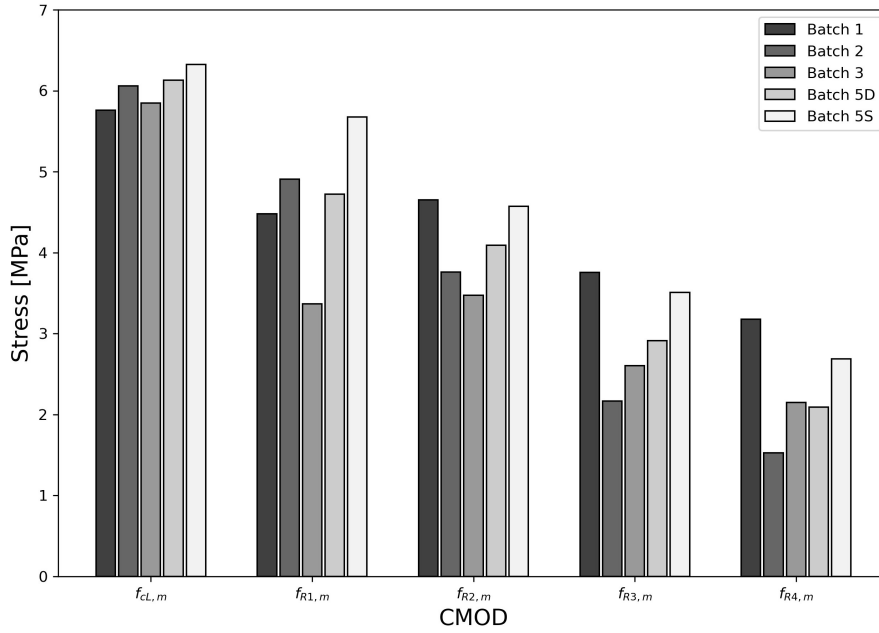


Figure 5.2: Comparison of the mean residual flexural tensile strength

Based on the results obtained from Table 5.2, there are certain variations regarding the concrete mixtures. Batch 5S exhibits the highest residual strength for $CMOD=0.5\text{ mm}$. This may be attributed to the distinctive casting method related to this batch, NS14651, which sets it apart from the other batches. In contrast, batch 3 exhibits the lowest residual strength. Therefore, compared to basalt fibres, steel fibres gives in general significantly higher residual strength for $CMOD=0.5\text{ mm}$. However, note that for $CMOD=2.5\text{ mm}$ batch 2 turned out to have the lowest residual strength, despite a high value for $CMOD=0.5\text{ mm}$. Figure 5.1 and Table 5.2 shows a large scatter within each batch, as assumed for small specimens. However, batch 5D differs from the other batches with a significantly lower coefficient of variation.

5.3 Plate Bending Test

The plate bending test was carried out as described in chapter 3.3. From this test, the obtained results are presented in load-displacement curves for all the tested elements. In addition, registration of the first crack and photos of the final crack pattern is presented.

5.3.1 Load-Displacement

During the testing of the elements some irregularities in both the elements and the test rig were detected. When the elements were installed in the rig, some gaps were noticeably large between the supports and the element. Hence, resulting in a spurious deflection in the early stage of the test. The load-displacement curve is expected to behave linearly before cracking, as shown in chapter 2.3, and therefore the plots are adjusted for this. This was done by extending the linear part of the curve and adjusting for the spurious deflection, as shown in Figure 5.3.

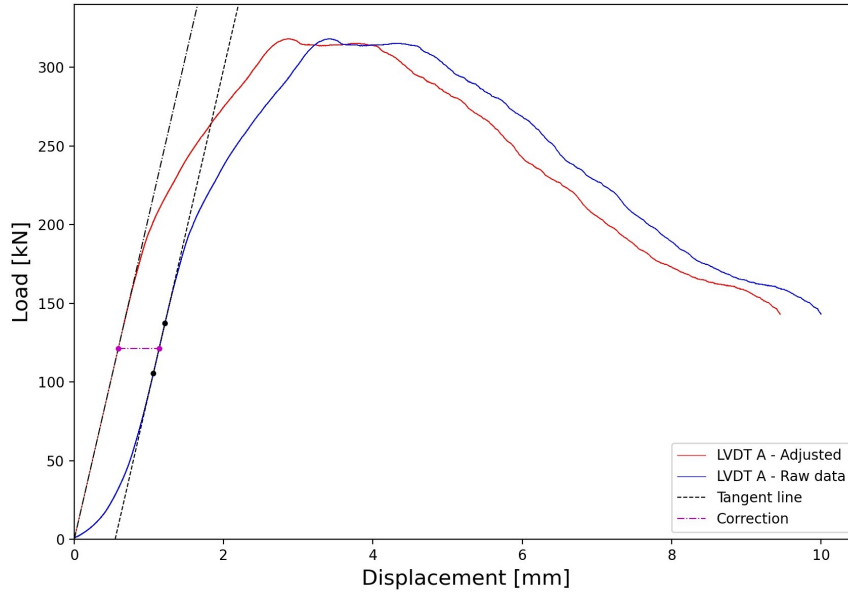


Figure 5.3: Illustration of adjusted curve for LVDT A in first plate (ID-1)

Regarding all the following plots, the curves show the relation between load and measured displacement. All the curves represent measurements from the LVDTs at different positions, as described in Figure 3.8 in chapter 3.3. To summarize, LVDT A-E is placed centric at the bottom side and LVDT F-G at the corners on the top side. This applies to all plots, except those for the large slabs. For the large slabs, LVDT A-E is stated similarly, while the LVDTs at the corners are replaced with LVDT H-I. In addition, LVDT F-G is placed on the bottom side closer to the support and LVDT M-J is placed centric on the top side. Additionally, the ultimate load P_{ULS} is represented at the peak load.

The results obtained for the small slabs with only fibre reinforcement are shown in Figure 5.4.

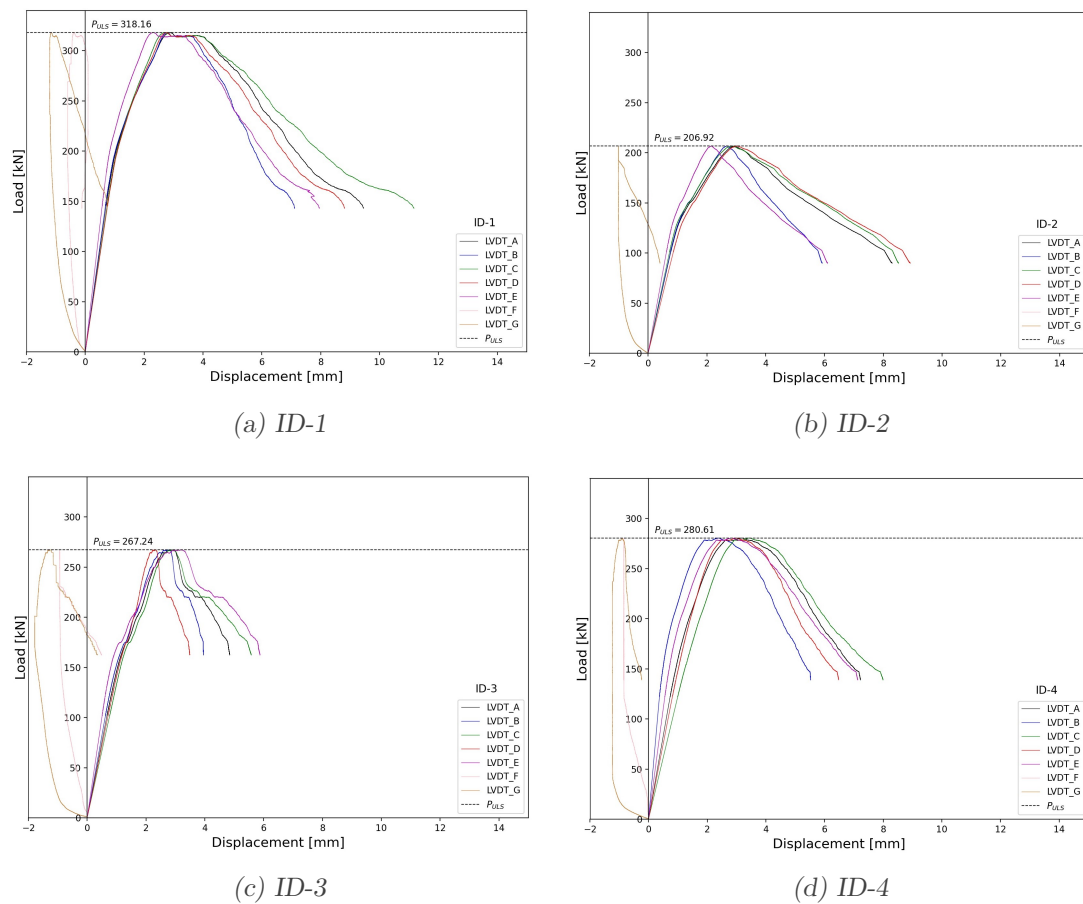


Figure 5.4: Load-displacement curve for small slabs with fibre reinforcement

Based on the results for elements 1-4 it is clear that element 1 exhibits the highest ultimate load. Additionally, it was expected that element 4 would maintain similar results given that these two were identical. However, element 1 exhibits a 13 % higher load compared to element 4. Furthermore, the plot of element 2, with only basalt fibres, exhibits a 23-35 % lower ultimate load compared to the three other slabs. Also, note that element 3, despite an unstable concrete mixture, exhibits nearly similar results as elements 1 and 4.

The results obtained for the small walls with only fibre reinforcement are shown in Figure 5.5.

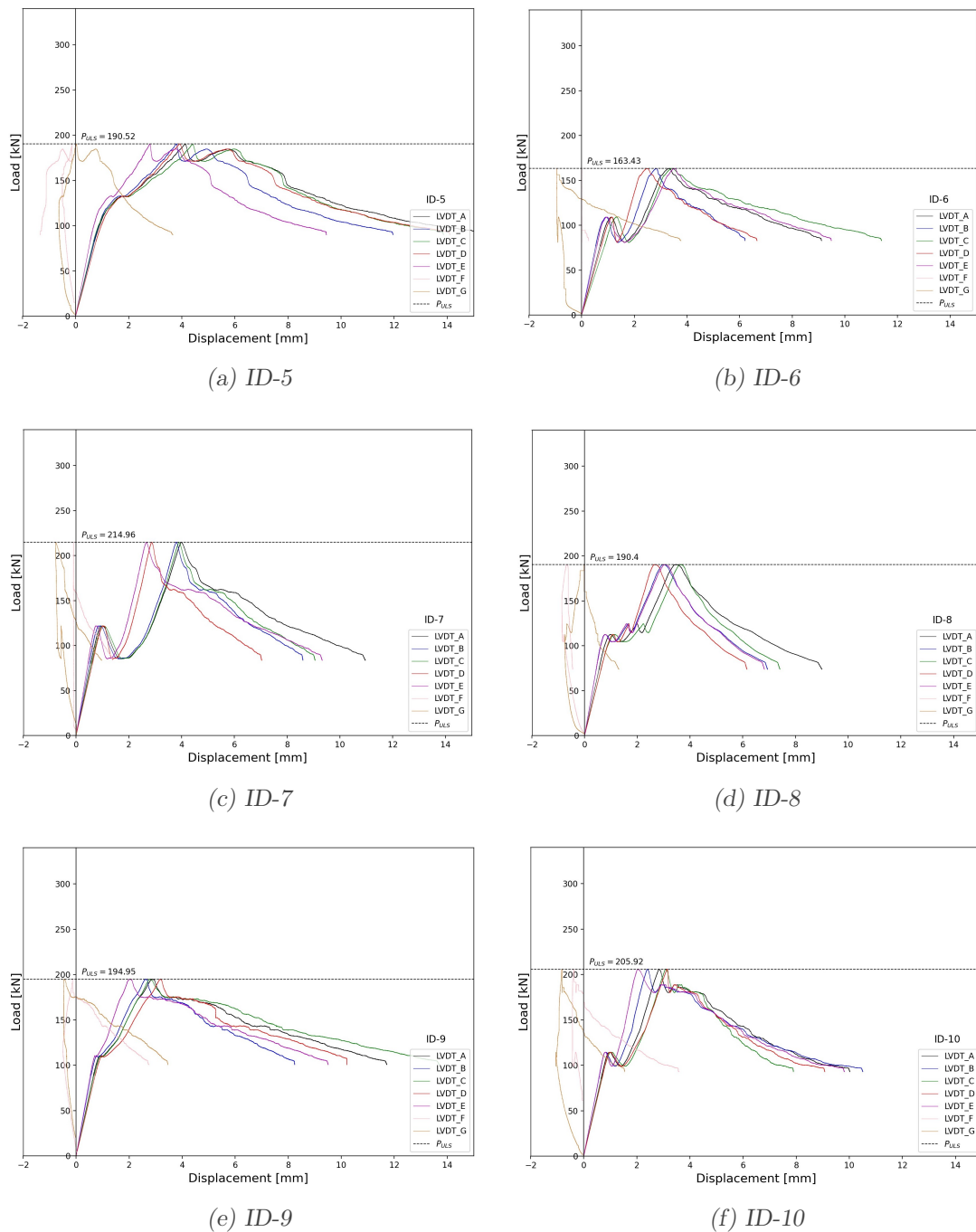


Figure 5.5: Load-displacement curve for small walls with fibre reinforcement

As presented above, the results from elements 5-10 contain a distinct curve behaviour that separates them from the small slabs. For instance, a relatively large load drop can be seen before reaching the ultimate load. The walls with the highest ultimate load are elements 7 and 10, which implement a vibrating concrete mixture. In contrast, element 6 with an unstable concrete mixture, exhibits 24 % lower ultimate load compared to element 7. Furthermore, for these small walls with only fibre reinforcement, there is no crucial difference between steel- and basalt fibres.

The results obtained for the small slabs with fibre- and conventional reinforcement are shown in Figure 5.6.

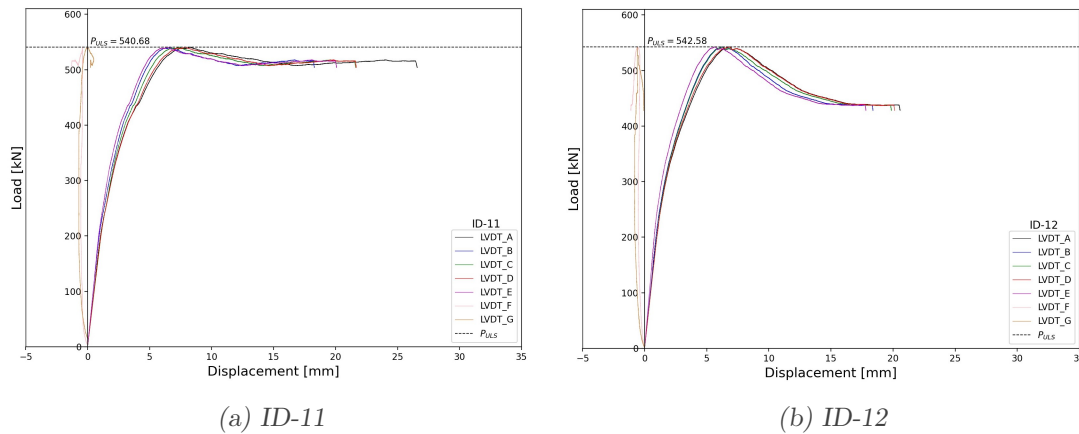


Figure 5.6: Load-displacement curve for small slabs with fibre- and conventional reinforcement

Considering elements 11 and 12, the elements exhibit approx. similar ultimate load. Also, the curve shows strain-softening and considerably more ductile behaviour. Specifically, element 11 exhibits a minimal decrease in load after yielding. In comparison, element 12 exhibits a larger decrease in load after yielding, before stabilizing in a ductile behaviour. It should be noted that the only difference between these two elements is the stability of the concrete.

The results obtained for the small walls with fibre- and conventional reinforcement are shown in Figure 5.7.

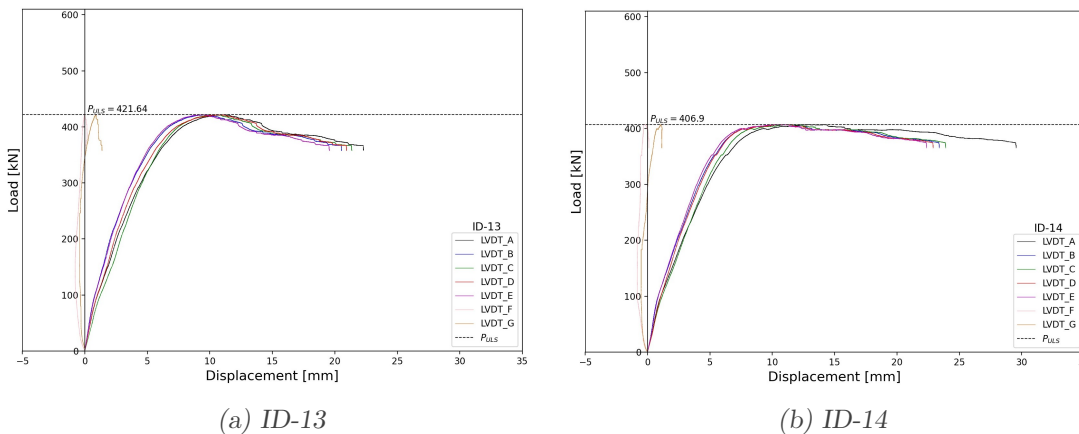


Figure 5.7: Load-displacement curve for small walls with fibre- and conventional reinforcement

Based on the results for elements 13 and 14, there is no significant difference between the stable and unstable concrete mixture. The ultimate load is only separated by 4 %. Both before and after yielding the curve behave similarly. After yielding, both curves show plastic deformation with high ductility.

The results obtained for the large slabs with fibre- and conventional reinforcement are shown in Figure 5.8.

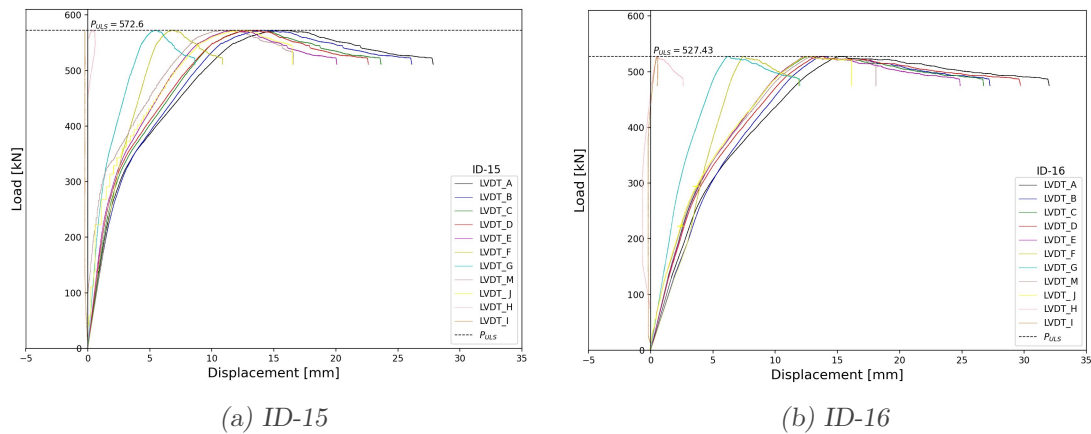


Figure 5.8: Load-displacement curve for large slabs with fibre- and conventional reinforcement

Regarding the large slabs, elements 15 and 16, the only difference was supposed to be the casting procedure for the two elements. However, element 16 was 20-30 mm thinner, hence, they are not directly comparable. As shown in the load-displacement curve, both elements show a low reduction in load as the deformation increases. This indicates a strain-softening behaviour with plastic deformation after reaching the ultimate load. Despite the 17 % variation in thickness, there is only a slight difference of 8 % in the ultimate load. Furthermore, the curves show a clear transition from linear-elastic behaviour to non-linear behaviour when the elements reach the proportionality limit. To summarise, the ultimate load for elements 1-16 is presented in Table 5.3.

Table 5.3: Ultimate load

Experiment		Experiment	
ID	P_{ULS} [kN]	ID	P_{ULS} [kN]
1	318.16	9	194.95
2	206.92	10	205.92
3	267.24	11	540.68
4	280.61	12	542.58
5	190.52	13	421.64
6	163.43	14	406.90
7	214.96	15	572.60
8	190.40	16	527.44

5.3.2 Crack Pattern

All elements were analysed regarding the development of the first crack in relation to the load, as shown in Table 5.4. The results were obtained from the photos taken during the test. However, without the camera covering the entire element, it is not possible to conclude with certainty that it is the first crack. Despite this, the load corresponding to the first crack complies well with the plots when the limit of proportionality is reached.

Table 5.4: Crack registration

ID	First crack		Ultimate failure
	Load [kN]	UTIL [%]	[kN]
1	206	65 %	318.16
2	131	63 %	206.92
3	120	45 %	267.24
4	170	61 %	280.61
5	121	64 %	190.52
6	107	65 %	163.43
7	119	55 %	214.96
8	110	58 %	190.40
9	108	55 %	194.95
10	111	54 %	205.92
11	200	37 %	540.68
12	187	35 %	542.58
13	100	24 %	421.64
14	88	22 %	406.90
15	300	52 %	572.60
16	273	52 %	527.44

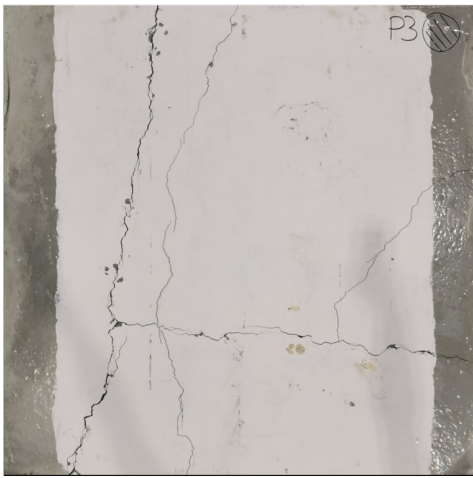
With the previously described test setup, the failure mechanism was assumed as shown in Figure 4.5 from the yield line analysis. However, due to no additional conventional reinforcement in elements 1-10, the assumed crack pattern was not expected to be fully developed. The final crack pattern from the elements with only fibre reinforcement is shown in Figure 5.9 and 5.10. Further, the elements with both fibre- and conventional reinforcement are shown in Figure 5.11, 5.12 and 5.14.



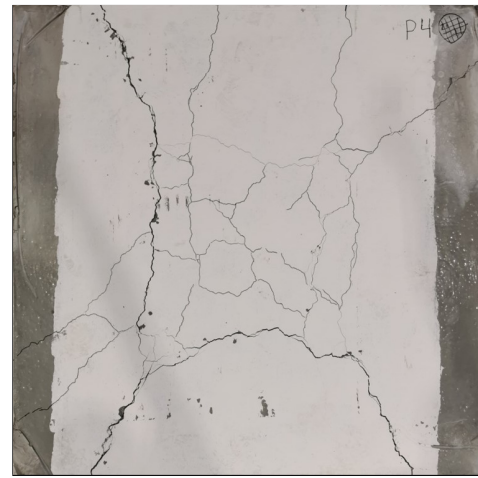
(a) ID-1



(b) ID-2



(c) ID-3



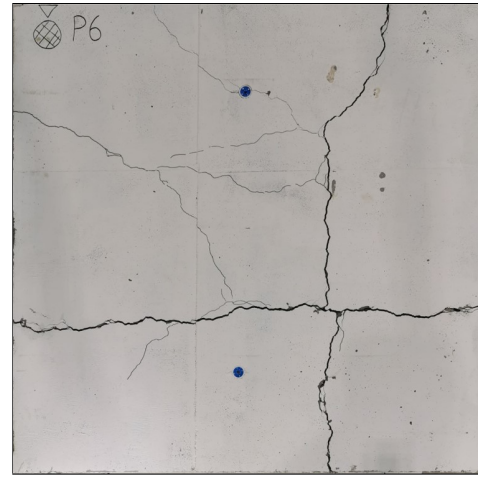
(d) ID-4

Figure 5.9: Crack pattern for the small slabs with fibre reinforcement

The crack pattern observed in the small slabs indicates a relatively well-developed failure pattern. Clearly, it shows some similarity to the assumed pattern, especially element 4 in Figure 5.9d.



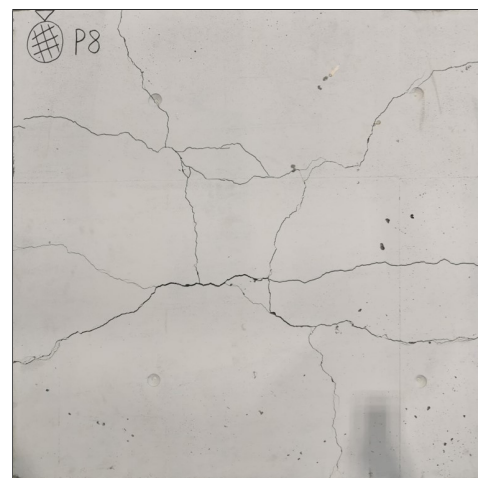
(a) ID-5



(b) ID-6



(c) ID-7



(d) ID-8



(e) ID-9



(f) ID-10

Figure 5.10: Crack pattern for the small walls with fibre reinforcement

The small walls show some similarities to the assumed crack pattern and are also relatively well developed. Note that the crack in Figure 5.10e and 5.10f follows the formwork joint and creates nearly straight cracks.



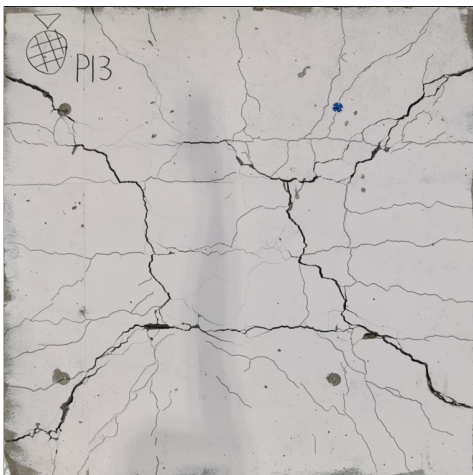
(a) ID-11



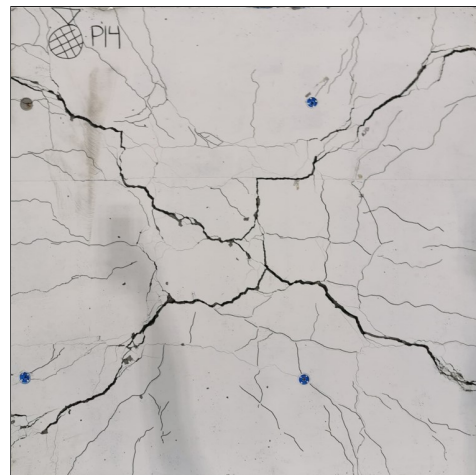
(b) ID-12

Figure 5.11: Crack pattern for the small slabs with fibre- and conventional reinforcement

The small slabs with additional conventional reinforcement shows a clear failure mechanism with multiple secondary cracks. Figure 5.11b is almost identical to the assumed pattern, where the four point loads cause a square of yield lines in the middle. However, the inner square is slightly smaller than the assumed pattern. Regarding Figure 5.11a, the square is not as well developed where the pattern resembles a single point load in the centre of the element.



(a) ID-13



(b) ID-14

Figure 5.12: Crack pattern for the small walls with fibre- and conventional reinforcement

The crack pattern from the small walls with conventional reinforcement in two layers shows a similar tendency to the previous ones. Figure 5.12a has a relatively well developed pattern in the inner square, while the cracks in Figure 5.12b connect in the centre. Also, these elements show more systematic and parallel secondary cracks. Unlike all the other elements, elements 13 and 14 were the only element that exhibits cracks at the top surface from the loading points towards each respective corner, see Figure 5.13. However, these crack on the top surface was not present until the test was way past the ultimate load.

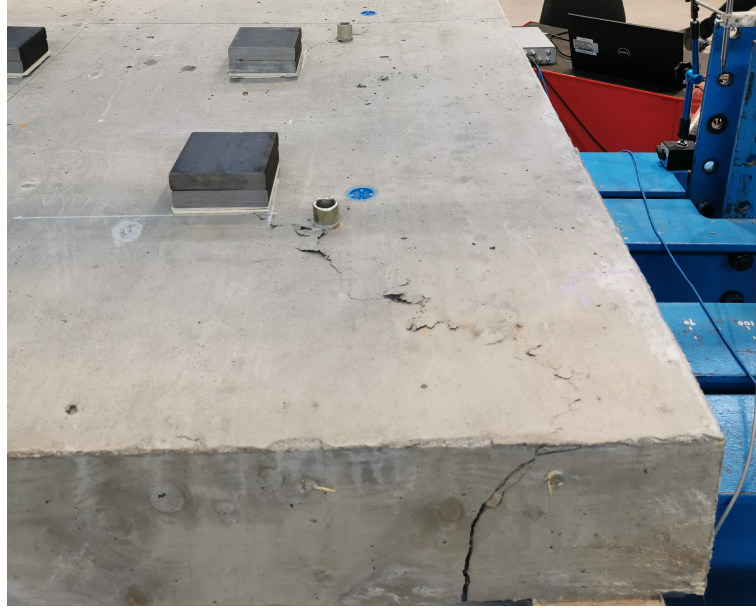
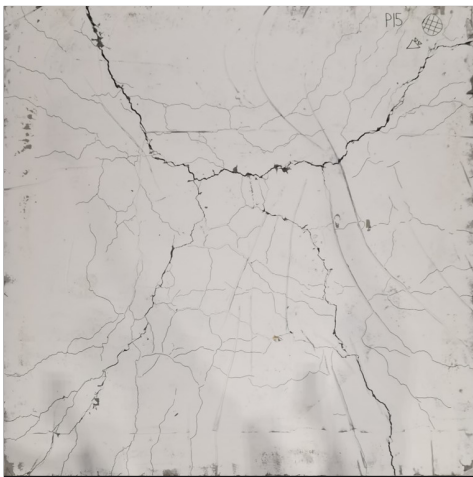
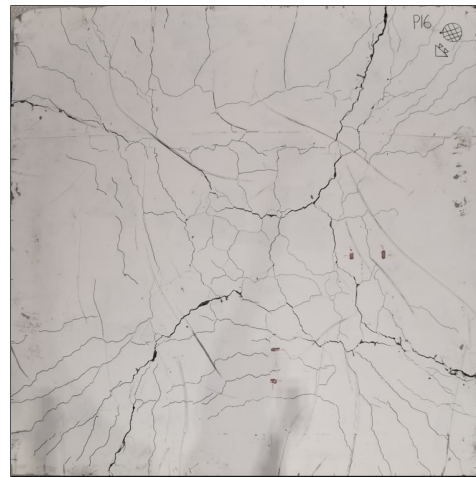


Figure 5.13: Crack at the top surface on element 13.



(a) ID-15



(b) ID-16

Figure 5.14: Crack pattern for the large walls with fibre- and conventional reinforcement

As Figure 5.14 shows, the large slabs with additional conventional reinforcement exhibit more secondary cracks where the failure mechanism is not as clear compared to the smaller element. However, the largest cracks form a pattern that may resemble the assumed failure mechanism.

5.4 Inductive Test

To study the fibre content and orientation, samples from the beams and plates were tested. The result from the inductive test of the standard beams is presented in Table 5.5. From this, a large scatter in fibre content (c_f) can be observed with a range from 24 to 58 kg/m^3 . Regarding the orientation approx. 40-50 % of the fibres are orientated along the length axis of the beams. Due to the wall effect, it was expected a high fibre orientation in the length axis. Also, note that the y-axis, which is the vertical axis, has the lowest contribution for each cube, except for B5-1D(2).

Table 5.5: Fibre content and orientation in cubes

Cube	C_f [kg/m ³]	C_x [%]	C_y [%]	C_z [%]
B1-1(1)	34.12	45.1	24.2	30.7
B1-1(2)	37.71	41.5	25.0	33.5
B1-6(1)	40.71	47.9	17.4	34.7
B1-6(2)	34.12	46.4	18.4	35.1
B2-1(1)	29.32	48.5	23.0	28.4
B2-1(2)	28.42	51.0	18.5	30.5
B2-7(1)	31.72	51.8	20.0	28.2
B2-7(2)	23.92	50.5	21.0	28.5
B5-1D(1)	34.72	51.6	21.0	27.5
B5-1D(2)	32.62	45.9	28.5	25.6
B5-6D(1)	33.22	44.4	22.5	33.0
B5-6D(2)	32.32	55.1	18.7	26.3
B5-1S(1)	54.20	50.7	20.6	28.7
B5-1S(2)	47.61	44.0	19.9	36.1
B5-2S(1)	45.81	40.5	22.8	36.7
B5-2S(2)	57.80	41.2	20.6	38.2

Regarding the core samples from the plates, only element 1, 5, 9, 13 and 14 has been tested, with four to six cylinders from each element. Figure 5.15 shows the fibre content from each sample and the corresponding location from where it was sampled. Likewise, also the cylinders have a large scatter in fibre content.

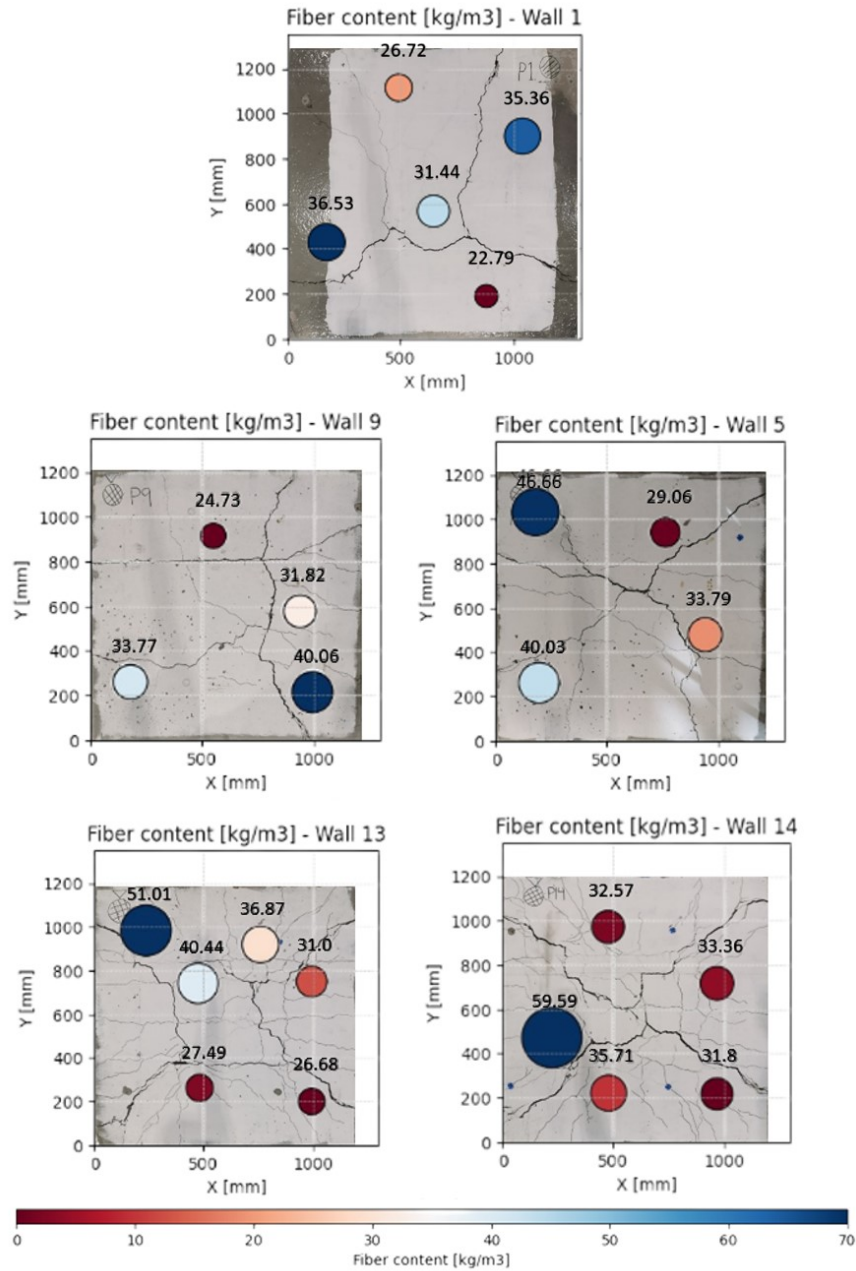


Figure 5.15: Fibre content in samples from elements

As previously stated, the isotropy factor for the cylindrical specimens can be calculated, and plots of the result are presented in Figure 5.16. Regarding the plots, a round shape illustrates an isotropic orientation. In contrast, the longer the major axis in the ellipse is, the more anisotropic it is, with the main orientation along the major axis. The isotropy factor for each sample is presented in Table 5.6.

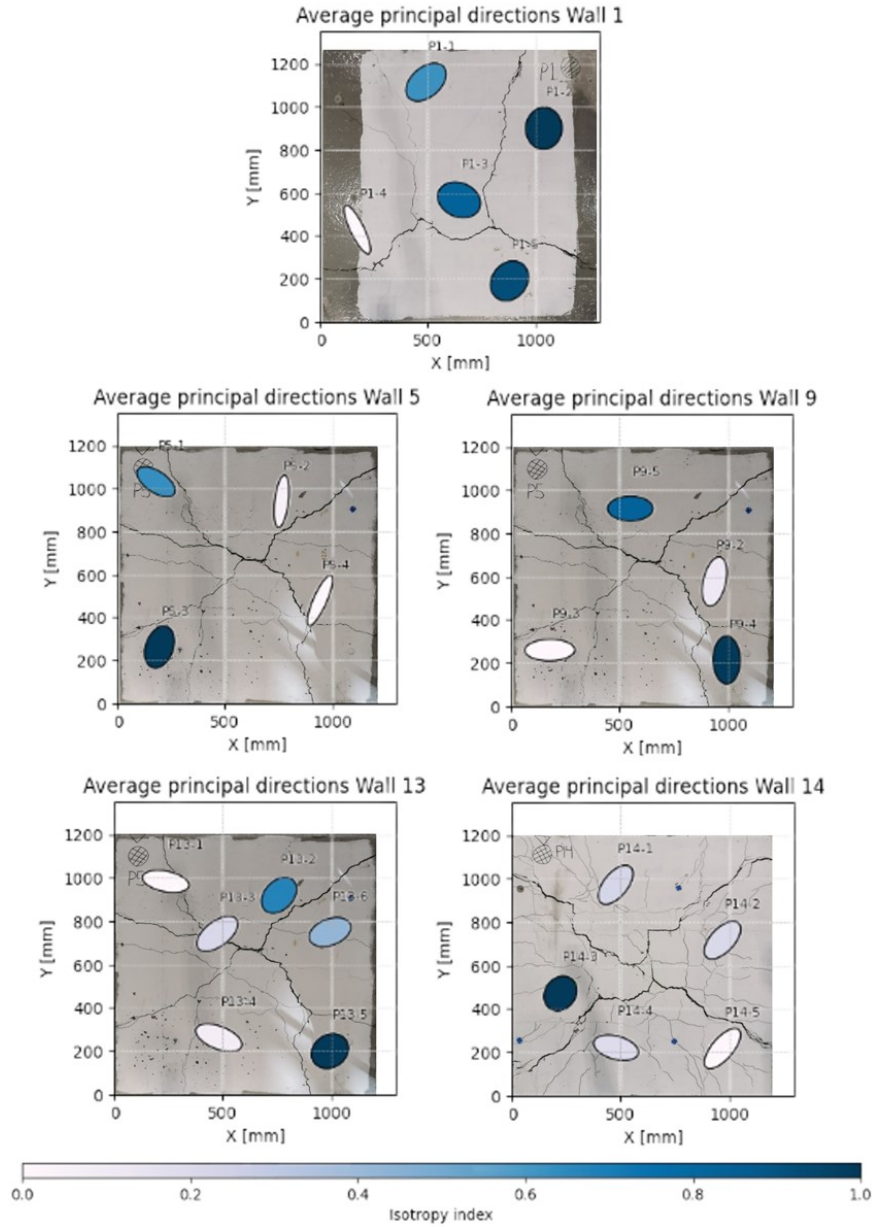


Figure 5.16: Isotropy factor in samples from elements

Table 5.6: Isotropy factor in the core samples

Cylinder	Isotropy factor				
	P1	P5	P9	P13	P14
1	0.636	0.493	-	0.436	0.519
2	0.870	0.265	0.449	0.701	0.512
3	0.765	0.639	0.433	0.520	0.834
4	0.259	0.247	0.568	0.467	0.508
5	0.822	-	0.544	0.833	0.429
6	-	-	-	0.604	-

6 Calculation Results

Based on the results from the laboratory tests, a comparison with calculated results, according to the guidelines in the EC2 and NB38, is conducted. There are performed calculations in both the ultimate limit state and serviceability limit state.

6.1 Ultimate Load

The ultimate load is calculated with two different methods, using yield line analysis and strip method as described in chapter 4.3. To determine the moment capacity, an approach from both EC2 and NB38 is used with mean and characteristic strength. Due to the low amount of reinforcement, the strain in the most tensioned fibre was the limited factor. Hence, the parameters k_1 and k_2 were included as the concrete capacity was not fully utilized. The calculations of the ultimate loads can be found in appendix E with the related moment in appendix D.

The first case presented in Table 6.1 is calculated using mean residual tensile strength according to EC2. Since the calculation use mean strength, the geometric factor κ_G is not included, while the orientation factor κ_0 is included. The orientation factor is equal to 1.0 for the slabs and 0.5 for the walls. This applies to all the following cases.

Table 6.1: Ultimate load using mean value according to EC2

ID	M_{Rd}	Yield line		Strip method		Experiment
	[kNm]	P_{ULS} [kN]	UTIL [%]	P_{ULS} [kN]	UTIL [%]	P_{ULS} [kN]
1	13.48	254.97	80	196.13	62	318.16
2	9.40	177.79	86	136.76	66	206.92
3	7.87	148.89	56	114.53	43	267.24
4	13.48	254.97	91	196.13	70	280.61
5	6.81	100.97	53	83.82	44	190.52
6	3.97	58.56	36	48.80	30	163.43
7D	5.30	78.29	36	65.24	30	214.96
7S	6.38	94.24	44	78.53	37	214.96
8	4.74	70.02	37	58.35	31	190.40
9	6.81	100.59	52	83.82	43	194.95
10D	5.30	78.29	38	65.24	32	205.92
10S	6.38	94.24	46	78.53	38	205.92
11	31.60	597.55	111	459.65	85	540.68
12	26.15	494.55	91	380.43	70	542.58
13	27.10	400.19	95	333.49	79	421.64
14	24.35	359.60	88	299.66	74	406.90
15	42.13	749.05	131	374.52	65	572.60
16	31.60	561.80	107	280.90	53	527.44

Case two presented in Table 6.2 is calculated according to EC2 with characteristic strength. Clearly, the calculated capacity decreases. However, when using the characteristic residual tensile strength, κ_G is included which will restrict the decrease depending on the size of the failure mechanism. For the given failure mechanism κ_G varies between 1.24 and 1.5, depending on the element size and height of the compression zone.

Table 6.2: Ultimate load using characteristic value according to EC2

ID	M_{Rd} [kNm]	Yield line		Strip method		Experiment
		P_{ULS} [kN]	UTIL [%]	P_{ULS} [kN]	UTIL [%]	P_{ULS} [kN]
1	8.27	156.41	49	120.31	38	318.16
2	7.07	133.77	65	102.90	50	206.92
3	5.20	98.32	37	75.63	28	267.24
4	8.27	156.41	56	120.31	43	280.61
5	4.16	61.43	32	51.19	27	190.52
6	2.61	38.50	24	32.08	20	163.43
7D	3.17	46.84	22	39.03	18	214.96
7S	4.76	70.35	33	58.62	27	214.96
8	3.55	52.48	28	43.74	23	190.40
9	4.16	61.43	32	51.19	26	194.95
10D	3.17	46.84	23	39.03	19	205.92
10S	4.76	70.35	34	58.62	28	205.92
11	26.29	497.20	92	382.46	71	540.68
12	23.35	441.59	81	339.68	63	542.58
13	24.33	359.33	85	299.44	71	421.64
14	22.86	337.62	83	281.35	69	406.90
15	36.78	653.78	114	326.89	57	572.60
16	27.41	487.28	92	243.64	46	527.44

Case three presented in Table 6.3 is calculated according to NB38 with mean strength. The only parameter separating this calculation method from the EC2 is the scaling factor when transforming $f_{R,3k}$ to f_{Ftuk} . With a higher factor for calculations according to NB38, a higher capacity is achieved for calculation with mean strength.

Table 6.3: Ultimate load using mean value according to NB38

ID	M_{Rd} [kNm]	Yield line		Strip method		Experiment P_{ULS} [kN]
		P_{ULS} [kN]	UTIL [%]	P_{ULS} [kN]	UTIL [%]	
1	15.09	285.25	90	219.42	69	318.16
2	10.53	199.02	96	153.10	74	206.92
3	8.82	166.73	62	128.25	48	267.24
4	15.09	285.25	102	219.42	78	280.61
5	7.63	112.62	59	93.85	49	190.52
6	4.44	65.59	40	54.66	33	163.43
7D	5.94	87.66	41	73.05	34	214.96
7S	7.14	105.51	49	87.92	41	214.96
8	5.31	78.42	41	65.35	34	190.4
9	7.63	112.62	58	93.85	48	194.95
10D	5.94	87.66	43	73.05	35	205.92
10S	7.14	105.51	51	87.92	43	205.92
11	33.16	627.10	116	482.38	89	540.68
12	27.07	511.91	94	393.78	73	542.58
13	27.88	411.78	98	343.15	81	421.64
14	24.80	366.32	90	305.27	75	406.9
15	44.28	787.18	137	393.59	69	572.6
16	33.16	589.58	112	294.79	56	527.44

Finally, in case four presented in Table 6.4, the calculations are performed with characteristic strength according to NB38. Similarly to case three, the transformation from $f_{R,3k}$ to f_{Ftuk} is higher. However, when calculating according to NB38, the κ_G is not considered. Hence, the characteristic capacity is lower considering that $\kappa_G > 1.12$ for case two.

Table 6.4: Ultimate load using characteristic value according to NB38

ID	M_{Rd} [kNm]	Yield line		Strip method		Experiment
		P_{ULS} [kN]	UTIL [%]	P_{ULS} [kN]	UTIL [%]	P_{ULS} [kN]
1	7.40	139.94	44	107.65	34	318.16
2	6.32	119.58	58	91.99	44	206.92
3	4.64	87.78	33	67.52	25	267.24
4	7.40	139.94	50	107.65	38	280.61
5	3.73	55.16	29	45.96	24	190.52
6	2.34	34.51	21	28.76	18	163.43
7D	2.84	42.01	20	35.01	16	214.96
7S	4.28	63.20	29	52.66	24	214.96
8	3.19	47.09	25	39.24	21	190.4
9	3.73	55.16	28	45.96	24	194.95
10D	2.84	42.01	20	35.01	17	205.92
10S	4.28	63.20	31	52.66	26	205.92
11	25.50	482.16	89	370.89	69	540.68
12	22.85	432.04	80	332.34	61	542.58
13	23.95	353.74	84	294.78	70	421.64
14	22.63	334.17	82	278.47	68	406.9
15	33.28	591.70	103	295.85	52	572.6
16	25.50	453.31	86	226.65	43	527.44

6.2 Crack Width Calculation

The maximum calculated crack widths for element 11 at four different load applications are presented in Table 6.5. The selection of element 11 is because of the demand that the LVDTs should measure perpendicular to the crack. To illustrate, the load-elongation curve in Figure 6.1 indicates that element 11 obtain a valid result for the crack width. The results calculated from both EC2 and NB38 were compared to the actual crack width maintained in the experiment. Appendix F shows complete crack width calculations.

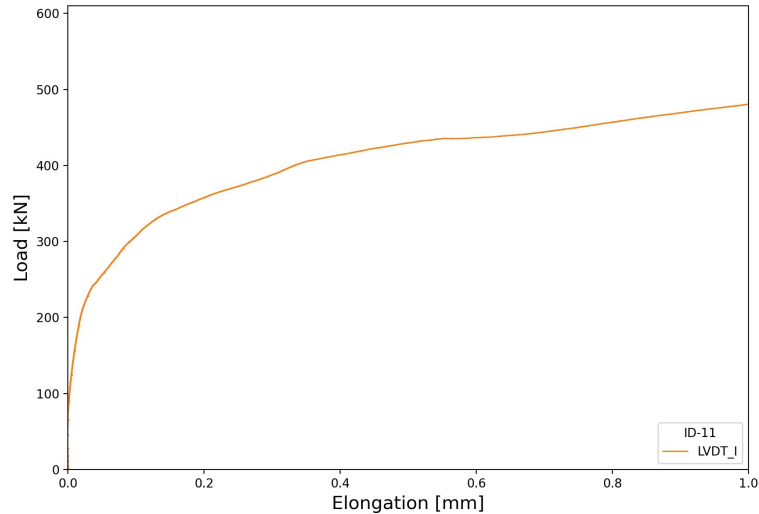


Figure 6.1: Load-elongation curve from LVDTs measuring crack-openings

Table 6.5: Calculated crack widths for element 11

Approx. load [kN]	w_k (EC2) [mm]	w_k (NB38) [mm]	w_k (Experiment) [mm]
250	0.048	0.025	0.045
300	0.087	0.053	0.091
350	0.128	0.088	0.179
400	0.169	0.121	0.333

Crack width calculation from the two first loads, based on EC2, showed nearly similar crack width obtained from the experiment. However, when the load increases further there will be a significant difference between the calculated and the experimental crack width. Furthermore, the results obtained from NB38 were considerably less than for EC2.

7 Discussion

All the results from calculations and testing will be discussed in this chapter. In short, a comparison of how the casting method, concrete mixture and reinforcement influence the behaviour and the strength properties of the elements. This also includes how fibre orientation and distribution are affected. Also, different uncertainty that has appeared throughout the study will be discussed. Further, the results obtained from calculation rules in EC2 and NB38 are compared to the experimental test result.

7.1 Experimental Series

The experimental series gave in general good and interesting results for all the conducted tests. There are some limitations to the results due to the limited number of tested elements. Hence, in some areas, further investigations are required in order to draw any conclusion.

7.1.1 Experimental Error

Within the experimental series, various sources of error were prominent, most of which have been previously presented. These sources of error may exert an influence on the test results.

Considering the compression test, it should be noted that no specimens for batch 5 were tested due to poor casting. However, the variation in compressive strength is small. Therefore, similar properties obtained for batch 1 were used in the calculation for batch 5.

For the three-point bending test, there were seven beam specimens that should be tested for each batch. However, one beam from batch 5D was considered invalid due to incomplete test execution. Additionally, one beam from batch 5S was not tested due to poor casting. As a result, these batches had six samples instead of seven. The effect will vary depending on the residual flexural tensile strength for the missing test sample. To elaborate, if the beam specimen would exhibit a significantly higher or lower value in comparison to the rest, this would exert an influence on the result, specifically for batch 5D and batch 5S.

The bending test for elements contains various sources of error. For several elements, it could be observed a gap between the element and the roller support, as shown in Figure 7.1. This could in the worst case lead to a behaviour where the element is working as a one-way slab rather than a two-way slab until the deflection is large enough for the element to be in contact with the entire surface of the roller support. With regard to this, it should be mentioned that the first crack often appeared before full contact was achieved.



Figure 7.1: Gap between element and roller support

Furthermore, as a consequence of the inaccurate placement of lifting anchors, the four point loads were moved closer to the centre than first planned. As a result, the calculated ultimate load will exhibit a lower value the closer to the centre these point loads are localized. Then, it could have an influence on the calculated walls in comparison to the slabs, which exhibits different distance. Also, the plywood, placed on the top surface to mitigate irregularities, may have a slight influence on the presented load-displacement curves. Moreover, the varying cross section thickness, especially in the slabs with an uneven top surface, and the distance between rebars may have a slight impact on the results.

These sources of error are important to acknowledge. Nonetheless, the experimental series is still successful and it is upon these results the conclusion is drawn.

7.1.2 Comparison of Residual Tensile Strength

The comparison between the residual flexural tensile strength, obtained from the three-point bending test, variate regarding the concrete mixture. Figure 7.2 summarise the mean residual flexural tensile strength for the different concrete mixtures.

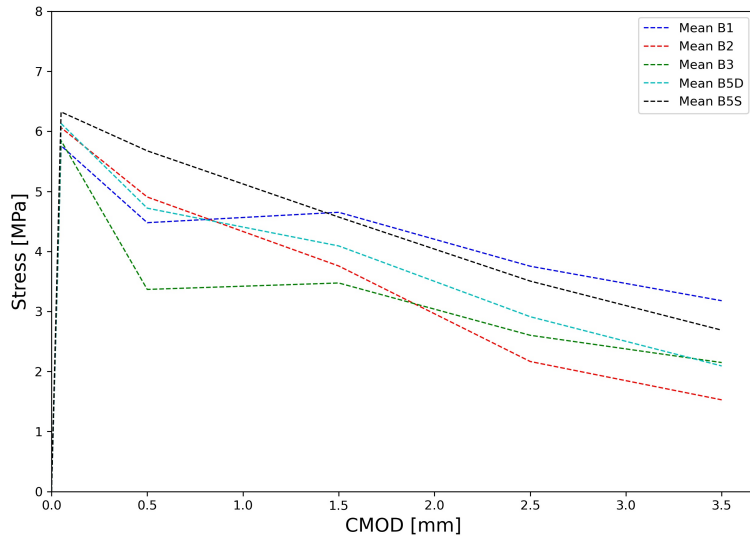


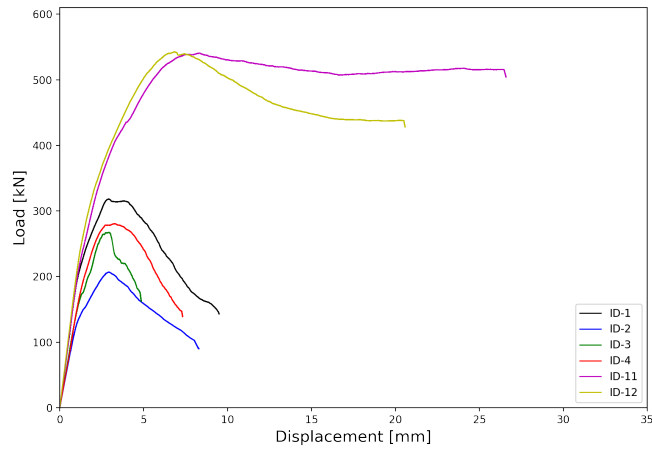
Figure 7.2: Comparison of mean residual flexural tensile strength

In general, the mixtures with steel fibres performed better compared to basalt fibres. However, it can be observed large variation between the mixtures with steel fibres. For instance, a stable concrete mixture is superior compared to an unstable concrete mixture, especially in ULS. Also, the concrete mixture based on the casting method from NS14651 exhibits the highest value until the limit of proportionality is reached. Thus, it should be mentioned that the capacity decreases more rapidly parallel with increasing crack width. Moreover, the casting method from NS14651 performed better than the Danish. This may be due to a significantly larger fibre content in the specimens casted from NS14651, resulting in a higher proportion of effective fibres after cracking.

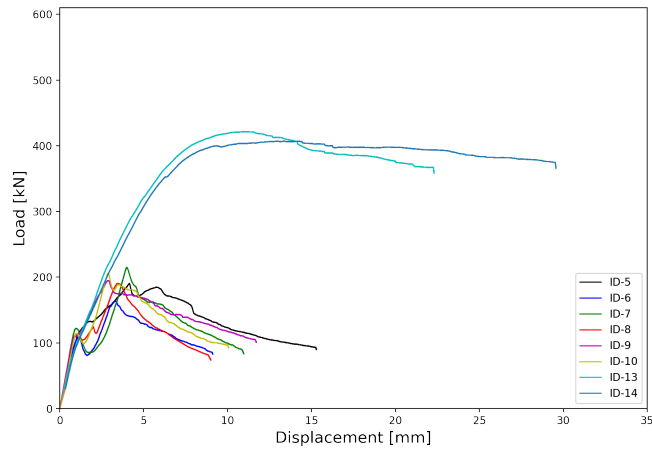
It should also be mentioned that the results for each individual sample within the batches indicated a significant scatter of the Stress-CMOD curves. This may be a result of a small crack area, resulting in a large variability of the amount of fibres intersecting the crack. Additionally, irregularities in shape or notch can also have an influence.

7.1.3 Comparison of Elements

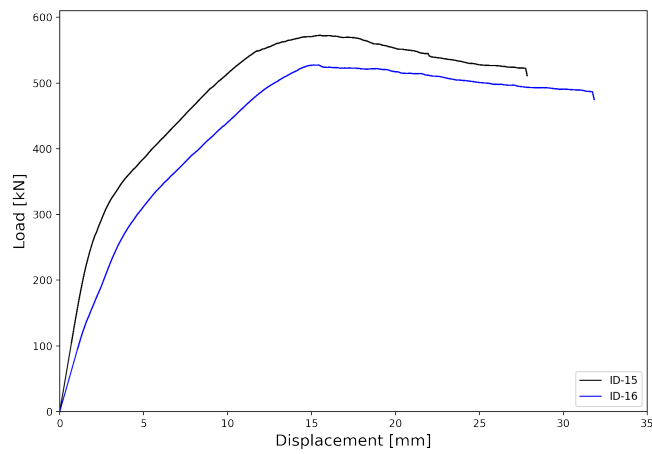
Based on the findings from the experimental tests there are rather large variations in the results when comparing the elements. As expected, and also indicated in Figure 7.4, there is a significant difference between elements with only fibre reinforcement compared to elements with fibre- and conventional reinforcement.



(a) Small slabs



(b) Small walls



(c) Large slabs

Figure 7.3: Comparison of elements

It can be observed that elements with rebars in addition to fibre will reach a significantly higher ultimate load. Specifically, these slabs reach approx. 85 % and 103 % higher ultimate load, for stable- and unstable concrete mixtures, respectively. Likewise, the walls reach approx. 120 % and 150 % higher ultimate load, for stable- and unstable concrete mixtures, respectively. With regard to this, it should also be mentioned that the elements with fibre- and conventional reinforcement had no significant difference in capacity between stable and unstable concrete mixtures. On the other hand, for the elements with only fibre reinforcement, it can be observed a lower capacity when applying an unstable concrete mixture. Thus, a stable concrete mixture gives the most favourable results, and this is also consistent with the study from the literature. Another essential observation is seen for the vertically casted elements with batch 5. Despite the fact that these are vibrated, there are no signs of negative effects. On the contrary, the two wall elements that exhibit the highest ultimate load are vibrated.

Furthermore, elements with combined reinforcement achieve a higher ductility due to the rebar's ability to maintain a high capacity after reaching the ultimate load. On the contrary, the post-peak load for the element with only fibre reinforcement decreases rapidly, hence, does not achieve as good ductility. This was as expected with a fibre concentration below 1 %, which usually results in strain-softening for FRC. However, a slight difference in behaviour after the ultimate load can be observed when comparing the slabs and walls with only fibre, where the load in the walls decreases slower compared to the slabs. Despite the fact that the slabs reached a significantly higher ultimate load, the walls achieved a greater deformation before the load was reduced to 50 % of the peak load. This may indicate a slightly higher ductility for the walls.

An interesting observation is seen regarding a prominent difference in load behaviour between horizontal and vertical casted elements. It can be observed a relatively large load-drop when the vertically casted elements reached approx. 60 % of the ultimate load. This coincides with the initiation of the first crack. The load-drop can be attributed to the fact that the fibres do not contribute sufficient residual tensile strength after the first crack. Hence, a load-drop can be seen. This drop continues until the internal stress is redistributed, and the load increases again. However, why this phenomenon only occurs for the vertically casted elements is uncertain.

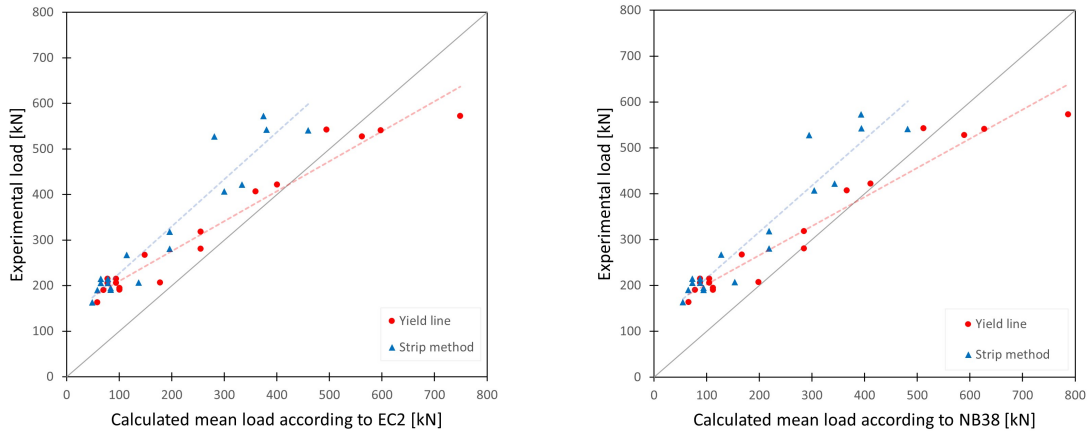
In the comparison between steel- and basalt fibres, the horizontally casted elements clearly indicate that steel fibres give superior results. In contrast, for the vertically casted elements, basalt fibres actually exhibit comparable results to steel fibres. However, due to the limited number of BFRC elements for comparison, no conclusions can be drawn. According to the residual flexural tensile strength, a substantial difference between steel- and basalt fibre would be expected. However, that is not the case. This may be due to a more beneficial fibre distribution and orientation in the vertically casted element than the beam specimens from the three-point bending test.

7.2 Comparing of Calculated- and Laboratory Results

To compare the experimental test and the calculation, the most representative calculation is done with mean strength values, as these calculations should represent the average results. However, with only two equal elements at most, the average test result of the element would most likely deviate from the average if the number of samples had been increased. This can be seen in the result from the three-point bending test, where the result has a large scatter in capacity even for similar specimens with equal properties. Hence, the result from one specimen can deviate somewhat from the mean values. For the three-point bending test, the specimens are relatively small, and a large scatter was expected. In contrast, a smaller scatter is expected for larger plate elements when they are equally sized with similar properties, as explained in chapter 4.2.

7.2.1 Ultimate Load

In the calculation of the mean ultimate load capacity, it was expected a higher capacity for yield line analysis compared to the strip method. This was also the case for all the calculations presented in the results. However, the difference between elements 15 and 16 should be noted, where the yield line analysis results in 100 % higher capacity compared to the strip method, while for the other elements, the difference is only 20-30 %. As these two methods represent an upper- and lower-bound theorem, the experimental result was expected between those. In general, this was not the case for the smaller elements. By studying the trendlines in Figure 7.4, the strip method has a trendline parallel to the exact value on the lower bound side. On the contrary, the trendline for the yield line analysis has an increasing utilization starting on the safe side.



(a) Calculation according to EC2

(b) Calculation according to NB38

Figure 7.4: Comparison of mean calculated capacity and experimental capacity

With only three calculations above the experimental load, it is reasonable to assume that the calculated moment capacity may be too low. One of the factors that influence the calculated moment capacity is the orientation factor κ_0 . For the vertically casted elements with only fibre reinforcement, the utilization was significantly low, which can imply that the assumed orientation

factor for walls, $\kappa_0 = 0.5$, is too conservative. However, when the conventional reinforcement is included, the calculation coincides significantly better with the laboratory results. Hence, it appears that the rebars have a greater influence on the fibre orientation in vertically casted elements, compared to the horizontally casted elements. Regarding the yield line analysis, it should also be noted that the assumed failure pattern was not the case for every plate. Hence, the calculated ultimate load can for that reason deviate from the tested ultimate load.

In addition, calculations with characteristic strength were performed and compared with the experimental results. These calculations are statistically expected to be conservative. Also, the yield line analysis results in a too high capacity for element 15, as shown in Figure 7.5. In relation to this, and the large variation between the yield line analysis and strip method for elements 15 and 16, uncertainty regarding the yield line calculation for the large elements should be noted.

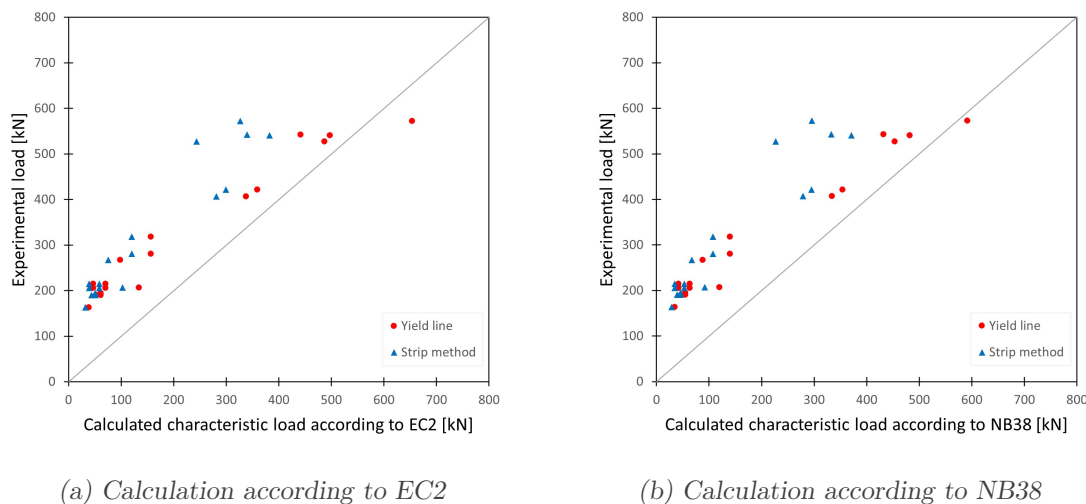


Figure 7.5: Comparison of characteristic calculated capacity and experimental capacity

7.2.2 Crack Width Calculation

As mentioned in chapter 6.2, crack width calculations from load in SLS, according to EC2, showed nearly similar crack width obtained from the experiment. However, when the load increases further there will be a significant difference between the calculated and the experimental crack width. The reason behind this can be attributed to the size of the load and the reinforcement stress. At the two final calculation the load are likely to have passed the SLS and the calculation of the reinforcement stress is no longer valid. Additionally, it can be a consequence of significantly higher stress within the element, subjected to the corresponding load when running the experimental test. Also, the result may exhibit variation due to the non-linear crack formation, causing uneven measurements by the LVDTs. Furthermore, the results from NB38 were considerably less. The difference between calculation rules in EC2 and NB38 will be discussed in chapter 7.2.3. Finally, it is important to note that the calculations are based on one element. Therefore, no definitive conclusion can be drawn.

7.2.3 Comparing of EC2 and NB38

Regarding the strength of FRC, EC2 and NB38 calculates the residual tensile strength differently. For the mean calculations, it is mainly the scaling factor from the transformation from linear elastic stress distribution to a rigid-plastic model that separates the residual tensile strength calculations. Hence, the calculation according to NB38 results in a higher fibre contribution, as the height of the tension zone is larger compared to EC2. However, in a calculation with characteristic strength where the scaling factor is still larger for NB38, the size of the failure mechanism can have a larger influence, resulting in a higher strength for FRC according to EC2. This was the case for all the calculations performed on the elements where κ_G was at least 1.24 and even reached the maximum value of 1.5 for element 15.

With regard to the calculated crack width, the results from NB38 were considerably less than for EC2. This could potentially be attributed to the fact that the characteristic residual tensile strength is calculated differently in NB38 compared to EC2. Hence, the fibres contribute more, lowering the calculated strain and stress in the rebars.

7.3 Fibre Orientation and Distribution

The fibre content and orientation study is based on the inductive test, which is a relatively new method to determine the fibres distribution. The results obtained seem reliable and confirmed some of the expectations.

The cubes from the standard beams were expected to have variations in fibre content and orientation. This was attributed to the fact that the standard beams with the lowest and highest obtained residual tensile strength represented each batch.

When comparing the average fibre content in the x-direction for each beam, presented in Table 7.1, the beams with the lowest f_{R3} also have the lowest fibre content in the x-direction. For batch 5 casted according to NS14651, the total fibre content is lowest for the beam with the highest residual strength. However, with a larger fraction orientated in the x-direction, this beam exhibits the highest effective fibre content. When comparing the casting methods all the beams show a clear result of the wall-effect with a uniaxial orientation. However, batch 5 casted according to NS14651 has a lower fraction orientated in the x-direction compared to the other, which may be due to a lower wall-effect when the concrete is poured from three points. Also, the high fibre content of these beams should be noted. This is likely to have a significant influence on the high obtained residual tensile strength.

Table 7.1: Average fibre content orientated in x-direction in the beams

Average Beam	C_f [kg/m ³]	C_x [%]	Amount [kg/m ³]	Test result f_{R3}
B1-1	35.92	43.3	15.54	Low
B1-6	37.41	47.2	17.65	High
B2-1	28.87	49.7	14.36	High
B2-7	27.82	51.2	14.23	Low
B5-1D	33.67	48.7	16.41	High
B5-6D	32.77	49.8	16.31	Low
B5-1S	50.90	47.3	24.10	High
B5-2S	51.80	40.9	21.18	Low

Regarding the fibre content in the plate elements, the result in Figure 5.15 shows a large scatter within each element. As the results from the standard beams are used to determine the residual tensile strength, the correlation of fibre distribution between the tested beams and plate elements is related through κ_0 . According to EC2 and NB38, there are no reductions for horizontally casted elements while for vertically casted elements, the residual tensile strength is reduced to 50 % with $\kappa_0 = 0.5$.

For element 1 the orientation can be related to the beams where the fraction of fibres orientated out of the plane is low due to the wall-effect and flow of the fresh concrete. The element shows a relatively even orientation in the x- and y directions, indicating an even planer orientation. Regarding the orientation, the fibres seem to be more isotropic close to the casting point, and further away the fibres show the tendency of being orientated perpendicular to the flow direction, as anticipated in chapter 2.5.1.

For the walls without conventional reinforcement, elements 5-10, the reduction in κ_0 seems conservative as the calculated capacity exhibits a very low utilization. When studying the inductive test results, elements 5 and 9 exhibit generally the lowest isotropy factor, with the dominating directions in either x or y direction. However, there is no consistency in which direction that has the highest fraction. With the lowest content orientated out of the plane (z-direction), most of the fibres are orientated parallel to the flow direction, indicating a strong wall-effect. Furthermore, compared to elements 5 and 9, a variation was expected as the rebars may influence the wall-effect for elements 13 and 14.

When studying the crack patterns in correlation with the fibre orientation in Figure 5.16, numerous cracks show the tendency to occur parallel to the dominating fibre direction. However, the observations obtained from the inductive test are based on a limited number of samples. Therefore, to draw a conclusion, more samples need to be tested.

8 Conclusions

In this thesis, a full-scale experimental investigation has been conducted for 16 plate elements, where the objective was to compare different casting methods for horizontal and vertical casted elements. The comparison involved the use of SFRC and BFRC, with and without the inclusion of rebars. Also, the fibre content and distribution have been investigated related to the obtained capacity and crack pattern for the elements. Moreover, the obtained test results have been compared with the results derived from calculation rules according to EC2 and NB38.

The obtained residual tensile strength shows a clear favourable effect for the use of steel fibre compared to basalt fibre immediately after cracking. However, with increasing crack width, a stable SCC is required to maintain a high residual tensile strength. For VCC the casting method according to NS-EN 14651 exhibits the highest result and also a significantly smaller scatter in the obtained result.

With respect to the plate bending test, a significantly higher capacity is achieved for FRC when conventional reinforcement is included. Also, a higher ductility is reached, which increases the safety of load-bearing FRC structures. Moreover, the horizontally casted elements performed in general better than the vertically casted elements. The observation indicates a larger difference for steel fibres compared to basalt fibre between slabs and walls. That aside, elements with steel- and basalt fibres obtained similarly ultimate load for the vertically casted elements. However, elements with steel fibres reached a higher ductility than those with basalt fibres. Further, stable- and unstable SCC show less variation in the elements, despite the significant difference in residual tensile strength according to the three-point bending test. In comparison, the VCC show no negative sign of being vibrated, as the element with VCC achieved the highest ultimate load in the vertically casted elements.

In the comparison of calculated and experimental ultimate load, the yield line was in general more exact. However, the strip method shows a constant deviation from the experimental value. Related to the calculated ultimate load for walls, the orientation factor κ_0 is too conservative when it reduces the capacity by half. Furthermore, the crack width calculations according to EC2 provide accurate results in SLS compared to NB38. However, since this calculation is based on a single tested element, further testing is required to conclude.

The fibre content and distribution obtained from the inductive test show a clear correlation with the residual flexural tensile strength. For the beam specimens, the fibre content varies a lot, while the orientation along the length axis of the beam shows more consistency independent of the concrete mixture. The fibre content and orientation from the plates are obtained from a small sample. Hence, any final conclusions can be drawn from this. However, both the vertically and horizontally casted elements show in general a planer orientation. Also, for the horizontally casted element, the orientation coincides with the theory, where the fibres tend to be orientated perpendicular to the flow direction.

Further Work

In order to manage the work associated with this thesis within the given time, certain limitations and prioritizations were implemented. As a consequence, there are several results that require more testing before a final conclusion. Therefore, suggestions for further work are provided.

- Perform more testing of elements with stable self compacting SFRC and stable BFRC to give a more reliable comparison.
- Study the relation between fibre orientation in beam specimens and vertically casted elements to determine a more optimal orientation factor κ_0 . This involves inductive testing of several samples of the tested elements.
- Obtain several crack measurements to compare the crack width calculations.
- In further testing, some changes in the plate bending test would be advisable. Loading from the bottom side with supports on the top side would give a better overview of the crack propagation.

References

- [1] Kanstad T, Døssland ÅL, Vatnar A, Mathisen AE, Brå H, and Hisdal JM et al. Fiberarmert betong i bærende konstruksjoner. *Publikasjon nr.38*, 2020.
- [2] fib. *fib Model Code for Concrete Structure 2010*, volume 1. Ernst & Sohn, 2013.
- [3] Ilakya T and Thaarani S. A comparative study of fibres in concrete. 2015. URL <https://www.ijert.org/research/a-comparitive-study-of-fibres-in-concrete-IJERTCONV3IS04065.pdf>.
- [4] Mujalli MA, Dirar S, Mushtaha E, Hussien A, and Maksoud A. Evaluation of the tensile characteristics and bond behaviour of steel fibre-reinforced concrete: An overview. 2022. URL <https://www.mdpi.com/2079-6439/10/12/104>.
- [5] Susetyo J. *Fibre Reinforcement for Shrinkage Crack Control in Prestressed, Precast Segmental Bridges*. PhD thesis, University of Toronto, Toronto, 2009.
- [6] Døssland ÅL. *Fibre Reinforcement in Load Carrying Concrete Structures*. PhD thesis, The Norwegian University of Science and Technology (NTNU), Trondheim, 2008.
- [7] Marcalikova Z, Cajka R, Bilek V, Bujdos D, and Sucharda O. Determination of mechanical characteristics for fiber-reinforced concrete with straight and hooked fibers. 2020. URL <https://www.mdpi.com/2073-4352/10/6/545>.
- [8] Standard Norge. NS-EN14889-1:2006. Fibres for concrete - Part 1: Steel fibres - Definitions, specifications and conformity [Internet]. Standard norge, 2006, . URL <https://standard.no>.
- [9] Kanstad T et al. Forslag til retningslinjer for dimensjonering, utførelse og kontroll av fiberarmerte betongkonstruksjoner. SINTEF. COIN Project report 29, 2011.
- [10] Jalasutram S, Sahoo DR, and Matsagar V. Experimental investigation of the mechanical properties of basalt fiber-reinforced concrete. 2017. URL <https://doi.org/10.1002/suco.201500216>.
- [11] Li Z, Shen A, Zeng G, Chen Z, and Guo Y. Research progress on properties of basalt fiber-reinforced cement concrete. 2022. URL <https://www.sciencedirect.com/science/article/pii/S2352492822016658>.
- [12] Wei B, Cao H, and Song S. Degradation of basalt fibre and glass fibre/epoxy resin composites in seawater. 2011. URL <https://www.sciencedirect.com/science/article/pii/S0010938X10004841>.
- [13] Löfgren I. *Fibre-reinforced Concrete for Industrial Construction - a fracture mechanics approach to material testing and structural analysis*. PhD thesis, Chalmers University of

Technology, Göteborg, 2005.

- [14] Rossi P, Daviau-Desnoyers D, and Tailhan JL. Analysis of cracking in steel fibre-reinforced concrete (sfrc) structures in bending using probabilistic modelling. 2015. URL <https://doi.org/10.1002/suco.201400081>.
- [15] Le LA, Nguyen GD, Bui HH, Sheikh AH, and Kotousov A. Incorporation of micro-cracking and fibre bridging mechanisms in constitutive modelling of fibre reinforced concrete. 2019. URL <https://doi.org/10.1016/j.jmps.2019.103732>.
- [16] Zirgulis G, Svec O, Geiker MR, Cwirzen A, and Kanstad T. Influence of reinforcing bar layout on fibre orientation and distribution in slabs cast from fibre-reinforced self-compacting concrete (frscc). volume 17 of *Structural concrete: journal of the FIB*. Ernst & Sohn, 2016.
- [17] Torrents JM, Blanco A, Pujadas P, Aguado A, Juan-García P, and Sánchez-Moragues MÁ. Inductive method for assessing the amount and orientation of steel fibers in concrete. *Materials and Structures*, 2012. URL <https://doi.org/10.1617/s11527-012-9858-6>.
- [18] Cavalaro SHP, López R, Torrents JM, and Aguado A. Improved assessment of fibre content and orientation with inductive method in sfrc. *Materials and Structures*, 2014. URL <https://doi.org/10.1617/s11527-014-0279-6>.
- [19] Cavalaro SHP, López-Carreño R, Torrents JM, Aguado A, and Juan-García P. Assessment of fibre content and 3d profile cylindrical sfrc specimens. *Materials and Structures*, 2015. URL <https://doi.org/10.1617/s11527-014-0521-2>.
- [20] Sørensen SI. *Betongkonstruksjoner - Beregning of dimensjonering etter Eurocode 2*, volume 2. Fagbokforlaget, 2013.
- [21] Kennedy G and Goodchild CH. Practical yield line design. The Concrete Centre, 2004.
- [22] Standard Norge. NS-EN12390-3:2019. Testing hardened concrete - Part 3: Compressive strength of test specimens [Internet]. Standard norge, 2019, . URL <https://www.standard.no>.
- [23] Standard Norge. NS-EN14651. Prøvningsmetode for betong med metalliske fibre - Måling av bøyestrekfasthet (proporsjonalitetsgrense og restfastheter) [Internet]. Standard norge, 2008, . URL <https://www.standard.no/nettbutikk/sokeresultater/?search=NS-EN14651>.
- [24] Matthys S and Triantafillou T. *fib Bulletin 90*, volume 1. fib, 2019.
- [25] European Committee for Standardization. Eurocode 2: Design of concrete structures — part 1-1: General rules and rules for buildings, bridges and civil engineering structures. European committee for standardization, 2022.

Appendix

A Drawings

- A.1 As-built drawing
- A.2 Core drilling position

B Concrete properties

- B.1 Concrete recipe
- B.2 Compression test
- B.3 Compressive and tensile strength

C Characteristic residual tensile strength

D Moment capacity

- D.1 Moment capacity - EC2 - mean
- D.2 Moment capacity - EC2 - Characteristic
- D.3 Moment capacity - NB38 - mean
- D.4 Moment capacity - NB38 - Characteristic

E Calculated ultimate load

- E.1 Ultimate load with yield line theory
- E.2 Ultimate load with strip method

F Crack width calculation

- F.1 Crack Width Calculation - EC2 - 250 kN loading
- F.2 Crack Width Calculation - EC2 - 300 kN loading
- F.3 Crack Width Calculation - EC2 - 350 kN loading
- F.4 Crack Width Calculation - EC2 - 400 kN loading
- F.5 Crack Width Calculation - NB38 - 250 kN loading
- F.6 Crack Width Calculation - NB38 - 300 kN loading
- F.7 Crack Width Calculation - NB38 - 350 kN loading
- F.8 Crack Width Calculation - NB38 - 400 kN loading

G Inductive test

- G.1 Fibre orientation in cubes
- G.2 Fibre orientation in cylinders

A Drawings

A.1 As-built drawing

Plate 1.3x1.3x0.15 - Uarmerte

Batch 1 #1
Stabil
Fiber 1

Batch 3 #2
Stabil
Fiber 2

Batch 2 #3
Ustabil
Fiber 1

Batch 1 #4
Stabil
Fiber 1

Veggskiver 1.2x1.2x0.15 - Uarmerte

Batch 1 #5
Stabil
Fiber 1

Batch 2 #6
Ustabil
Fiber 1

Batch 5 #7
VB Bef.
Fiber 1

Batch 3 #8
Stabil
Fiber 2

Batch 1 #9
Stabil
Fiber 1

Batch 5 #10
VB Bef.
Fiber 1

Plate 1.3x1.3x0.15 - Armerte

Batch 1 #11
Stabil
Fiber 1

Arm. $\phi 10cc250$
overdekning
25mm

Batch 2 #12
Ustabil
Fiber 1

Arm. $\phi 10cc250$
overdekning
25mm

Veggskiver 1.2x1.2x0.15 - Armerte

Batch 1 #13
Stabil
Fiber 1

Arm. B.S.
 $\phi 10cc250$
overdekning
15mm

Batch 2 #14
Ustabil
Fiber 1

Arm. B.S.
 $\phi 10cc250$
overdekning
15mm

Plate 3.1x3.1x0.18 - Armerte
Utstøping fra ett punkt

Batch 1 #15
Stabil
Fiber 1

Arm. $\phi 10cc250$
overdekning
25mm

Batch 1 #16
Stabil
Fiber 1

Arm. $\phi 10cc250$
overdekning
25mm

Veggskiver 2.5x7.05x0.20 - Uarmerte - utstøping fra ett punkt

Batch 1 #17
Stabil
Fiber 1

STØPEORDRE

Veggskiver 2.5x7.5x0.20 - Uarmerte - utstøping fra flere (2) punkt

Batch 1 #18
Stabil
Fiber 1

MERK !
Nøyaktig plassering av boresylindere må bestemmes

Terning 100x100x100
Batch 1, 2, 3 og 5 24stk.

3 stk. testes etter 28 dager

B1-1	B1-1	B1-1	B5-1
B1-2	B1-2	B1-2	B5-2
B1-3	B1-3	B1-3	B5-3

3 stk. testes etter 91 dager

B1-4	B1-4	B1-4	B5-4
B1-5	B1-5	B1-5	B5-5
B1-6	B1-6	B1-6	B5-6
B1-7	B1-7	B1-7	B5-7

'Work diagram'
 $\phi 150 \times 300$ eller $\phi 100 \times 200$
Batch 1, 2, 3 og 5
12stk.

B1-1	B1-1	B1-1	B5-1
B1-2	B1-2	B1-2	B5-2
B1-3	B1-3	B1-3	B5-3

Batch 1	B1-1	B1-2	B1-3	B1-4	B1-5	B1-6	B1-7
Merk: Støping etter dansk støpeordre							
(7stk.)							

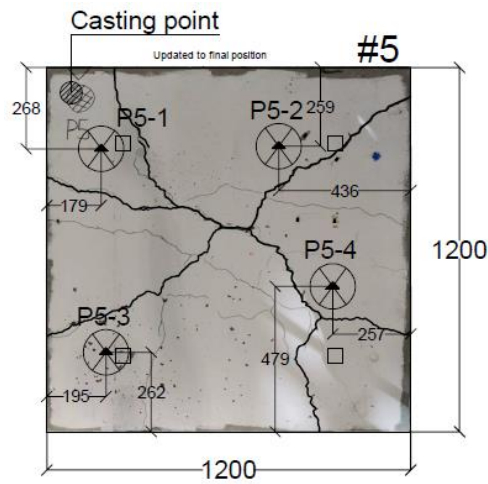
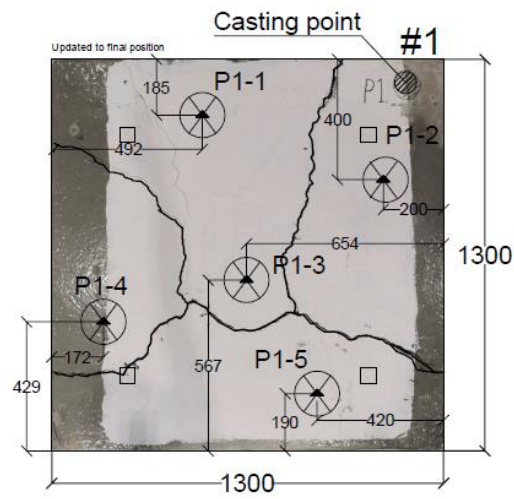
Batch 2	B2-1	B2-2	B2-3	B2-4	B2-5	B2-6	B2-7
Merk: Støping etter dansk støpeordre							
(7stk.)							

Batch 3	B3-1	B3-2	B3-3	B3-4	B3-5	B3-6	B3-7
Merk: Støping etter dansk støpeordre							
(7stk.)							

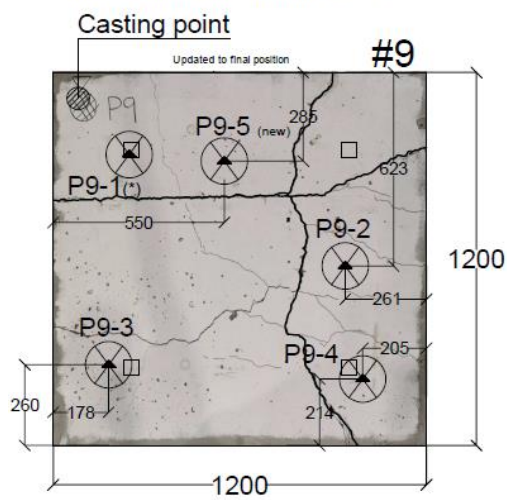
Batch 5	B5-1	B5-2	B5-3	B5-4	B5-5	B5-6	B5-7
Merk: Støping etter dansk støpeordre							
(7stk.)							

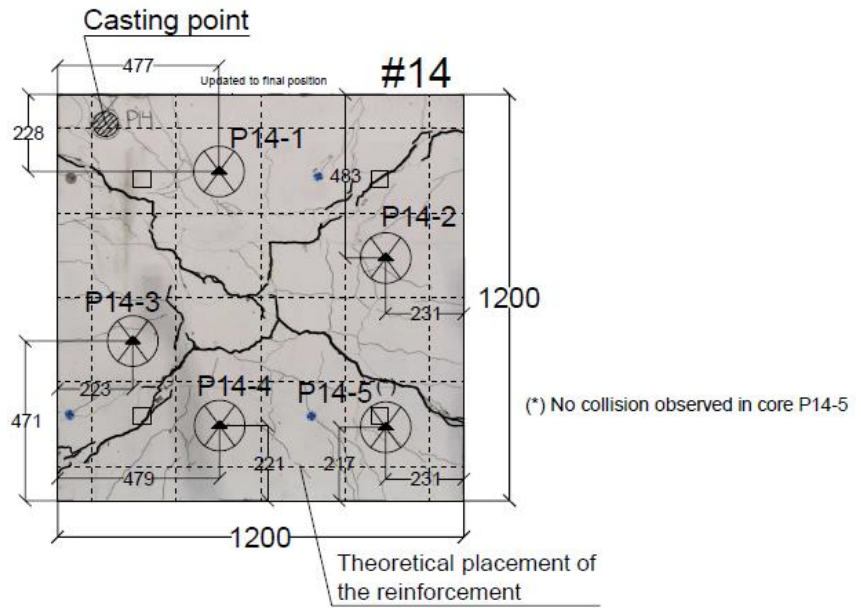
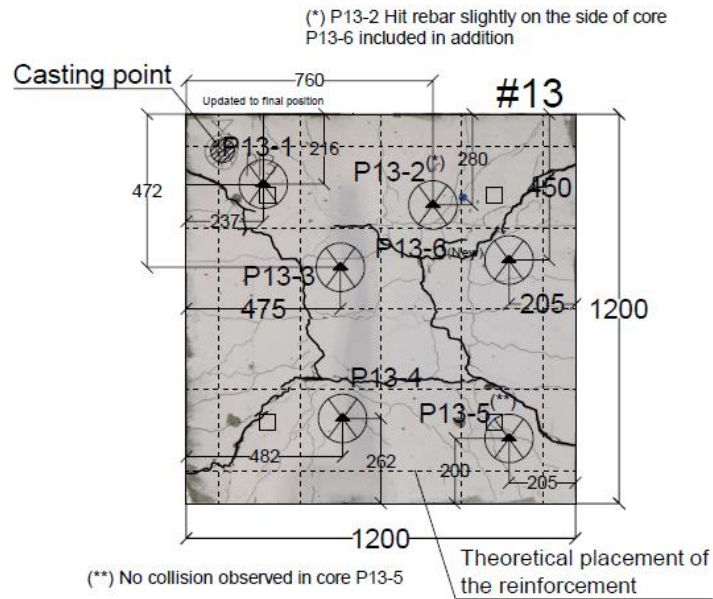
Batch 5	B5-1	B5-2	B5-3	B5-4	B5-5	B5-6	B5-7
Merk: Støping etter dansk støpeordre							
(7stk.)							

A.2 Core drilling position



(*) P9-1 can't be used because collision with anchor
 No collision observed in the rest of cores





B Concrete properties

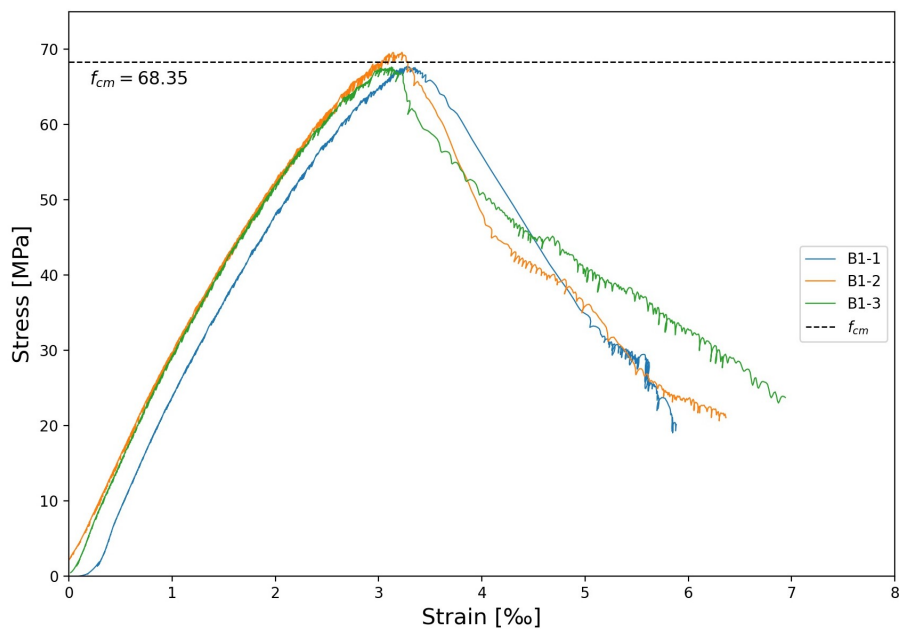
B.1 Concrete recipe

B45 M40 D22 SKB LKB		BETONG ØST					
Avdeling 313, Rudshøgda							
Resept:	4770	Avdeling:	313 - Rudshøgda				
	B45 M40 D22 SKB LKB						
Fasthetskklasse:	B45	Luftinnhold:	20 liter	Karbonklasse:	Lavkarbon A		
Bestandighetsklasse:	M40	Basis synk:	650 mm	CO2 (A1-A3):	217,81 kg		
Masseforhold (V/C):	0,398	D-max:	22 mm				
Materiale	Prop	Masse (kg)	Densitet	Volum (l)	Vann (l)	Pris	CO2 (kg)
1350 11-16RHP	30,00 %	517,6	2,68	193,1	0,0		2,51
1351 16-22RHP	10,00 %	172,5	2,68	64,4	0,0		0,84
1633 0-8V	60,00 %	1 027,5	2,66	386,3	0,0		2,52
Sum tilslag		1 717,7		643,8			5,86
2001 STD FA	80,00 %	340,8	3,00	113,6	0,0		199,42
3001 SILIKA	5,00 %	21,3	2,20	9,7	0,0		1,48
3007 FA	15,00 %	63,9	2,30	27,8	0,0		1,96
6013 SR-N	1,28 %	5,5	1,05	5,2	0,0		3,06
6207 SCC10	0,47 %	2,0	1,02	2,0	0,0		0,01
Vann		178,0	1,00	178,0	178,0		
Luft	2,00 %	0,0	0,00	20,0	0,0		
Totalt		2 329,1		1 000,0	178,0		211,81

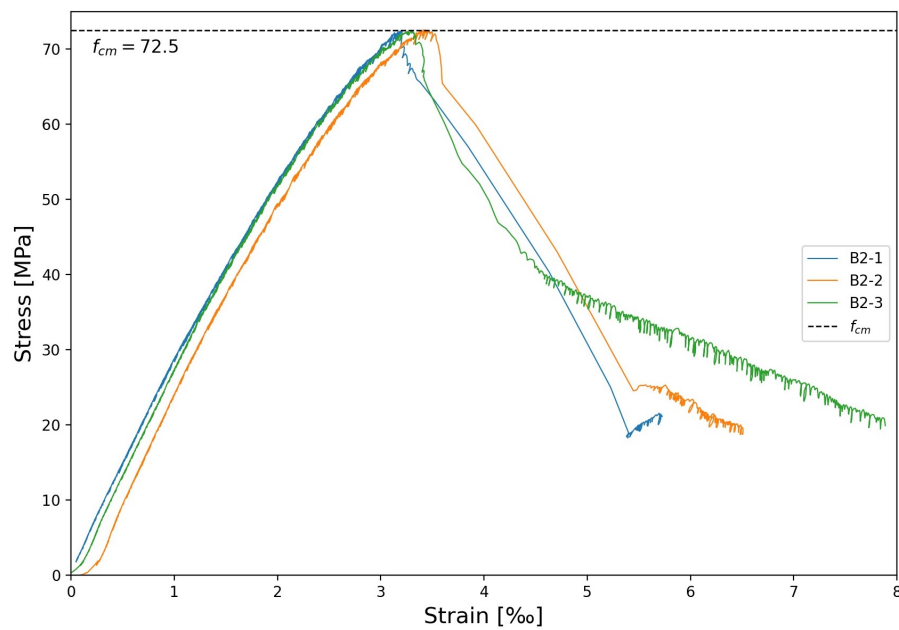
Recipe of SCC low carbon concrete

B.2 Compression test

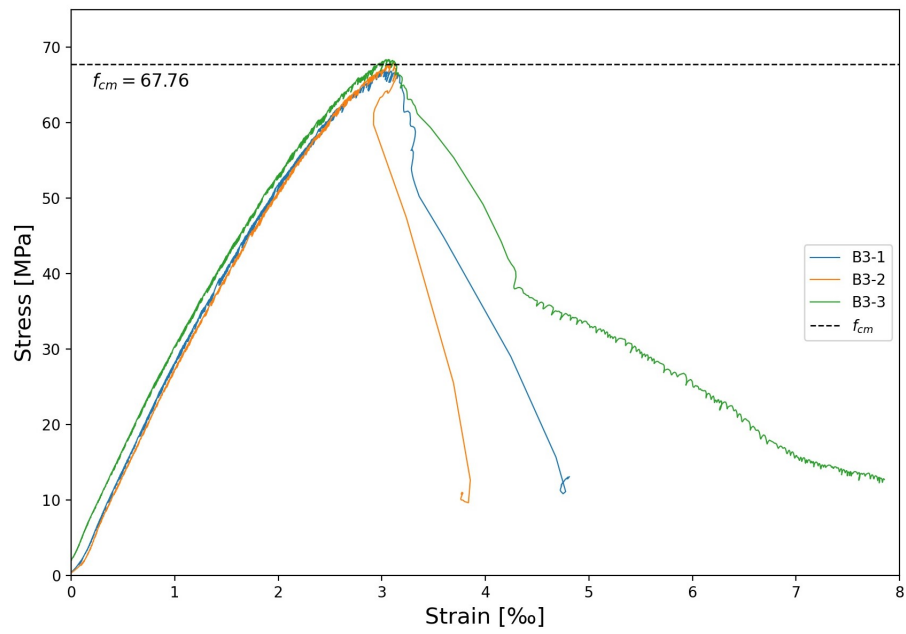
Batch 1



Batch 2



Batch 3



B.3 Compressive and tensile strength

Compressive and tensile strength of concrete

All calculations derived from formulas in New EC2 (Table 5.1)

Values from f_{cm} is derived from the compressive test

NB! Batch 5 with no valid results from compressive test -> Used the same as for Batch 1

Batch 1:

$$f_{cm} := 68.35 \text{ MPa}$$

$$f_{ck} := f_{cm} - 8 = 60.35 \text{ MPa}$$

$$f_{ctm} := 1.1 \cdot f_{ck}^{\frac{1}{3}} = 4.31 \text{ MPa} \quad (f_{ck} > 50 \text{ MPa})$$

$$f_{ctk;0.05} := 0.7 \cdot f_{ctm} = 3.02 \text{ MPa}$$

$$k_E := 0.7 \cdot 9500 = 6650 \quad (\text{Sandstone aggregates})$$

$$E_{cm} := k_E \cdot f_{cm}^{\frac{1}{3}} = 27189 \text{ MPa}$$

Batch 2:

$$f_{cm} := 72.50 \text{ MPa}$$

$$f_{ck} := f_{cm} - 8 = 64.5 \text{ MPa}$$

$$f_{ctm} := 1.1 \cdot f_{ck}^{\frac{1}{3}} = 4.41 \text{ MPa} \quad (f_{ck} > 50 \text{ MPa})$$

$$f_{ctk;0.05} := 0.7 \cdot f_{ctm} = 3.09 \text{ MPa}$$

$$k_E := 0.7 \cdot 9500 = 6650 \quad (\text{Sandstone aggregates})$$

$$E_{cm} := k_E \cdot f_{cm}^{\frac{1}{3}} = 27729 \text{ MPa}$$

Batch 3:

$$f_{cm} := 67.76 \text{ MPa}$$

$$f_{ck} := f_{cm} - 8 = 59.76 \text{ MPa}$$

$$f_{ctm} := 1.1 \cdot f_{ck}^{\frac{1}{3}} = 4.3 \text{ MPa} \quad (f_{ck} > 50 \text{ MPa})$$

$$f_{ctk;0.05} := 0.7 \cdot f_{ctm} = 3.01 \text{ MPa}$$

$$k_E := 0.7 \cdot 9500 = 6650 \quad (\text{Sandstone aggregates})$$

$$E_{cm} := k_E \cdot f_{cm}^{\frac{1}{3}} = 27111 \text{ MPa}$$

C Characteristic residual tensile strength

Characteristic residual tensile strength

Values from $f_{R.1m}$ and $f_{R.3m}$ is derived from the Three point bending test

Batch 1:

Residual flexural tensile strength with $CMOD_1 := 0.5 \text{ mm}$

$$f_{R.1m} := 4.48 \text{ MPa}$$

Mean residual flexural tensile strength

Residual flexural tensile strength with $CMOD_3 := 2.5 \text{ mm}$

$$f_{R.3m} := 3.75 \text{ MPa}$$

Mean residual flexural tensile strength

$$k := 1.7$$

Factor dependent on the number of test specimens

$$s_{d,i} = \sqrt{\frac{\sum (f_{R,i} - f_{R.im})^2}{n-1}}$$

Standard deviation of the samples

$$s_{d,1} := 1.24 \text{ MPa}$$

$$s_{d,3} := 1.13 \text{ MPa}$$

$$f_{R.1k} := \min(f_{R.1m} - k \cdot s_{d,1}, 0.6 \cdot f_{R.1m}) = 2.37 \text{ MPa}$$

Characteristic residual flexural tensile strength

$$f_{R.3k} := \min(f_{R.3m} - k \cdot s_{d,3}, 0.6 \cdot f_{R.3m}) = 1.83 \text{ MPa}$$

Batch 2:

Residual flexural tensile strength with $CMOD_1 := 0.5 \text{ mm}$

$$f_{R.1m} := 4.91 \text{ MPa}$$

Mean residual flexural tensile strength

Residual flexural tensile strength with $CMOD_3 := 2.5 \text{ mm}$

$$f_{R.3m} := 2.17 \text{ MPa}$$

Mean residual flexural tensile strength

$$k := 1.7$$

Factor dependent on the number of test specimens

$$s_{d,i} = \sqrt{\frac{\sum (f_{R,i} - f_{R.im})^2}{n-1}}$$

Standard deviation of the samples

$$s_{d,1} := 1.29 \text{ MPa}$$

$$s_{d,3} := 0.61 \text{ MPa}$$

$$f_{R.1k} := \min(f_{R.1m} - k \cdot s_{d,1}, 0.6 \cdot f_{R.1m}) = 2.72 \text{ MPa}$$

Characteristic residual flexural tensile strength

$$f_{R.3k} := \min(f_{R.3m} - k \cdot s_{d,3}, 0.6 \cdot f_{R.3m}) = 1.13 \text{ MPa}$$

Batch 3:Residual flexural tensile strength with $CMOD_1 := 0.5 \text{ mm}$

$$f_{R.1m} := 3.37 \text{ MPa}$$

Mean residual flexural tensile strength

Residual flexural tensile strength with $CMOD_3 := 2.5 \text{ mm}$

$$f_{R.3m} := 2.60 \text{ MPa}$$

Mean residual flexural tensile strength

$$k := 1.7$$

Factor dependent on the number of test specimens

$$s_{d.i} = \sqrt{\frac{\sum (f_{R.i} - f_{R.im})^2}{n - 1}}$$

Standard deviation of the samples

$$s_{d.1} := 0.73 \text{ MPa}$$

$$s_{d.3} := 0.59 \text{ MPa}$$

$$f_{R.1k} := \min(f_{R.1m} - k \cdot s_{d.1}, 0.6 \cdot f_{R.1m}) = 2.02 \text{ MPa}$$

Characteristic residual flexural tensile strength

$$f_{R.3k} := \min(f_{R.3m} - k \cdot s_{d.3}, 0.6 \cdot f_{R.3m}) = 1.56 \text{ MPa}$$

Batch 5 (Danish casting method):Residual flexural tensile strength with $CMOD_1 := 0.5 \text{ mm}$

$$f_{R.1m} := 4.72 \text{ MPa}$$

Mean residual flexural tensile strength

Residual flexural tensile strength with $CMOD_3 := 2.5 \text{ mm}$

$$f_{R.3m} := 2.91 \text{ MPa}$$

$$k := 1.7$$

Factor dependent on the number of test specimens

$$s_{d.i} = \sqrt{\frac{\sum (f_{R.i} - f_{R.im})^2}{n - 1}}$$

Standard deviation of the samples

$$s_{d.1} := 1.03 \text{ MPa}$$

$$s_{d.3} := 0.89 \text{ MPa}$$

$$f_{R.1k} := \min(f_{R.1m} - k \cdot s_{d.1}, 0.6 \cdot f_{R.1m}) = 2.83 \text{ MPa}$$

Characteristic residual flexural tensile strength

$$f_{R.3k} := \min(f_{R.3m} - k \cdot s_{d.3}, 0.6 \cdot f_{R.3m}) = 1.40 \text{ MPa}$$

Batch 5 (NS14651 casting method):Residual flexural tensile strength with $CMOD_1 := 0.5 \text{ mm}$

$$f_{R.1m} := 5.68 \text{ MPa}$$

Mean residual flexural tensile strength

Residual flexural tensile strength with $CMOD_3 := 2.5 \text{ mm}$

$$f_{R.3m} := 3.50 \text{ MPa}$$

Mean residual flexural tensile strength

$$k := 1.7$$

Factor dependent on the
number of test specimens

$$s_{d,i} = \sqrt{\frac{\sum (f_{R,i} - f_{R.im})^2}{n - 1}}$$

Standard deviation of the samples

$$s_{d,1} := 0.91 \text{ MPa} \quad s_{d,3} := 0.57 \text{ MPa}$$

$$f_{R.1k} := \min(f_{R.1m} - k \cdot s_{d,1}, 0.6 \cdot f_{R.1m}) = 3.41 \text{ MPa}$$

Characteristic residual
flexural tensile strength

$$f_{R.3k} := \min(f_{R.3m} - k \cdot s_{d,3}, 0.6 \cdot f_{R.3m}) = 2.10 \text{ MPa}$$

D Moment capacity

D.1 Moment capacity - EC2 - mean

1

fcd	68.35	eps fibmax	20	epsc	0.925
b	1000			x = alfa * h	
h	150	Lin	500	alfa	0.0442055
d	0	Lout	400	x=	6.63082437
d'	0	Lsup	275	k1	0.39119792
As	0	Lcr	3.55563	k2	0.34852217
As'	0	kG	1		
sigma s	0	fR3	3.75	Tc=	177297.486
eps s2	0.00	k0	1	Tc/S	1.00
sigma s'	0	fFtud	1.2375		
S1=	0	fib=	177419	Mom-cap	
S2=	0			MRd	13.48

2

fcd	67.76	eps fibmax	20	epsc	0.76
b	1000			x = alfa * h	
h	150	Lin	500	alfa	0.03660886
d	0	Lout	400	x=	5.49132948
d'	0	Lsup	275	k1	0.33186667
As	0	Lcr	3.55563	k2	0.34541985
As'	0	kG	1		
sigma s	0	fR3	2.60	Tc=	123485.093
eps s2	0.00	k0	1	Tc/S	1.00
sigma s'	0	fFtud	0.858		
S1=	0	fib=	123988	Mom-cap	
S2=	0			MRd	9.40

3

fcd	72.50	eps fibmax	20	epsc	0.665
b	1000			x = alfa * h	
h	150	Lin	500	alfa	0.03218001
d	0	Lout	400	x=	4.82700218
d'	0	Lsup	275	k1	0.29564792
As	0	Lcr	3.55563	k2	0.34372071
As'	0	kG	1		
sigma s	0	fR3	2.17	Tc=	103464.252
eps s2	0.00	k0	1	Tc/S	1.00
sigma s'	0	fFtud	0.7161		
S1=	0	fib=	103958	Mom-cap	
S2=	0			MRd	7.87

4

fcd	68.35	eps fibmax	20	epsc	0.925
b	1000			x = alfa * h	
h	150	Lin	500	alfa	0.0442055
d	0	Lout	400	x=	6.63082437
d'	0	Lsup	275	k1	0.39119792
As	0	Lcr	3.55563	k2	0.34852217
As'	0	kG	1		
sigma s	0	fR3	3.75	Tc=	177297.486
eps s2	0.00	k0	1	Tc/S	1.00
sigma s'	0	fFtud	1.2375		
S1=	0	fib=	177419	Mom-cap	
S2=	0			MRd	13.48

5

fcd	68.35	eps fibmax	20	epsc	0.635
b	1000			x = alfa * h	
h	150	Lin	400	alfa	0.03077296
d	0	Lout	400	x=	4.61594378
d'	0	Lsup	325	k1	0.28389792
As	0	Lcr	3.43848	k2	0.34319664
As'	0	kG	1		
sigma s	0	fR3	3.75	Tc=	89569.7239
eps s2	0.00	k0	0.5	Tc/S	1.00
sigma s'	0	fFtud	0.61875		
S1=	0	fib=	89956.4	Mom-cap	
S2=	0			MRd	6.81

6

fcd	72.50	eps fibmax	20	epsc	0.462
b	1000			x = alfa * h	
h	150	Lin	400	alfa	0.02257844
d	0	Lout	400	x=	3.38676571
d'	0	Lsup	325	k1	0.213213
As	0	Lcr	3.43848	k2	0.3402853
As'	0	kG	1		
sigma s	0	fR3	2.17	Tc=	52352.4296
eps s2	0.00	k0	0.5	Tc/S	1.00
sigma s'	0	fFtud	0.35805		
S1=	0	fib=	52494.9	Mom-cap	
S2=	0			MRd	3.97

7D

fcd	68.35	eps fibmax	20	epsc	0.557
b	1000			x = alfa * h	
h	150	Lin	400	alfa	0.02709539
d	0	Lout	400	x=	4.06430899
d'	0	Lsup	325	k1	0.25264592
As	0	Lcr	3.43848	k2	0.34186111
As'	0	kG	1		
sigma s	0	fR3	2.91	Tc=	70183.9037
eps s2	0.00	k0	0.5	Tc/S	1.00
sigma s'	0	fFtud	0.48015		
S1=	0	fib=	70071	Mom-cap	
S2=	0			MRd	5.30

7S

fcd	68.35	eps fibmax	20	epsc	0.615
b	1000			x = alfa * h	
h	150	Lin	400	alfa	0.02983265
d	0	Lout	400	x=	4.47489692
d'	0	Lsup	325	k1	0.27598125
As	0	Lcr	3.43848	k2	0.34285051
As'	0	kG	1		
sigma s	0	fR3	3.51	Tc=	84411.4056
eps s2	0.00	k0	0.5	Tc/S	1.00
sigma s'	0	fFtud	0.57915		
S1=	0	fib=	84280.9	Mom-cap	
S2=	0			MRd	6.38

8

fcd	67.76	eps fibmax	20	epsc	0.527
b	1000			x = alfa * h	
h	150	Lin	400	alfa	0.0256735
d	0	Lout	400	x=	3.85102548
d'	0	Lsup	325	k1	0.24035592
As	0	Lcr	3.43848	k2	0.34135757
As'	0	kG	1		
sigma s	0	fR3	2.60	Tc=	62719.7916
eps s2	0.00	k0	0.5	Tc/S	1.00
sigma s'	0	fFtud	0.429		
S1=	0	fib=	62697.9	Mom-cap	
S2=	0			MRd	4.74

9

fcd	68.35	eps fibmax	20	epsc	0.635
b	1000			x = alfa * h	
h	150	Lin	400	alfa	0.03077296
d	0	Lout	400	x=	4.61594378
d'	0	Lsup	325	k1	0.28389792
As	0	Lcr	3.43848	k2	0.34319664
As'	0	kG	1		
sigma s	0	fR3	3.75	Tc=	89569.7239
eps s2	0.00	k0	0.5	Tc/S	1.00
sigma s'	0	fFtud	0.61875		
S1=	0	fib=	89956.4	Mom-cap	
S2=	0			MRd	6.81

10D

fcd	68.35	eps fibmax	20	epsc	0.557
b	1000			x = alfa * h	
h	150	Lin	400	alfa	0.02709539
d	0	Lout	400	x=	4.06430899
d'	0	Lsup	325	k1	0.25264592
As	0	Lcr	3.43848	k2	0.34186111
As'	0	kG	1		
sigma s	0	fR3	2.91	Tc=	70183.9037
eps s2	0.00	k0	0.5	Tc/S	1.00
sigma s'	0	fFtud	0.48015		
S1=	0	fib=	70071	Mom-cap	
S2=	0			MRd	5.30

10S

fcd	68.35	eps fibmax	20	epsc	0.615
b	1000			x = alfa * h	
h	150	Lin	400	alfa	0.02983265
d	0	Lout	400	x=	4.47489692
d'	0	Lsup	325	k1	0.27598125
As	0	Lcr	3.43848	k2	0.34285051
As'	0	kG	1		
sigma s	0	fR3	3.51	Tc=	84411.4056
eps s2	0.00	k0	0.5	Tc/S	1.00
sigma s'	0	fFtud	0.57915		
S1=	0	fib=	84280.9	Mom-cap	
S2=	0			MRd	6.38

11

fcd	68.35	eps fibmax	20	epsc	1.33
b	1000			x = alfa * h	
h	150	Lin	500	alfa	0.06235349
d	120	Lout	400	x=	9.35302391
d'	0	Lsup	275	k1	0.51759167
As	314	Lcr	3.55563	k2	0.35706638
As'	0	kG	1		
sigma s	500	fR3	3.75	Tc=	330885.578
eps s2	0.00	k0	1	Tc/S	1.00
sigma s'	0	fFtud	1.2375		
S1=	157000	fib=	174051	Mom-cap	
S2=	0			MRd	31.60

12

fcd	72.5	eps fibmax	20	epsc	1.11
b	1000			x = alfa * h	
h	150	Lin	500	alfa	0.05258171
d	120	Lout	400	x=	7.88725722
d'	0	Lsup	275	k1	0.452325
As	314	Lcr	3.55563	k2	0.35224949
As'	0	kG	1		
sigma s	500	fR3	2.17	Tc=	258651.263
eps s2	0.00	k0	1	Tc/S	1.00
sigma s'	0	fFtud	0.7161		
S1=	157000	fib=	101767	Mom-cap	
S2=	0			MRd	26.15

13

fcd	68.35	eps fibmax	20	epsc	1.35
b	1000			x = alfa * h	
h	150	Lin	400	alfa	0.06323185
d	130	Lout	400	x=	9.48477752
d'	20	Lsup	325	k1	0.523125
As	314	Lcr	3.43848	k2	0.35752688
As'	314	kG	1		
sigma s	500	fR3	3.75	Tc=	339133.852
eps s2	1.50	k0	0.5	Tc/S	1.00
sigma s'	299.33	fFtud	0.61875		
S1=	157000	fib=	86943.8	Mom-cap	
S2=	93991			MRd	27.10

14

fcd	72.5	eps fibmax	20	epsc	1.23
b	1000			x = alfa * h	
h	150	Lin	400	alfa	0.05793688
d	130	Lout	400	x=	8.69053227
d'	20	Lsup	325	k1	0.488925
As	314	Lcr	3.43848	k2	0.3548218
As'	314	kG	1		
sigma s	500	fR3	2.17	Tc=	308053.84
eps s2	1.60	k0	0.5	Tc/S	1.00
sigma s'	320.13	fFtud	0.35805		
S1=	157000	fib=	50595.9	Mom-cap	
S2=	100522			MRd	24.35

15

fcd	68.35	eps fibmax	20	epsc	1.27
b	1000			x = alfa * h	
h	180	Lin	900	alfa	0.05970851
d	150	Lout	550	x=	10.7475317
d'	0	Lsup	450	k1	0.50059167
As	314	Lcr	6.14558	k2	0.35570825
As'	0	kG	1		
sigma s	500	fR3	3.75	Tc=	367731.532
eps s2	0.00	k0	1	Tc/S	1.00
sigma s'	0	fFtud	1.2375		
S1=	157000	fib=	209450	Mom-cap	
S2=	0			MRd	42.13

16

fcd	68.35	eps fibmax	20	epsc	1.33
b	1000			x = alfa * h	
h	150	Lin	900	alfa	0.06235349
d	120	Lout	550	x=	9.35302391
d'	0	Lsup	450	k1	0.51759167
As	314	Lcr	6.14558	k2	0.35706638
As'	0	kG	1		
sigma s	500	fR3	3.75	Tc=	330885.578
eps s2	0.00	k0	1	Tc/S	1.00
sigma s'	0	fFtud	1.2375		
S1=	157000	fib=	174051	Mom-cap	
S2=	0			MRd	31.60

ID	f _{R,3m}	k ₀	k _G	f _{Ftud}	M _{Rd}	Yield line Theory		Strip method		Lab result
						P _{ULS}	Utilization	P _{ULS}	Utilization	
1	3.75	1.0	1.0	1.24	13.48	254.97	80 %	196.13	62 %	318.16
2	2.60	1.0	1.0	0.86	9.40	177.79	86 %	136.76	66 %	206.92
3	2.17	1.0	1.0	0.72	7.87	148.89	56 %	114.53	43 %	267.24
4	3.75	1.0	1.0	1.24	13.48	254.97	91 %	196.13	70 %	280.61
5	3.75	0.5	1.0	0.62	6.81	100.59	53 %	83.82	44 %	190.52
6	2.17	0.5	1.0	0.36	3.97	58.56	36 %	48.80	30 %	163.43
7D	2.91	0.5	1.0	0.48	5.30	78.29	36 %	65.24	30 %	214.96
7S	3.51	0.5	1.0	0.58	6.38	94.24	44 %	78.53	37 %	214.96
8	2.60	0.5	1.0	0.43	4.74	70.02	37 %	58.35	31 %	190.4
9	3.75	0.5	1.0	0.62	6.81	100.59	52 %	83.82	43 %	194.95
10D	2.91	0.5	1.0	0.48	5.30	78.29	38 %	65.24	32 %	205.92
10S	3.51	0.5	1.0	0.58	6.38	94.24	46 %	78.53	38 %	205.92
11	3.75	1.0	1.0	1.24	31.60	597.55	111 %	459.65	85 %	540.68
12	2.17	1.0	1.0	0.72	26.15	494.55	91 %	380.43	70 %	542.58
13	3.75	0.5	1.0	0.62	27.10	400.19	95 %	333.49	79 %	421.64
14	2.17	0.5	1.0	0.36	24.35	359.60	88 %	299.66	74 %	406.9
15	3.75	1.0	1.0	1.24	42.13	749.05	131 %	374.52	65 %	572.6
16	3.75	1.0	1.0	1.24	31.60	561.80	107 %	280.90	53 %	527.44

D.2 Moment capacity - EC2 - Characteristic

1

fcd	45	eps fibmax	20	epsc	0.89
b	1000			x = alfa * h	
h	150	Lin	500	alfa	0.0426041
d	0	Lout	400	x=	6.3906175
d'	0	Lsup	275	k1	0.3789917
As	0	Lcr	3.555635	k2	0.3478474
As'	0	kG	1.255311		
sigma s	0	fR3	1.83	Tc=	108989.59
eps s2	0.00	k0	1	Tc/S	1.00
sigma s'	0	fFtud	0.758082		
S1=	0	fib=	108867.8	Mom-cap	
S2=	0			MRd	8.27

2

fcd	45	eps fibmax	20	epsc	0.815
b	1000			x = alfa * h	
h	150	Lin	500	alfa	0.0391545
d	0	Lout	400	x=	5.8731684
d'	0	Lsup	275	k1	0.3521479
As	0	Lcr	3.555635	k2	0.346432
As'	0	kG	1.256231		
sigma s	0	fR3	1.56	Tc=	93070.081
eps s2	0.00	k0	1	Tc/S	1.00
sigma s'	0	fFtud	0.646708		
S1=	0	fib=	93207.95	Mom-cap	
S2=	0			MRd	7.07

3

fcd	45	eps fibmax	20	epsc	0.69
b	1000			x = alfa * h	
h	150	Lin	500	alfa	0.0333494
d	0	Lout	400	x=	5.0024166
d'	0	Lsup	275	k1	0.305325
As	0	Lcr	3.555635	k2	0.344162
As'	0	kG	1.257779		
sigma s	0	fR3	1.14	Tc=	68731.329
eps s2	0.00	k0	1	Tc/S	1.00
sigma s'	0	fFtud	0.473177		
S1=	0	fib=	68609.46	Mom-cap	
S2=	0			MRd	5.20

4

fcd	45	eps fibmax	20	epsc	0.89
b	1000			x = alfa * h	
h	150	Lin	500	alfa	0.0426041
d	0	Lout	400	x=	6.3906175
d'	0	Lsup	275	k1	0.3789917
As	0	Lcr	3.555635	k2	0.3478474
As'	0	kG	1.255311		
sigma s	0	fR3	1.83	Tc=	108989.59
eps s2	0.00	k0	1	Tc/S	1.00
sigma s'	0	fFtud	0.758082		
S1=	0	fib=	108867.8	Mom-cap	
S2=	0			MRd	8.27

5

fcd	45	eps fibmax	20	epsc	0.61
b	1000			x = alfa * h	
h	150	Lin	400	alfa	0.0295973
d	0	Lout	400	x=	4.4395924
d'	0	Lsup	325	k1	0.2739917
As	0	Lcr	3.438478	k2	0.3427644
As'	0	kG	1.250253		
sigma s	0	fR3	1.83	Tc=	54738.51
eps s2	0.00	k0	0.5	Tc/S	1.00
sigma s'	0	fFtud	0.377514		
S1=	0	fib=	54951.08	Mom-cap	
S2=	0			MRd	4.16

6

fcd	45	eps fibmax	20	epsc	0.477
b	1000			x = alfa * h	
h	150	Lin	400	alfa	0.0232944
d	0	Lout	400	x=	3.4941642
d'	0	Lsup	325	k1	0.2195393
As	0	Lcr	3.438478	k2	0.3405305
As'	0	kG	1.251879		
sigma s	0	fR3	1.14	Tc=	34519.778
eps s2	0.00	k0	0.5	Tc/S	1.00
sigma s'	0	fFtud	0.235478		
S1=	0	fib=	34498.95	Mom-cap	
S2=	0			MRd	2.61

7D

fcd	45	eps fibmax	20	epsc	0.53
b	1000			x = alfa * h	
h	150	Lin	400	alfa	0.0258159
d	0	Lout	400	x=	3.8723819
d'	0	Lsup	325	k1	0.2415917
As	0	Lcr	3.438478	k2	0.3414077
As'	0	kG	1.251228		
sigma s	0	fR3	1.39	Tc=	42099.084
eps s2	0.00	k0	0.5	Tc/S	1.00
sigma s'	0	fFtud	0.286969		
S1=	0	fib=	41934.13	Mom-cap	
S2=	0			MRd	3.17

7S

fcd	45	eps fibmax	20	epsc	0.657
b	1000			x = alfa * h	
h	150	Lin	400	alfa	0.0318052
d	0	Lout	400	x=	4.7707799
d'	0	Lsup	325	k1	0.2925293
As	0	Lcr	3.438478	k2	0.3435804
As'	0	kG	1.249684		
sigma s	0	fR3	2.10	Tc=	62801.67
eps s2	0.00	k0	0.5	Tc/S	1.00
sigma s'	0	fFtud	0.433015		
S1=	0	fib=	62886.49	Mom-cap	
S2=	0			MRd	4.76

8

fcd	45	eps fibmax	20	epsc	0.562
b	1000			x = alfa * h	
h	150	Lin	400	alfa	0.027332
d	0	Lout	400	x=	4.0997957
d'	0	Lsup	325	k1	0.2546797
As	0	Lcr	3.438478	k2	0.3419456
As'	0	kG	1.250837		
sigma s	0	fR3	1.56	Tc=	46986.058
eps s2	0.00	k0	0.5	Tc/S	1.00
sigma s'	0	fFtud	0.321966		
S1=	0	fib=	46974.84	Mom-cap	
S2=	0			MRd	3.55

9

fcd	45	eps fibmax	20	epsc	0.61
b	1000			x = alfa * h	
h	150	Lin	400	alfa	0.0295973
d	0	Lout	400	x=	4.4395924
d'	0	Lsup	325	k1	0.2739917
As	0	Lcr	3.438478	k2	0.3427644
As'	0	kG	1.250253		
sigma s	0	fR3	1.83	Tc=	54738.51
eps s2	0.00	k0	0.5	Tc/S	1.00
sigma s'	0	fFtud	0.377514		
S1=	0	fib=	54951.08	Mom-cap	
S2=	0			MRd	4.16

10D

fcd	45	eps fibmax	20	epsc	0.53
b	1000			x = alfa * h	
h	150	Lin	400	alfa	0.0258159
d	0	Lout	400	x=	3.8723819
d'	0	Lsup	325	k1	0.2415917
As	0	Lcr	3.438478	k2	0.3414077
As'	0	kG	1.251228		
sigma s	0	fR3	1.39	Tc=	42099.084
eps s2	0.00	k0	0.5	Tc/S	1.00
sigma s'	0	fFtud	0.286969		
S1=	0	fib=	41934.13	Mom-cap	
S2=	0			MRd	3.17

10S

fcd	45	eps fibmax	20	epsc	0.657
b	1000			x = alfa * h	
h	150	Lin	400	alfa	0.0318052
d	0	Lout	400	x=	4.7707799
d'	0	Lsup	325	k1	0.2925293
As	0	Lcr	3.438478	k2	0.3435804
As'	0	kG	1.249684		
sigma s	0	fR3	2.10	Tc=	62801.67
eps s2	0.00	k0	0.5	Tc/S	1.00
sigma s'	0	fFtud	0.433015		
S1=	0	fib=	62886.49	Mom-cap	
S2=	0			MRd	4.76

11

fcd	45	eps fibmax	20	epsc	1.49
b	1000			x = alfa * h	
h	150	Lin	500	alfa	0.0693346
d	120	Lout	400	x=	10.400186
d'	0	Lsup	275	k1	0.5599917
As	314	Lcr	3.555635	k2	0.3608647
As'	0	kG	1.248183		
sigma s	500	fR3	1.83	Tc=	262080.79
eps s2	0.00	k0	1	Tc/S	1.00
sigma s'	0	fFtud	0.753778		
S1=	157000	fib=	105227.2	Mom-cap	
S2=	0			MRd	26.29

12

fcd	45	eps fibmax	20	epsc	1.35
b	1000			x = alfa * h	
h	150	Lin	500	alfa	0.0632319
d	120	Lout	400	x=	9.4847775
d'	0	Lsup	275	k1	0.523125
As	314	Lcr	3.555635	k2	0.3575269
As'	0	kG	1.24981		
sigma s	500	fR3	1.14	Tc=	223277.59
eps s2	0.00	k0	1	Tc/S	1.00
sigma s'	0	fFtud	0.470179		
S1=	157000	fib=	66067.26	Mom-cap	
S2=	0			MRd	23.35

13

fcd	45	eps fibmax	20	epsc	1.59
b	1000			x = alfa * h	
h	150	Lin	400	alfa	0.0736452
d	130	Lout	400	x=	11.046781
d'	20	Lsup	325	k1	0.584325
As	314	Lcr	3.438478	k2	0.3633787
As'	314	kG	1.238894		
sigma s	500	fR3	1.83	Tc=	290470.96
eps s2	1.29	k0	0.5	Tc/S	1.00
sigma s'	257.7333	fFtud	0.374084		
S1=	157000	fib=	51980.17	Mom-cap	
S2=	80928.27			MRd	24.33

14

fcd	45	eps fibmax	20	epsc	1.53
b	1000			x = alfa * h	
h	150	Lin	400	alfa	0.0710636
d	130	Lout	400	x=	10.659545
d'	20	Lsup	325	k1	0.569925
As	314	Lcr	3.438478	k2	0.3618568
As'	314	kG	1.23956		
sigma s	500	fR3	1.14	Tc=	273381.35
eps s2	1.34	k0	0.5	Tc/S	1.00
sigma s'	268.1333	fFtud	0.233161		
S1=	157000	fib=	32488.78	Mom-cap	
S2=	84193.87			MRd	22.86

15

fcd	45	eps fibmax	20	epsc	1.47
b	1000			x = alfa * h	
h	180	Lin	900	alfa	0.0684676
d	150	Lout	550	x=	12.324173
d'	0	Lsup	450	k1	0.554925
As	314	Lcr	6.145584	k2	0.3603753
As'	0	kG	1.5		
sigma s	500	fR3	1.83	Tc=	307754.63
eps s2	0.00	k0	1	Tc/S	1.00
sigma s'	0	fFtud	0.90585		
S1=	157000	fib=	151889.1	Mom-cap	
S2=	0			MRd	36.78

16

fcd	45	eps fibmax	20	epsc	1.54
b	1000			x = alfa * h	
h	150	Lin	900	alfa	0.0714949
d	120	Lout	550	x=	10.724234
d'	0	Lsup	450	k1	0.5723667
As	314	Lcr	6.145584	k2	0.3621076
As'	0	kG	1.427965		
sigma s	500	fR3	1.83	Tc=	276218.73
eps s2	0.00	k0	1	Tc/S	1.00
sigma s'	0	fFtud	0.862348		
S1=	157000	fib=	120104.2	Mom-cap	
S2=	0			MRd	27.41

ID	f _{R,3k}	k ₀	k _G	f _{Ftud}	M _{Rd}	Yield line theory		Strip method		Lab result
						P _{ULS}	Utilization	P _{ULS}	Utilization	
1	1.83	1.0	1.26	0.76	8.27	156.41	49 %	120.31	38 %	318.16
2	1.56	1.0	1.26	0.65	7.07	133.77	65 %	102.90	50 %	206.92
3	1.14	1.0	1.26	0.47	5.20	98.32	37 %	75.63	28 %	267.24
4	1.83	1.0	1.26	0.76	8.27	156.41	56 %	120.31	43 %	280.61
5	1.83	0.5	1.25	0.38	4.16	61.43	32 %	51.19	27 %	190.52
6	1.14	0.5	1.25	0.24	2.61	38.50	24 %	32.08	20 %	163.43
7D	1.39	0.5	1.25	0.29	3.17	46.84	22 %	39.03	18 %	214.96
7S	2.10	0.5	1.25	0.43	4.76	70.35	33 %	58.62	27 %	214.96
8	1.56	0.5	1.25	0.32	3.55	52.48	28 %	43.74	23 %	190.4
9	1.83	0.5	1.25	0.38	4.16	61.43	32 %	51.19	26 %	194.95
10D	1.39	0.5	1.25	0.29	3.17	46.84	23 %	39.03	19 %	205.92
10S	2.10	0.5	1.25	0.43	4.76	70.35	34 %	58.62	28 %	205.92
11	1.83	1.0	1.25	0.75	26.29	497.20	92 %	382.46	71 %	540.68
12	1.14	1.0	1.25	0.47	23.35	441.59	81 %	339.68	63 %	542.58
13	1.83	0.5	1.24	0.37	24.33	359.33	85 %	299.44	71 %	421.64
14	1.14	0.5	1.24	0.23	22.86	337.62	83 %	281.35	69 %	406.9
15	1.83	1.0	1.50	0.91	36.78	653.78	114 %	326.89	57 %	572.6
16	1.83	1.0	1.43	0.86	27.41	487.28	92 %	243.64	46 %	527.44

D.3 Moment capacity - NB38 - mean

1

fcd	68.35	eps fibmax	20	epsc	0.985
b	1000			x = alfa * h	
h	150	Lin	500	alfa	0.0469383
d	0	Lout	400	x=	7.0407434
d'	0	Lsup	275	k1	0.4116479
As	0	Lcr	3.555635	k2	0.3497009
As'	0	kG	1		
sigma s	0	fR3	3.75	Tc=	198099.31
eps s2	0.00	k0	1	Tc/S	1.00
sigma s'	0	fFtud	1.3875		
S1=	0	fib=	198356	Mom-cap	
S2=	0			MRd	15.09

2

fcd	67.76	eps fibmax	20	epsc	0.81
b	1000			x = alfa * h	
h	150	Lin	500	alfa	0.0389236
d	0	Lout	400	x=	5.8385392
d'	0	Lsup	275	k1	0.350325
As	0	Lcr	3.555635	k2	0.3463391
As'	0	kG	1		
sigma s	0	fR3	2.60	Tc=	138595.37
eps s2	0.00	k0	1	Tc/S	1.00
sigma s'	0	fFtud	0.962		
S1=	0	fib=	138683.3	Mom-cap	
S2=	0			MRd	10.53

3

fcd	72.50	eps fibmax	20	epsc	0.71
b	1000			x = alfa * h	
h	150	Lin	500	alfa	0.034283
d	0	Lout	400	x=	5.1424433
d'	0	Lsup	275	k1	0.3129917
As	0	Lcr	3.555635	k2	0.344518
As'	0	kG	1		
sigma s	0	fR3	2.17	Tc=	116691.79
eps s2	0.00	k0	1	Tc/S	1.00
sigma s'	0	fFtud	0.8029		
S1=	0	fib=	116306.1	Mom-cap	
S2=	0			MRd	8.82

4

fcd	68.35	eps fibmax	20	epsc	0.985
b	1000			x = alfa * h	
h	150	Lin	500	alfa	0.0469383
d	0	Lout	400	x=	7.0407434
d'	0	Lsup	275	k1	0.4116479
As	0	Lcr	3.555635	k2	0.3497009
As'	0	kG	1		
sigma s	0	fR3	3.75	Tc=	198099.31
eps s2	0.00	k0	1	Tc/S	1.00
sigma s'	0	fFtud	1.3875		
S1=	0	fib=	198356	Mom-cap	
S2=	0			MRd	15.09

5

fcd	68.35	eps fibmax	20	epsc	0.675
b	1000			x = alfa * h	
h	150	Lin	400	alfa	0.0326481
d	0	Lout	400	x=	4.8972189
d'	0	Lsup	325	k1	0.2995313
As	0	Lcr	3.438478	k2	0.3438967
As'	0	kG	1		
sigma s	0	fR3	3.75	Tc=	100260.57
eps s2	0.00	k0	0.5	Tc/S	1.00
sigma s'	0	fFtud	0.69375		
S1=	0	fib=	100665.1	Mom-cap	
S2=	0			MRd	7.63

6

fcd	72.50	eps fibmax	20	epsc	0.49
b	1000			x = alfa * h	
h	150	Lin	400	alfa	0.0239141
d	0	Lout	400	x=	3.5871157
d'	0	Lsup	325	k1	0.2249917
As	0	Lcr	3.438478	k2	0.3407441
As'	0	kG	1		
sigma s	0	fR3	2.17	Tc=	58512.657
eps s2	0.00	k0	0.5	Tc/S	1.00
sigma s'	0	fFtud	0.40145		
S1=	0	fib=	58777.45	Mom-cap	
S2=	0			MRd	4.44

7D

fcd	68.35	eps fibmax	20	epsc	0.59
b	1000			x = alfa * h	
h	150	Lin	400	alfa	0.0286547
d	0	Lout	400	x=	4.298203
d'	0	Lsup	325	k1	0.2659917
As	0	Lcr	3.438478	k2	0.3424214
As'	0	kG	1		
sigma s	0	fR3	2.91	Tc=	78143.611
eps s2	0.00	k0	0.5	Tc/S	1.00
sigma s'	0	fFtud	0.53835		
S1=	0	fib=	78438.56	Mom-cap	
S2=	0			MRd	5.94

7S

fcd	68.35	eps fibmax	20	epsc	0.652
b	1000			x = alfa * h	
h	150	Lin	400	alfa	0.0315708
d	0	Lout	400	x=	4.7356188
d'	0	Lsup	325	k1	0.2905747
As	0	Lcr	3.438478	k2	0.3434929
As'	0	kG	1		
sigma s	0	fR3	3.51	Tc=	94053.076
eps s2	0.00	k0	0.5	Tc/S	1.00
sigma s'	0	fFtud	0.64935		
S1=	0	fib=	94327.43	Mom-cap	
S2=	0			MRd	7.14

8

fcd	67.76	eps fibmax	20	epsc	0.56
b	1000			x = alfa * h	
h	150	Lin	400	alfa	0.0272374
d	0	Lout	400	x=	4.0856031
d'	0	Lsup	325	k1	0.2538667
As	0	Lcr	3.438478	k2	0.3419118
As'	0	kG	1		
sigma s	0	fR3	2.60	Tc=	70280.567
eps s2	0.00	k0	0.5	Tc/S	1.00
sigma s'	0	fFtud	0.481		
S1=	0	fib=	70184.82	Mom-cap	
S2=	0			MRd	5.31

9

fcd	68.35	eps fibmax	20	epsc	0.675
b	1000			x = alfa * h	
h	150	Lin	400	alfa	0.0326481
d	0	Lout	400	x=	4.8972189
d'	0	Lsup	325	k1	0.2995313
As	0	Lcr	3.438478	k2	0.3438967
As'	0	kG	1		
sigma s	0	fR3	3.75	Tc=	100260.57
eps s2	0.00	k0	0.5	Tc/S	1.00
sigma s'	0	fFtud	0.69375		
S1=	0	fib=	100665.1	Mom-cap	
S2=	0			MRd	7.63

10D

fcd	68.35	eps fibmax	20	epsc	0.59
b	1000			x = alfa * h	
h	150	Lin	400	alfa	0.0286547
d	0	Lout	400	x=	4.298203
d'	0	Lsup	325	k1	0.2659917
As	0	Lcr	3.438478	k2	0.3424214
As'	0	kG	1		
sigma s	0	fR3	2.91	Tc=	78143.611
eps s2	0.00	k0	0.5	Tc/S	1.00
sigma s'	0	fFtud	0.53835		
S1=	0	fib=	78438.56	Mom-cap	
S2=	0			MRd	5.94

10S

fcd	68.35	eps fibmax	20	epsc	0.652
b	1000			x = alfa * h	
h	150	Lin	400	alfa	0.0315708
d	0	Lout	400	x=	4.7356188
d'	0	Lsup	325	k1	0.2905747
As	0	Lcr	3.438478	k2	0.3434929
As'	0	kG	1		
sigma s	0	fR3	3.51	Tc=	94053.076
eps s2	0.00	k0	0.5	Tc/S	1.00
sigma s'	0	fFtud	0.64935		
S1=	0	fib=	94327.43	Mom-cap	
S2=	0			MRd	7.14

11

fcd	68.35	eps fibmax	20	epsc	1.38
b	1000			x = alfa * h	
h	150	Lin	500	alfa	0.0645463
d	120	Lout	400	x=	9.6819457
d'	0	Lsup	275	k1	0.5313
As	314	Lcr	3.555635	k2	0.3582251
As'	0	kG	1		
sigma s	500	fR3	3.75	Tc=	351593.61
eps s2	0.00	k0	1	Tc/S	1.00
sigma s'	0	fFtud	1.3875		
S1=	157000	fib=	194691.3	Mom-cap	
S2=	0			MRd	33.16

12

fcd	72.5	eps fibmax	20	epsc	1.14
b	1000			x = alfa * h	
h	150	Lin	500	alfa	0.0539262
d	120	Lout	400	x=	8.0889309
d'	0	Lsup	275	k1	0.4617
As	314	Lcr	3.555635	k2	0.3528807
As'	0	kG	1		
sigma s	500	fR3	2.17	Tc=	270762.81
eps s2	0.00	k0	1	Tc/S	1.00
sigma s'	0	fFtud	0.8029		
S1=	157000	fib=	113940.4	Mom-cap	
S2=	0			MRd	27.07

13

fcd	68.35	eps fibmax	20	epsc	1.37
b	1000			x = alfa * h	
h	150	Lin	400	alfa	0.0641086
d	130	Lout	400	x=	9.6162845
d'	20	Lsup	325	k1	0.5285917
As	314	Lcr	3.438478	k2	0.3579914
As'	314	kG	1		
sigma s	500	fR3	3.75	Tc=	347429.06
eps s2	1.48	k0	0.5	Tc/S	1.00
sigma s'	295.8667	fFtud	0.69375		
S1=	157000	fib=	97391.2	Mom-cap	
S2=	92902.13			MRd	27.88

14

fcd	72.5	eps fibmax	20	epsc	1.24
b	1000			x = alfa * h	
h	150	Lin	400	alfa	0.0583804
d	130	Lout	400	x=	8.7570621
d'	20	Lsup	325	k1	0.4918667
As	314	Lcr	3.438478	k2	0.355042
As'	314	kG	1		
sigma s	500	fR3	2.17	Tc=	312279.76
eps s2	1.59	k0	0.5	Tc/S	1.00
sigma s'	318.4	fFtud	0.40145		
S1=	157000	fib=	56701.98	Mom-cap	
S2=	99977.6			MRd	24.80

15

fcd	68.35	eps fibmax	16.66667	epsc	1.19
b	1000			x = alfa * h	
h	180	Lin	900	alfa	0.0666418
d	150	Lout	550	x=	11.99552
d'	0	Lsup	450	k1	0.4769917
As	314	Lcr	6.145584	k2	0.3539501
As'	0	kG	1		
sigma s	500	fR3	3.75	Tc=	391082.5
eps s2	0.00	k0	1	Tc/S	1.00
sigma s'	0	fFtud	1.3875		
S1=	157000	fib=	233106.2	Mom-cap	
S2=	0			MRd	44.28

16

fcd	68.35	eps fibmax	20	epsc	1.38
b	1000			x = alfa * h	
h	150	Lin	900	alfa	0.0645463
d	120	Lout	550	x=	9.6819457
d'	0	Lsup	450	k1	0.5313
As	314	Lcr	6.145584	k2	0.3582251
As'	0	kG	1		
sigma s	500	fR3	3.75	Tc=	351593.61
eps s2	0.00	k0	1	Tc/S	1.00
sigma s'	0	fFtud	1.3875		
S1=	157000	fib=	194691.3	Mom-cap	
S2=	0			MRd	33.16

ID	f _{R,3m}	k ₀	k _G	f _{Ftud}	M _{Rd}	Yield line theory		Strip method		Lab result
						P _{ULS}	Utilization	P _{ULS}	Utilization	
1	3.75	1.0	1.0	1.39	15.09	285.25	90 %	219.42	69 %	318.16
2	2.60	1.0	1.0	0.96	10.53	199.02	96 %	153.10	74 %	206.92
3	2.17	1.0	1.0	0.80	8.82	166.73	62 %	128.25	48 %	267.24
4	3.75	1.0	1.0	1.39	15.09	285.25	102 %	219.42	78 %	280.61
5	3.75	0.5	1.0	0.69	7.63	112.62	59 %	93.85	49 %	190.52
6	2.17	0.5	1.0	0.40	4.44	65.59	40 %	54.66	33 %	163.43
7D	2.91	0.5	1.0	0.54	5.94	87.66	41 %	73.05	34 %	214.96
7S	3.51	0.5	1.0	0.65	7.14	105.51	49 %	87.92	41 %	214.96
8	2.60	0.5	1.0	0.48	5.31	78.42	41 %	65.35	34 %	190.4
9	3.75	0.5	1.0	0.69	7.63	112.62	58 %	93.85	48 %	194.95
10D	2.91	0.5	1.0	0.54	5.94	87.66	43 %	73.05	35 %	205.92
10S	3.51	0.5	1.0	0.65	7.14	105.51	51 %	87.92	43 %	205.92
11	3.75	1.0	1.0	1.39	33.16	627.10	116 %	482.38	89 %	540.68
12	2.17	1.0	1.0	0.80	27.07	511.91	94 %	393.78	73 %	542.58
13	3.75	0.5	1.0	0.69	27.88	411.78	98 %	343.15	81 %	421.64
14	2.17	0.5	1.0	0.40	24.80	366.32	90 %	305.27	75 %	406.9
15	3.75	1.0	1.0	1.39	44.28	787.18	137 %	393.59	69 %	572.6
16	3.75	1.0	1.0	1.39	33.16	589.58	112 %	294.79	56 %	527.44

D.4 Moment capacity - NB38 - Characteristic

1

fcd	45	eps fibmax	20	epsc	0.835
b	1000			x = alfa * h	
h	150	Lin	500	alfa	0.0400768
d	0	Lout	400	x=	6.0115191
d'	0	Lsup	275	k1	0.3593979
As	0	Lcr	3.555635	k2	0.3468054
As'	0	kG	1		
sigma s	0	fR3	1.83	Tc=	97223.734
eps s2	0.00	k0	1	Tc/S	1.00
sigma s'	0	fFtud	0.6771		
S1=	0	fib=	97494.6	Mom-cap	
S2=	0			MRd	7.40

2

fcd	45	eps fibmax	20	epsc	0.765
b	1000			x = alfa * h	
h	150	Lin	500	alfa	0.0368408
d	0	Lout	400	x=	5.5261257
d'	0	Lsup	275	k1	0.3337313
As	0	Lcr	3.555635	k2	0.345511
As'	0	kG	1		
sigma s	0	fR3	1.56	Tc=	82990.838
eps s2	0.00	k0	1	Tc/S	1.00
sigma s'	0	fFtud	0.5772		
S1=	0	fib=	83390.32	Mom-cap	
S2=	0			MRd	6.32

3

fcd	45	eps fibmax	20	epsc	0.65
b	1000			x = alfa * h	
h	150	Lin	500	alfa	0.031477
d	0	Lout	400	x=	4.7215496
d'	0	Lsup	275	k1	0.2897917
As	0	Lcr	3.555635	k2	0.3434579
As'	0	kG	1		
sigma s	0	fR3	1.14	Tc=	61571.958
eps s2	0.00	k0	1	Tc/S	1.00
sigma s'	0	fFtud	0.4218		
S1=	0	fib=	61278.45	Mom-cap	
S2=	0			MRd	4.64

4

fcd	45	eps fibmax	20	epsc	0.835
b	1000			x = alfa * h	
h	150	Lin	500	alfa	0.0400768
d	0	Lout	400	x=	6.0115191
d'	0	Lsup	275	k1	0.3593979
As	0	Lcr	3.555635	k2	0.3468054
As'	0	kG	1		
sigma s	0	fR3	1.83	Tc=	97223.734
eps s2	0.00	k0	1	Tc/S	1.00
sigma s'	0	fFtud	0.6771		
S1=	0	fib=	97494.6	Mom-cap	
S2=	0			MRd	7.40

5

fcd	45	eps fibmax	20	epsc	0.577
b	1000			x = alfa * h	
h	150	Lin	400	alfa	0.028041
d	0	Lout	400	x=	4.2061525
d'	0	Lsup	325	k1	0.2607559
As	0	Lcr	3.438478	k2	0.3421999
As'	0	kG	1		
sigma s	0	fR3	1.83	Tc=	49355.062
eps s2	0.00	k0	0.5	Tc/S	1.00
sigma s'	0	fFtud	0.33855		
S1=	0	fib=	49358.51	Mom-cap	
S2=	0			MRd	3.73

6

fcd	45	eps fibmax	20	epsc	0.45
b	1000			x = alfa * h	
h	150	Lin	400	alfa	0.0220049
d	0	Lout	400	x=	3.3007335
d'	0	Lsup	325	k1	0.208125
As	0	Lcr	3.438478	k2	0.3400901
As'	0	kG	1		
sigma s	0	fR3	1.14	Tc=	30913.432
eps s2	0.00	k0	0.5	Tc/S	1.00
sigma s'	0	fFtud	0.2109		
S1=	0	fib=	30938.88	Mom-cap	
S2=	0			MRd	2.34

7D

fcd	45	eps fibmax	20	epsc	0.5
b	1000			x = alfa * h	
h	150	Lin	400	alfa	0.0243902
d	0	Lout	400	x=	3.6585366
d'	0	Lsup	325	k1	0.2291667
As	0	Lcr	3.438478	k2	0.3409091
As'	0	kG	1		
sigma s	0	fR3	1.39	Tc=	37728.659
eps s2	0.00	k0	0.5	Tc/S	1.00
sigma s'	0	fFtud	0.25715		
S1=	0	fib=	37631.71	Mom-cap	
S2=	0			MRd	2.84

7S

fcd	45	eps fibmax	20	epsc	0.62
b	1000			x = alfa * h	
h	150	Lin	400	alfa	0.0300679
d	0	Lout	400	x=	4.5101843
d'	0	Lsup	325	k1	0.2779667
As	0	Lcr	3.438478	k2	0.3429368
As'	0	kG	1		
sigma s	0	fR3	2.10	Tc=	56415.64
eps s2	0.00	k0	0.5	Tc/S	1.00
sigma s'	0	fFtud	0.3885		
S1=	0	fib=	56522.79	Mom-cap	
S2=	0			MRd	4.28

8

fcd	45	eps fibmax	20	epsc	0.53
b	1000			x = alfa * h	
h	150	Lin	400	alfa	0.0258159
d	0	Lout	400	x=	3.8723819
d'	0	Lsup	325	k1	0.2415917
As	0	Lcr	3.438478	k2	0.3414077
As'	0	kG	1		
sigma s	0	fR3	1.56	Tc=	42099.084
eps s2	0.00	k0	0.5	Tc/S	1.00
sigma s'	0	fFtud	0.2886		
S1=	0	fib=	42172.43	Mom-cap	
S2=	0			MRd	3.19

9

fcd	45	eps fibmax	20	epsc	0.577
b	1000			x = alfa * h	
h	150	Lin	400	alfa	0.028041
d	0	Lout	400	x=	4.2061525
d'	0	Lsup	325	k1	0.2607559
As	0	Lcr	3.438478	k2	0.3421999
As'	0	kG	1		
sigma s	0	fR3	1.83	Tc=	49355.062
eps s2	0.00	k0	0.5	Tc/S	1.00
sigma s'	0	fFtud	0.33855		
S1=	0	fib=	49358.51	Mom-cap	
S2=	0			MRd	3.73

10D

fcd	45	eps fibmax	20	epsc	0.5
b	1000			x = alfa * h	
h	150	Lin	400	alfa	0.0243902
d	0	Lout	400	x=	3.6585366
d'	0	Lsup	325	k1	0.2291667
As	0	Lcr	3.438478	k2	0.3409091
As'	0	kG	1		
sigma s	0	fR3	1.39	Tc=	37728.659
eps s2	0.00	k0	0.5	Tc/S	1.00
sigma s'	0	fFtud	0.25715		
S1=	0	fib=	37631.71	Mom-cap	
S2=	0			MRd	2.84

10S

fcd	45	eps fibmax	20	epsc	0.62
b	1000			x = alfa * h	
h	150	Lin	400	alfa	0.0300679
d	0	Lout	400	x=	4.5101843
d'	0	Lsup	325	k1	0.2779667
As	0	Lcr	3.438478	k2	0.3429368
As'	0	kG	1		
sigma s	0	fR3	2.10	Tc=	56415.64
eps s2	0.00	k0	0.5	Tc/S	1.00
sigma s'	0	fFtud	0.3885		
S1=	0	fib=	56522.79	Mom-cap	
S2=	0			MRd	4.28

11

fcd	45	eps fibmax	20	epsc	1.45
b	1000			x = alfa * h	
h	150	Lin	500	alfa	0.0675991
d	120	Lout	400	x=	10.13986
d'	0	Lsup	275	k1	0.5497917
As	314	Lcr	3.555635	k2	0.3598901
As'	0	kG	1		
sigma s	500	fR3	1.83	Tc=	250866.48
eps s2	0.00	k0	1	Tc/S	1.00
sigma s'	0	fFtud	0.6771		
S1=	157000	fib=	94699.3	Mom-cap	
S2=	0			MRd	25.50

12

fcd	45	eps fibmax	20	epsc	1.325
b	1000			x = alfa * h	
h	150	Lin	500	alfa	0.0621336
d	120	Lout	400	x=	9.3200469
d'	0	Lsup	275	k1	0.5161979
As	314	Lcr	3.555635	k2	0.3569519
As'	0	kG	1		
sigma s	500	fR3	1.14	Tc=	216494.5
eps s2	0.00	k0	1	Tc/S	1.00
sigma s'	0	fFtud	0.4218		
S1=	157000	fib=	59338.8	Mom-cap	
S2=	0			MRd	22.85

13

fcd	45	eps fibmax	20	epsc	1.57
b	1000			x = alfa * h	
h	150	Lin	400	alfa	0.0727863
d	130	Lout	400	x=	10.917942
d'	20	Lsup	325	k1	0.5795917
As	314	Lcr	3.438478	k2	0.3628668
As'	314	kG	1		
sigma s	500	fR3	1.83	Tc=	284757.66
eps s2	1.31	k0	0.5	Tc/S	1.00
sigma s'	261.2	fFtud	0.33855		
S1=	157000	fib=	47086.23	Mom-cap	
S2=	82016.8			MRd	23.95

14

fcd	45	eps fibmax	20	epsc	1.52
b	1000			x = alfa * h	
h	150	Lin	400	alfa	0.070632
d	130	Lout	400	x=	10.594796
d'	20	Lsup	325	k1	0.5674667
As	314	Lcr	3.438478	k2	0.3616071
As'	314	kG	1		
sigma s	500	fR3	1.14	Tc=	270548.7
eps s2	1.35	k0	0.5	Tc/S	1.00
sigma s'	269.8667	fFtud	0.2109		
S1=	157000	fib=	29400.56	Mom-cap	
S2=	84738.13			MRd	22.63

15	fcd	45	eps fibmax	16.66667	epsc	1.225
	b	1000			x = alfa * h	
	h	180	Lin	900	alfa	0.0684676
	d	150	Lout	550	x=	12.324173
	d'	0	Lsup	450	k1	0.4874479
	As	314	Lcr	6.145584	k2	0.354712
	As'	0	kG	1		
	sigma s	500	fR3	1.83	Tc=	270332.67
	eps s2	0.00	k0	1	Tc/S	1.00
	sigma s'	0	fFtud	0.6771		
	S1=	157000	fib=	113533.3	Mom-cap	
	S2=	0			MRd	33.28

16	fcd	45	eps fibmax	20	epsc	1.45
	b	1000			x = alfa * h	
	h	150	Lin	900	alfa	0.0675991
	d	120	Lout	550	x=	10.13986
	d'	0	Lsup	450	k1	0.5497917
	As	314	Lcr	6.145584	k2	0.3598901
	As'	0	kG	1		
	sigma s	500	fR3	1.83	Tc=	250866.48
	eps s2	0.00	k0	1	Tc/S	1.00
	sigma s'	0	fFtud	0.6771		
	S1=	157000	fib=	94699.3	Mom-cap	
	S2=	0			MRd	25.50

ID	f _{R,3k}	k ₀	k _G	f _{Ftud}	M _{Rd}	Yield line theory		Strip method		Lab result
						P _{ULS}	Utilization	P _{ULS}	Utilization	
1	1.83	1.0	1.00	0.68	7.40	139.94	44 %	107.65	34 %	318.16
2	1.56	1.0	1.00	0.58	6.32	119.58	58 %	91.99	44 %	206.92
3	1.14	1.0	1.00	0.42	4.64	87.78	33 %	67.52	25 %	267.24
4	1.83	1.0	1.00	0.68	7.40	139.94	50 %	107.65	38 %	280.61
5	1.83	0.5	1.00	0.34	3.73	55.16	29 %	45.96	24 %	190.52
6	1.14	0.5	1.00	0.21	2.34	34.51	21 %	28.76	18 %	163.43
7D	1.39	0.5	1.00	0.26	2.84	42.01	20 %	35.01	16 %	214.96
7S	2.10	0.5	1.00	0.39	4.28	63.20	29 %	52.66	24 %	214.96
8	1.56	0.5	1.00	0.29	3.19	47.09	25 %	39.24	21 %	190.4
9	1.83	0.5	1.00	0.34	3.73	55.16	28 %	45.96	24 %	194.95
10D	1.39	0.5	1.00	0.26	2.84	42.01	20 %	35.01	17 %	205.92
10S	2.10	0.5	1.00	0.39	4.28	63.20	31 %	52.66	26 %	205.92
11	1.83	1.0	1.00	0.68	25.50	482.16	89 %	370.89	69 %	540.68
12	1.14	1.0	1.00	0.42	22.85	432.04	80 %	332.34	61 %	542.58
13	1.83	0.5	1.00	0.34	23.95	353.74	84 %	294.78	70 %	421.64
14	1.14	0.5	1.00	0.21	22.63	334.17	82 %	278.47	68 %	406.9
15	1.83	1.0	1.00	0.68	33.28	591.70	103 %	295.85	52 %	572.6
16	1.83	1.0	1.00	0.68	25.50	453.31	86 %	226.65	43 %	527.44

E Calculated ultimate load

E.1 Ultimate load with yield line theory

Yield Line Theory

Moment obtained from EC, using mean strength values
Calculation of moment with k_0 and without k_G

Plate 1,2,3,4,11 and 12:

$$L := 1.3 \text{ m}$$

$$i = 1, 2, 3, 4, 11, 12$$

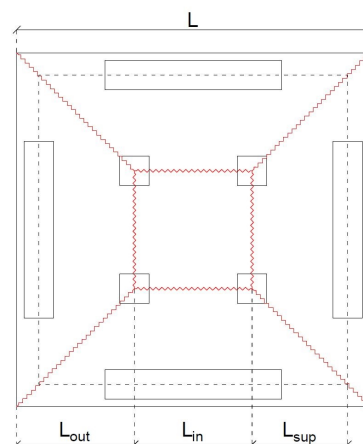
$$L_{out} := 0.4 \text{ m}$$

$$L_{in} := 0.5 \text{ m}$$

$$L_{sup} := 0.275 \text{ m}$$

$$w := 1 \text{ m} \quad (\text{Dummy})$$

$$m_{Rd,i} := \begin{bmatrix} 13.48 \\ 9.40 \\ 7.87 \\ 13.48 \\ 31.60 \\ 26.15 \end{bmatrix} \frac{\text{kN} \cdot \text{m}}{\text{m}}$$



External work:

$$W_{ext} = P \cdot w$$

Internal work:

$$W_{int} = M \cdot \theta = m_{Rd,i} \cdot L \cdot \theta$$

$$W_{int} := m_{Rd,i} \cdot \left(8 \cdot L_{out} \cdot \frac{w}{L_{sup}} + 4 \cdot L_{in} \cdot \frac{w}{L_{sup}} \right) = \begin{bmatrix} 254.89 \\ 177.75 \\ 148.81 \\ 254.89 \\ 597.53 \\ 494.47 \end{bmatrix} \text{ kN} \cdot \text{m}$$

Set external work equal internal work:

$$W_{ext} = W_{int}$$

$$P := \frac{W_{int}}{w} = \begin{bmatrix} 254.89 \\ 177.75 \\ 148.81 \\ 254.89 \\ 597.53 \\ 494.47 \end{bmatrix} \text{ kN} \quad \begin{bmatrix} ID1 \\ ID2 \\ ID3 \\ ID4 \\ ID11 \\ ID12 \end{bmatrix}$$

Yield Line Theory

Moment obtained from EC, using mean strength values

Calculation of moment with k_0 and without k_G

Plate 5,6,7,8,9,10,13 and 14:

$$L := 1.2 \text{ m}$$

$$i = 5, 6, 7 D, 7 S, 8, 9, 10 D, 10 S, 13, 14$$

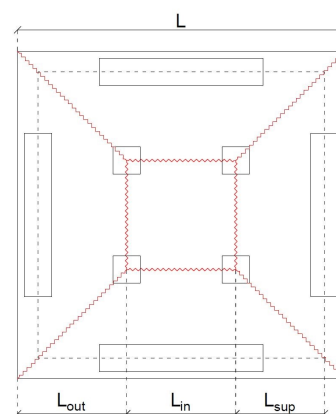
$$L_{out} := 0.4 \text{ m}$$

$$L_{in} := 0.4 \text{ m}$$

$$L_{sup} := 0.325 \text{ m}$$

$$w := 1 \text{ m} \quad (\text{Dummy})$$

$$m_{Rd,i} := \begin{bmatrix} 6.81 \\ 3.97 \\ 5.30 \\ 6.38 \\ 4.74 \\ 6.81 \\ 5.30 \\ 6.38 \\ 27.10 \\ 24.35 \end{bmatrix} \frac{kN \cdot m}{m}$$



External work:

$$W_{ext} = P \cdot w$$

Internal work:

$$W_{int} = M \cdot \theta = m_{Rd,i} \cdot L \cdot \theta$$

$$W_{int} := m_{Rd,i} \cdot \left(8 \cdot L_{out} \cdot \frac{w}{L_{sup}} + 4 \cdot L_{in} \cdot \frac{w}{L_{sup}} \right) = \begin{bmatrix} 100.58 \\ 58.63 \\ 78.28 \\ 94.23 \\ 70.01 \\ 100.58 \\ 78.28 \\ 94.23 \\ 400.25 \\ 359.63 \end{bmatrix} kN \cdot m$$

Set external work equal internal work:

$$W_{ext} = W_{int}$$

$$P := \frac{W_{int}}{w} = \begin{bmatrix} 100.58 \\ 58.63 \\ 78.28 \\ 94.23 \\ 70.01 \\ 100.58 \\ 78.28 \\ 94.23 \\ 400.25 \\ 359.63 \end{bmatrix} kN \quad \begin{bmatrix} ID5 \\ ID6 \\ ID7D \\ ID7S \\ ID8 \\ ID9 \\ ID10D \\ ID10S \\ ID13 \\ ID14 \end{bmatrix}$$

Yield Line Theory

Moment obtained from EC, using mean strength values
 Calculation of moment with k_0 and without k_G

Plate 15 and 16:

$$L := 2.0 \text{ m}$$

$$i = 15, 16$$

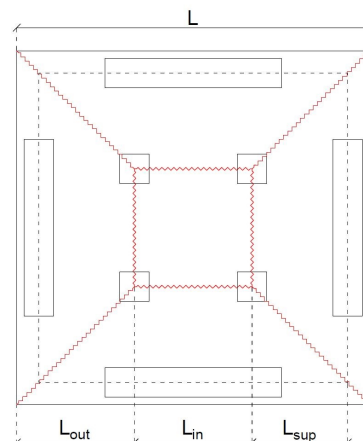
$$L_{out} := 0.55 \text{ m}$$

$$L_{in} := 0.90 \text{ m}$$

$$L_{sup} := 0.45 \text{ m}$$

$$w := 1 \text{ m} \quad (\text{Dummy})$$

$$m_{Rd,i} := \begin{bmatrix} 42.13 \\ 31.60 \end{bmatrix} \frac{\text{kN} \cdot \text{m}}{\text{m}}$$



External work:

$$W_{ext} = P \cdot w$$

Internal work:

$$W_{int} = M \cdot \theta = m_{Rd,i} \cdot L \cdot \theta$$

$$W_{int} := m_{Rd,i} \cdot \left(8 \cdot L_{out} \cdot \frac{w}{L_{sup}} + 4 \cdot L_{in} \cdot \frac{w}{L_{sup}} \right) = \begin{bmatrix} 748.98 \\ 561.78 \end{bmatrix} \text{ kN} \cdot \text{m}$$

Set external work equal internal work:

$$W_{ext} = W_{int}$$

$$P := \frac{W_{int}}{w} = \begin{bmatrix} 748.98 \\ 561.78 \end{bmatrix} \text{ kN} \quad \begin{bmatrix} ID15 \\ ID16 \end{bmatrix}$$

E.2 Ultimate load with strip method

Strip method

Moment obtained from EC, using mean strength values

Calculation of moment with k_0 and without k_G

Plate 1,2,3,4,11 and 12:

$$L := 1.3 \text{ m}$$

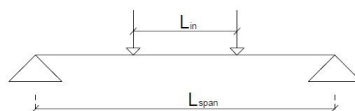
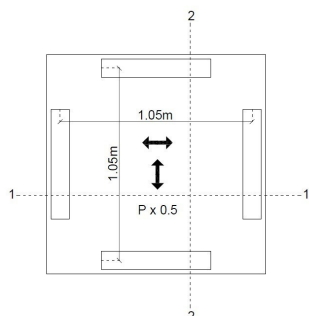
$$i = 1, 2, 3, 4, 11, 12$$

$$L_{out} := 0.4 \text{ m}$$

$$L_{in} := 0.5 \text{ m}$$

$$L_{span} := 1.05 \text{ m}$$

$$m_{Rd,i} := \begin{bmatrix} 13.48 \\ 9.40 \\ 7.87 \\ 13.48 \\ 31.60 \\ 26.15 \end{bmatrix} \frac{\text{kN} \cdot \text{m}}{\text{m}}$$



$$\gamma := 0.5$$

$$0 \leq \gamma \leq 1.0$$

In this case half the load is allocated uniformly to the strips in each direction, as indicated by the dispersion arrows in the figure.

Ultimate load:

$$m_{Rd,i} = \frac{(P \cdot \gamma)}{2} \cdot \frac{L_{span}}{2} - \frac{(P \cdot \gamma)}{2} \cdot \frac{L_{in}}{2}$$

$$m_{Rd,i} = \frac{(P \cdot \gamma)}{4} \cdot (L_{span} - L_{in})$$

$$P := \frac{4 \cdot m_{Rd,i}}{(L_{span} - L_{in}) \cdot \gamma} = \begin{bmatrix} 196.07 \\ 136.73 \\ 114.47 \\ 196.07 \\ 459.64 \\ 380.36 \end{bmatrix} \text{ kN} \quad \begin{bmatrix} ID1 \\ ID2 \\ ID3 \\ ID4 \\ ID11 \\ ID12 \end{bmatrix}$$

Since the plates are symmetric about both axis, it is reasonable that ultimate load is equal for both strip 1-1 and strip 2-2

Strip method

Moment obtained from EC, using mean strength values

Calculation of moment with k_0 and without k_G

Plate 5,6,7,8,9,10,13 and 14:

$$L := 1.2 \text{ m}$$

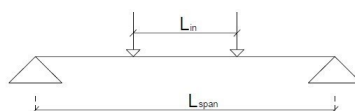
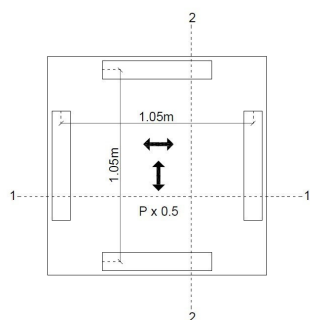
$$i = 5, 6, 7 D, 7 S, 8, 9, 10 D, 10 S, 13, 14$$

$$L_{out} := 0.4 \text{ m}$$

$$L_{in} := 0.4 \text{ m}$$

$$L_{span} := 1.05 \text{ m}$$

$$m_{Rd,i} := \begin{bmatrix} 6.81 \\ 3.97 \\ 5.30 \\ 6.38 \\ 4.74 \\ 6.81 \\ 5.30 \\ 6.38 \\ 27.10 \\ 24.35 \end{bmatrix} \frac{\text{kN} \cdot \text{m}}{\text{m}}$$



$$\gamma := 0.5$$

$$0 \leq \gamma \leq 1.0$$

In this case half the load is allocated uniformly to the strips in each direction, as indicated by the dispersion arrows in the figure.

Ultimate load:

$$m_{Rd,i} = \frac{(P \cdot \gamma)}{2} \cdot \frac{L_{span}}{2} - \frac{(P \cdot \gamma)}{2} \cdot \frac{L_{in}}{2}$$

$$m_{Rd,i} = \frac{(P \cdot \gamma)}{4} \cdot (L_{span} - L_{in})$$

$$P := \frac{4 \cdot m_{Rd,i}}{(L_{span} - L_{in}) \cdot \gamma} = \begin{bmatrix} 83.82 \\ 48.86 \\ 65.23 \\ 78.52 \\ 58.34 \\ 83.82 \\ 65.23 \\ 78.52 \\ 333.54 \\ 299.69 \end{bmatrix} \text{ kN} \quad \begin{bmatrix} ID5 \\ ID6 \\ ID7D \\ ID7S \\ ID8 \\ ID9 \\ ID10D \\ ID10S \\ ID13 \\ ID14 \end{bmatrix}$$

Since the plates are symmetric about both axis, it is reasonable that ultimate load is equal for both strip 1-1 and strip 2-2

Strip method

Moment obtained from EC, using mean strength values
 Calculation of moment with k_0 and without k_G

Plate 15 and 16:

$$L := 2.0 \text{ m}$$

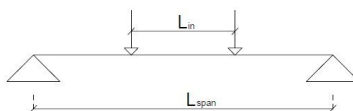
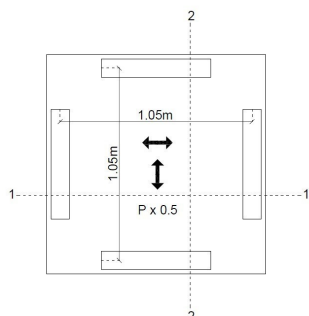
$$i = 15, 16$$

$$L_{out} := 0.55 \text{ m}$$

$$L_{in} := 0.90 \text{ m}$$

$$L_{span} := 1.80 \text{ m}$$

$$m_{Rd,i} := \begin{bmatrix} 42.13 \\ 31.60 \end{bmatrix} \frac{\text{kN} \cdot \text{m}}{\text{m}}$$



$$\gamma := 0.5$$

$$0 \leq \gamma \leq 1.0$$

In this case half the load is allocated uniformly to the strips in each direction, as indicated by the dispersion arrows in the figure.

Ultimate load:

$$m_{Rd,i} = \frac{(P \cdot \gamma)}{2} \cdot \frac{L_{span}}{2} - \frac{(P \cdot \gamma)}{2} \cdot \frac{L_{in}}{2}$$

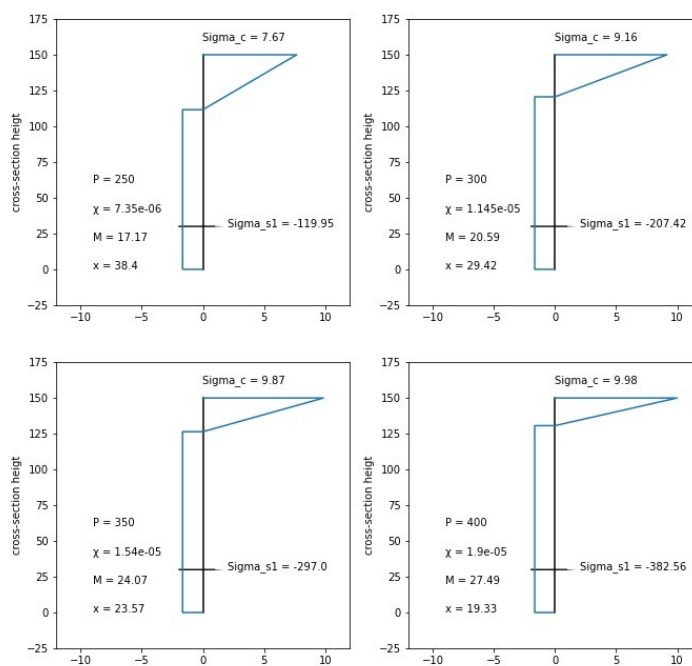
$$m_{Rd,i} = \frac{(P \cdot \gamma)}{4} \cdot (L_{span} - L_{in})$$

$$P := \frac{4 \cdot m_{Rd,i}}{(L_{span} - L_{in}) \cdot \gamma} = \begin{bmatrix} 374.49 \\ 280.89 \end{bmatrix} \text{ kN} \quad \begin{bmatrix} ID15 \\ ID16 \end{bmatrix}$$

Since the plates are symmetric about both axis, it is reasonable that ultimate load is equal for both strip 1-1 and strip 2-2

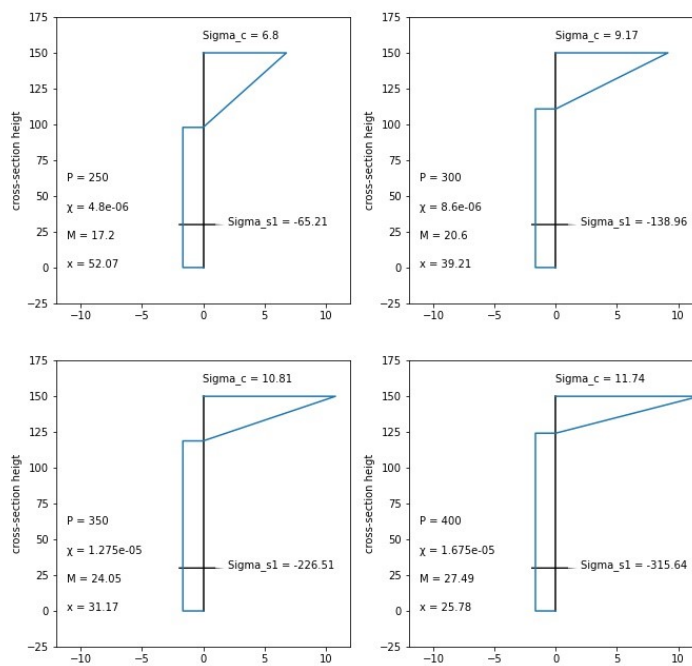
F Crack width calculation

Stress distribution in SLS according to EC2



Reinforcement stress in plate ID-11

Stress distribution in SLS according to NB38



Reinforcement stress in plate ID-11

F.1 Crack Width Calculation - EC2 - 250 kN loading

Calculation of crack width according to EC2

Element 11 - with 250 kN loading

Calculations of crack width only applies for elements with conventional reinforcement according to EC2

Dimensions:

$b := 1000 \text{ mm}$	One meter plate-strip
$l := 1300 \text{ mm}$	Plate length
$h := 150 \text{ mm}$	Plate thickness
$c := 25 \text{ mm}$	Cover

Conventional Reinforcement:

$f_{yk} := 500 \text{ MPa}$	
$n := 4$	Number of bars
$A_s := n \cdot 78.5 = 314 \text{ mm}^2$	Effective reinforcement area ($\phi 10cc250$)
$\phi := 10 \text{ mm}$	Bar diameter
$s := 250 \text{ mm}$	Spacing between bars
$E_s := 200000 \text{ MPa}$	Modulus of elasticity

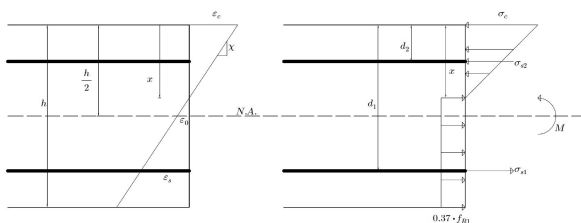
FRC properties:

$f_{ck} := 60.35 \text{ MPa}$	$f_{R.3m} := 3.75 \text{ MPa}$	$E_{cm} := 27189 \text{ MPa}$
$f_{ctm} := 4.31 \text{ MPa}$		
$f_{ct,eff} := f_{ctm} = 4.31 \text{ MPa}$		

Cross-section:

$x := 38 \text{ mm}$	$\sigma_c := 7.7 \text{ MPa}$	$\sigma_s := 120.0 \text{ MPa}$
----------------------	-------------------------------	---------------------------------

$$d := h - c - \frac{\phi}{2} = 120 \text{ mm} \quad z := d - \frac{1}{3} x = 107 \text{ mm}$$



Factor accounting for variation in fibre orientation:

$$\kappa_0 := 1.0$$

Mean residual tensile strength:

$$f_{Ftu.m} := \kappa_0 \cdot 0.33 \cdot f_{R.3m} = 1.24 \text{ MPa}$$

$$f_{R.3m} \text{ replaces the } \frac{f_{R.3k} \cdot \kappa_G}{\gamma_{SF}} \text{ in design residual tensile strength}$$

Uncracked cross-section:

$$A_c := b \cdot h = 150000 \text{ mm}^2$$

$$\eta := \frac{E_s}{E_{cm}} = 7.356$$

$$\alpha d := \frac{A_c \cdot 0.5 \cdot h + \eta \cdot A_s \cdot d}{A_c + \eta \cdot A_s} = 75.68 \text{ mm}$$

$$I_{cl} := \frac{b \cdot h^3}{12} + b \cdot h \cdot \left(\alpha d - \frac{h}{2} \right)^2 = 2.813 \cdot 10^8 \text{ mm}^2$$

$$I_{sl} := A_s \cdot (d - \alpha d)^2 = 6.167 \cdot 10^5 \text{ mm}^4$$

$$M_{cr} := \frac{I_{cl} + \eta \cdot I_{sl}}{h - \alpha d} \cdot f_{ctm} \cdot 10^{-6} = 16.58 \text{ kNm}$$

Minimum reinforcement:

$$k_h := 0.8 - 0.6 \cdot \frac{\min(b, h)}{1000} - 0.3 = 0.41 \quad \text{Use: } k_h := 0.5 \quad (\text{Requirements: } 0.5 - 0.8)$$

$$M_{R.min} \geq M_{cr}$$

$$M_{R.min} = f_{yk} \cdot A_{s.min} \cdot z + 0.4 f_{Ftu.m} \cdot b \cdot h^2$$

$$A_{s.min.1} := \frac{M_{cr} \cdot 10^6 - 0.4 f_{Ftu.m} \cdot b \cdot h^2}{f_{yk} \cdot z} = 101.38 \text{ mm}^2$$

$$A_{s.min.2} := \frac{0.2 k_h \cdot f_{ct.eff} \cdot A_c}{f_{yk}} = 129.3 \text{ mm}^2$$

$$A_{s.min} := \max(A_{s.min.1}, A_{s.min.2}) = 129.3 \text{ mm}^2$$

$$A_s \geq A_{s.min} \quad \rightarrow \text{OK}$$

Calculation of crack width:

Factor converting the mean crack width into a calculated crack width:

$$k_w := 1.3$$

Coefficient to account for the increase of crack width due to curvature:

$$a_{y,i} := c + \frac{\phi}{2} = 30 \text{ mm}$$

$$k_{1r} := \frac{h-x}{h-a_{y,i}-x} = 1.37 \quad (\text{one face in tension})$$

Tensile reinforcement ratio accounting for the different bond properties of reinforcing bars, referred to the effective concrete area:

$$h_{c,eff} := \min\left(c + 5\phi, 10\phi, 3.5c, h-x, \frac{h}{2}\right) = 75 \text{ mm} \quad (\text{single layer of bars})$$

$$b_{c,eff} := 4 \cdot 10\phi = 400 \text{ mm} \quad \text{Effective width (pr meter)}$$

$$A_{c,eff} := b_{c,eff} \cdot h_{c,eff} = 30000 \text{ mm}^2 \quad \text{Effective area (pr meter)}$$

$$\rho_{s,eff} := \frac{A_s}{A_{c,eff}} = 0.01$$

Mean crack spacing:

$$\text{For } s > 10\phi \quad s_{r,m,cal,F} := h-x = 112 \text{ mm}$$

The stress is equal to the design residual tensile strength for $CMOD_1$:

$$\sigma_s = 120 \text{ MPa}$$

$$k_t := 0.6 \quad (\text{Short term loading})$$

$$\alpha_e := \frac{E_s}{E_{cm}} = 7.36$$

Plates subjected to direct loads and stabilized cracking, where end restraint dominates, $\Delta\varepsilon$ may be determined as:

$$\Delta\varepsilon = \varepsilon_{sm} - \varepsilon_{cm}$$

$$\varepsilon_{dif,1} := \frac{\sigma_s - k_t \cdot \frac{f_{ct,eff}}{\rho_{s,eff}} \cdot (1 + \alpha_e \cdot \rho_{s,eff})}{E_s} = -0.00073 \quad \text{or} \quad \varepsilon_{dif,2} := (1 - k_t) \frac{\sigma_s}{E_s} = 0.00024$$

$$\Delta\varepsilon := \max(\varepsilon_{dif,1}, \varepsilon_{dif,2}) = 0.00024$$

Crack width:

$$w_{k.cal.F} := k_w \cdot k_{1r} \cdot s_{r.m.cal.F} \cdot \Delta\varepsilon = 0.048 \text{ mm}$$

Crack width limit:

$$\sigma_c = 7.7 \text{ MPa}$$

Stress for concrete

$$0.6 f_{ck} = 36.21 \text{ MPa}$$

$$\sigma_c \leq 0.6 f_{ck} \quad \rightarrow \text{OK}$$

F.2 Crack Width Calculation - EC2 - 300 kN loading

Calculation of crack width according to EC2

Element 11 - with 300 kN loading

Calculations of crack width only applies for elements with conventional reinforcement according to EC2

Dimensions:

$b := 1000 \text{ mm}$	One meter plate-strip
$l := 1300 \text{ mm}$	Plate length
$h := 150 \text{ mm}$	Plate thickness
$c := 25 \text{ mm}$	Cover

Conventional Reinforcement:

$f_{yk} := 500 \text{ MPa}$	
$n := 4$	Number of bars
$A_s := n \cdot 78.5 = 314 \text{ mm}^2$	Effective reinforcement area ($\phi 10cc250$)
$\phi := 10 \text{ mm}$	Bar diameter
$s := 250 \text{ mm}$	Spacing between bars
$E_s := 200000 \text{ MPa}$	Modulus of elasticity

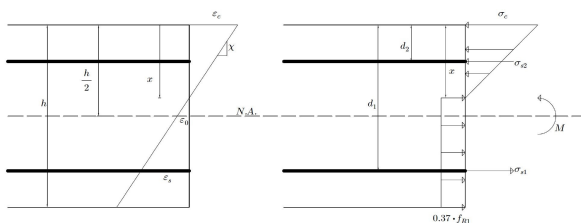
FRC properties:

$f_{ck} := 60.35 \text{ MPa}$	$f_{R.3m} := 3.75 \text{ MPa}$	$E_{cm} := 27189 \text{ MPa}$
$f_{ctm} := 4.31 \text{ MPa}$		
$f_{ct,eff} := f_{ctm} = 4.31 \text{ MPa}$		

Cross-section:

$x := 29 \text{ mm}$	$\sigma_c := 9.2 \text{ MPa}$	$\sigma_s := 207.4 \text{ MPa}$
----------------------	-------------------------------	---------------------------------

$$d := h - c - \frac{\phi}{2} = 120 \text{ mm} \quad z := d - \frac{1}{3} x = 110 \text{ mm}$$



Factor accounting for variation in fibre orientation:

$$\kappa_0 := 1.0$$

Mean residual tensile strength:

$$f_{Ftu.m} := \kappa_0 \cdot 0.33 \cdot f_{R.3m} = 1.24 \text{ MPa}$$

$$f_{R.3m} \text{ replaces the } \frac{f_{R.3k} \cdot \kappa_G}{\gamma_{SF}} \text{ in design residual tensile strength}$$

Uncracked cross-section:

$$A_c := b \cdot h = 150000 \text{ mm}^2$$

$$\eta := \frac{E_s}{E_{cm}} = 7.356$$

$$\alpha d := \frac{A_c \cdot 0.5 \cdot h + \eta \cdot A_s \cdot d}{A_c + \eta \cdot A_s} = 75.68 \text{ mm}$$

$$I_{cl} := \frac{b \cdot h^3}{12} + b \cdot h \cdot \left(\alpha d - \frac{h}{2} \right)^2 = 2.813 \cdot 10^8 \text{ mm}^2$$

$$I_{sl} := A_s \cdot (d - \alpha d)^2 = 6.167 \cdot 10^5 \text{ mm}^4$$

$$M_{cr} := \frac{I_{cl} + \eta \cdot I_{sl}}{h - \alpha d} \cdot f_{ctm} \cdot 10^{-6} = 16.58 \text{ kNm}$$

Minimum reinforcement:

$$k_h := 0.8 - 0.6 \cdot \frac{\min(b, h)}{1000} - 0.3 = 0.41 \quad \text{Use: } k_h := 0.5 \quad (\text{Requirements: } 0.5 - 0.8)$$

$$M_{R.min} \geq M_{cr}$$

$$M_{R.min} = f_{yk} \cdot A_{s.min} \cdot z + 0.4 f_{Ftu.m} \cdot b \cdot h^2$$

$$A_{s.min.1} := \frac{M_{cr} \cdot 10^6 - 0.4 f_{Ftu.m} \cdot b \cdot h^2}{f_{yk} \cdot z} = 98.62 \text{ mm}^2$$

$$A_{s.min.2} := \frac{0.2 k_h \cdot f_{ct.eff} \cdot A_c}{f_{yk}} = 129.3 \text{ mm}^2$$

$$A_{s.min} := \max(A_{s.min.1}, A_{s.min.2}) = 129.3 \text{ mm}^2$$

$$A_s \geq A_{s.min} \quad \rightarrow \text{OK}$$

Calculation of crack width:

Factor converting the mean crack width into a calculated crack width:

$$k_w := 1.3$$

Coefficient to account for the increase of crack width due to curvature:

$$a_{y,i} := c + \frac{\phi}{2} = 30 \text{ mm}$$

$$k_{1r} := \frac{h-x}{h-a_{y,i}-x} = 1.33 \quad (\text{one face in tension})$$

Tensile reinforcement ratio accounting for the different bond properties of reinforcing bars, referred to the effective concrete area:

$$h_{c,eff} := \min\left(c + 5\phi, 10\phi, 3.5c, h-x, \frac{h}{2}\right) = 75 \text{ mm} \quad (\text{single layer of bars})$$

$$b_{c,eff} := 4 \cdot 10\phi = 400 \text{ mm} \quad \text{Effective width (pr meter)}$$

$$A_{c,eff} := b_{c,eff} \cdot h_{c,eff} = 30000 \text{ mm}^2 \quad \text{Effective area (pr meter)}$$

$$\rho_{s,eff} := \frac{A_s}{A_{c,eff}} = 0.01$$

Mean crack spacing:

$$\text{For } s > 10\phi \quad s_{r,m,cal,F} := h-x = 121 \text{ mm}$$

The stress is equal to the design residual tensile strength for $CMOD_1$:

$$\sigma_s = 207.4 \text{ MPa}$$

$$k_t := 0.6 \quad (\text{Short term loading})$$

$$\alpha_e := \frac{E_s}{E_{cm}} = 7.36$$

Plates subjected to direct loads and stabilized cracking, where end restraint dominates, $\Delta\varepsilon$ may be determined as:

$$\Delta\varepsilon = \varepsilon_{sm} - \varepsilon_{cm}$$

$$\varepsilon_{dif,1} := \frac{\sigma_s - k_t \cdot \frac{f_{ct,eff}}{\rho_{s,eff}} \cdot (1 + \alpha_e \cdot \rho_{s,eff})}{E_s} = -0.00029 \quad \text{or} \quad \varepsilon_{dif,2} := (1 - k_t) \frac{\sigma_s}{E_s} = 0.00041$$

$$\Delta\varepsilon := \max(\varepsilon_{dif,1}, \varepsilon_{dif,2}) = 0.00041$$

Crack width:

$$w_{k.cal.F} := k_w \cdot k_{1r} \cdot s_{r.m.cal.F} \cdot \Delta\varepsilon = 0.087 \text{ mm}$$

Crack width limit:

$$\sigma_c = 9.2 \text{ MPa}$$

Stress for concrete

$$0.6 f_{ck} = 36.21 \text{ MPa}$$

$$\sigma_c \leq 0.6 f_{ck} \quad \rightarrow \text{OK}$$

F.3 Crack Width Calculation - EC2 - 350 kN loading

Calculation of crack width according to EC2

Element 11 - with 350 kN loading

Calculations of crack width only applies for elements with conventional reinforcement according to EC2

Dimensions:

$b := 1000 \text{ mm}$	One meter plate-strip
$l := 1300 \text{ mm}$	Plate length
$h := 150 \text{ mm}$	Plate thickness
$c := 25 \text{ mm}$	Cover

Conventional Reinforcement:

$f_{yk} := 500 \text{ MPa}$	
$n := 4$	Number of bars
$A_s := n \cdot 78.5 = 314 \text{ mm}^2$	Effective reinforcement area ($\phi 10cc250$)
$\phi := 10 \text{ mm}$	Bar diameter
$s := 250 \text{ mm}$	Spacing between bars
$E_s := 200000 \text{ MPa}$	Modulus of elasticity

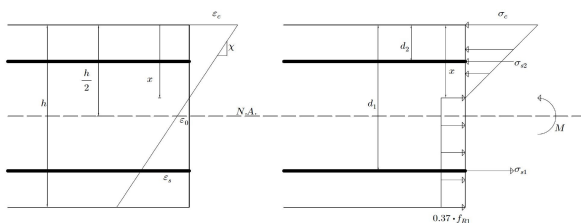
FRC properties:

$f_{ck} := 60.35 \text{ MPa}$	$f_{R.3m} := 3.75 \text{ MPa}$	$E_{cm} := 27189 \text{ MPa}$
$f_{ctm} := 4.31 \text{ MPa}$		
$f_{ct,eff} := f_{ctm} = 4.31 \text{ MPa}$		

Cross-section:

$x := 24 \text{ mm}$	$\sigma_c := 9.9 \text{ MPa}$	$\sigma_s := 297.0 \text{ MPa}$
----------------------	-------------------------------	---------------------------------

$$d := h - c - \frac{\phi}{2} = 120 \text{ mm} \quad z := d - \frac{1}{3} x = 112 \text{ mm}$$



Factor accounting for variation in fibre orientation:

$$\kappa_0 := 1.0$$

Mean residual tensile strength:

$$f_{Ftu.m} := \kappa_0 \cdot 0.33 \cdot f_{R.3m} = 1.24 \text{ MPa}$$

$$f_{R.3m} \text{ replaces the } \frac{f_{R.3k} \cdot \kappa_G}{\gamma_{SF}} \text{ in design residual tensile strength}$$

Uncracked cross-section:

$$A_c := b \cdot h = 150000 \text{ mm}^2$$

$$\eta := \frac{E_s}{E_{cm}} = 7.356$$

$$\alpha d := \frac{A_c \cdot 0.5 \cdot h + \eta \cdot A_s \cdot d}{A_c + \eta \cdot A_s} = 75.68 \text{ mm}$$

$$I_{cl} := \frac{b \cdot h^3}{12} + b \cdot h \cdot \left(\alpha d - \frac{h}{2} \right)^2 = 2.813 \cdot 10^8 \text{ mm}^2$$

$$I_{sl} := A_s \cdot (d - \alpha d)^2 = 6.167 \cdot 10^5 \text{ mm}^4$$

$$M_{cr} := \frac{I_{cl} + \eta \cdot I_{sl}}{h - \alpha d} \cdot f_{ctm} \cdot 10^{-6} = 16.58 \text{ kNm}$$

Minimum reinforcement:

$$k_h := 0.8 - 0.6 \cdot \frac{\min(b, h)}{1000} - 0.3 = 0.41 \quad \text{Use: } k_h := 0.5 \quad (\text{Requirements: } 0.5 - 0.8)$$

$$M_{R.min} \geq M_{cr}$$

$$M_{R.min} = f_{yk} \cdot A_{s.min} \cdot z + 0.4 f_{Ftu.m} \cdot b \cdot h^2$$

$$A_{s.min.1} := \frac{M_{cr} \cdot 10^6 - 0.4 f_{Ftu.m} \cdot b \cdot h^2}{f_{yk} \cdot z} = 97.15 \text{ mm}^2$$

$$A_{s.min.2} := \frac{0.2 k_h \cdot f_{ct.eff} \cdot A_c}{f_{yk}} = 129.3 \text{ mm}^2$$

$$A_{s.min} := \max(A_{s.min.1}, A_{s.min.2}) = 129.3 \text{ mm}^2$$

$$A_s \geq A_{s.min} \quad \rightarrow \text{OK}$$

Calculation of crack width:

Factor converting the mean crack width into a calculated crack width:

$$k_w := 1.3$$

Coefficient to account for the increase of crack width due to curvature:

$$a_{y,i} := c + \frac{\phi}{2} = 30 \text{ mm}$$

$$k_{1r} := \frac{h-x}{h-a_{y,i}-x} = 1.31 \quad (\text{one face in tension})$$

Tensile reinforcement ratio accounting for the different bond properties of reinforcing bars, referred to the effective concrete area:

$$h_{c,eff} := \min\left(c + 5\phi, 10\phi, 3.5c, h-x, \frac{h}{2}\right) = 75 \text{ mm} \quad (\text{single layer of bars})$$

$$b_{c,eff} := 4 \cdot 10\phi = 400 \text{ mm} \quad \text{Effective width (pr meter)}$$

$$A_{c,eff} := b_{c,eff} \cdot h_{c,eff} = 30000 \text{ mm}^2 \quad \text{Effective area (pr meter)}$$

$$\rho_{s,eff} := \frac{A_s}{A_{c,eff}} = 0.01$$

Mean crack spacing:

$$\text{For } s > 10\phi \quad s_{r,m,cal,F} := h-x = 126 \text{ mm}$$

The stress is equal to the design residual tensile strength for $CMOD_1$:

$$\sigma_s = 297 \text{ MPa}$$

$$k_t := 0.6 \quad (\text{Short term loading})$$

$$\alpha_e := \frac{E_s}{E_{cm}} = 7.36$$

Plates subjected to direct loads and stabilized cracking, where end restraint dominates, $\Delta\varepsilon$ may be determined as:

$$\Delta\varepsilon = \varepsilon_{sm} - \varepsilon_{cm}$$

$$\varepsilon_{dif,1} := \frac{\sigma_s - k_t \cdot \frac{f_{ct,eff}}{\rho_{s,eff}} \cdot (1 + \alpha_e \cdot \rho_{s,eff})}{E_s} = 0.00015 \quad \text{or} \quad \varepsilon_{dif,2} := (1 - k_t) \frac{\sigma_s}{E_s} = 0.00059$$

$$\Delta\varepsilon := \max(\varepsilon_{dif,1}, \varepsilon_{dif,2}) = 0.00059$$

Crack width:

$$w_{k.cal.F} := k_w \cdot k_{1r} \cdot s_{r.m.cal.F} \cdot \Delta\varepsilon = 0.128 \text{ mm}$$

Crack width limit:

$$\sigma_c = 9.9 \text{ MPa}$$

Stress for concrete

$$0.6 f_{ck} = 36.21 \text{ MPa}$$

$$\sigma_c \leq 0.6 f_{ck} \quad \rightarrow \text{OK}$$

F.4 Crack Width Calculation - EC2 - 400 kN loading

Calculation of crack width according to EC2

Element 11 - with 400 kN loading

Calculations of crack width only applies for elements with conventional reinforcement according to EC2

Dimensions:

$b := 1000 \text{ mm}$	One meter plate-strip
$l := 1300 \text{ mm}$	Plate length
$h := 150 \text{ mm}$	Plate thickness
$c := 25 \text{ mm}$	Cover

Conventional Reinforcement:

$f_{yk} := 500 \text{ MPa}$	
$n := 4$	Number of bars
$A_s := n \cdot 78.5 = 314 \text{ mm}^2$	Effective reinforcement area ($\phi 10cc250$)
$\phi := 10 \text{ mm}$	Bar diameter
$s := 250 \text{ mm}$	Spacing between bars
$E_s := 200000 \text{ MPa}$	Modulus of elasticity

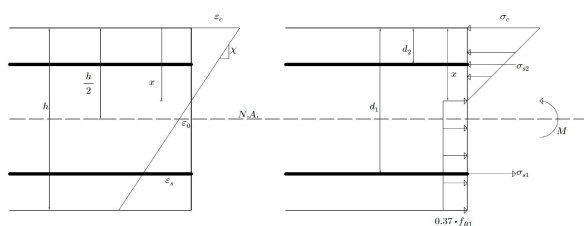
FRC properties:

$f_{ck} := 60.35 \text{ MPa}$	$f_{R,3m} := 3.75 \text{ MPa}$	$E_{cm} := 27189 \text{ MPa}$
$f_{ctm} := 4.31 \text{ MPa}$		
$f_{ct,eff} := f_{ctm} = 4.31 \text{ MPa}$		

Cross-section:

$x := 19 \text{ mm}$	$\sigma_c := 10.0 \text{ MPa}$	$\sigma_s := 382.6 \text{ MPa}$
----------------------	--------------------------------	---------------------------------

$$d := h - c - \frac{\phi}{2} = 120 \text{ mm} \quad z := d - \frac{1}{3} x = 114 \text{ mm}$$



Factor accounting for variation in fibre orientation:

$$\kappa_0 := 1.0$$

Mean residual tensile strength:

$$f_{Ftu.m} := \kappa_0 \cdot 0.33 \cdot f_{R.3m} = 1.24 \text{ MPa}$$

$$f_{R.3m} \text{ replaces the } \frac{f_{R.3k} \cdot \kappa_G}{\gamma_{SF}} \text{ in design residual tensile strength}$$

Uncracked cross-section:

$$A_c := b \cdot h = 150000 \text{ mm}^2$$

$$\eta := \frac{E_s}{E_{cm}} = 7.356$$

$$\alpha d := \frac{A_c \cdot 0.5 \cdot h + \eta \cdot A_s \cdot d}{A_c + \eta \cdot A_s} = 75.68 \text{ mm}$$

$$I_{cl} := \frac{b \cdot h^3}{12} + b \cdot h \cdot \left(\alpha d - \frac{h}{2} \right)^2 = 2.813 \cdot 10^8 \text{ mm}^2$$

$$I_{sl} := A_s \cdot (d - \alpha d)^2 = 6.167 \cdot 10^5 \text{ mm}^4$$

$$M_{cr} := \frac{I_{cl} + \eta \cdot I_{sl}}{h - \alpha d} \cdot f_{ctm} \cdot 10^{-6} = 16.58 \text{ kNm}$$

Minimum reinforcement:

$$k_h := 0.8 - 0.6 \cdot \frac{\min(b, h)}{1000} - 0.3 = 0.41 \quad \text{Use: } k_h := 0.5 \quad (\text{Requirements: } 0.5 - 0.8)$$

$$M_{R.min} \geq M_{cr}$$

$$M_{R.min} = f_{yk} \cdot A_{s.min} \cdot z + 0.4 f_{Ftu.m} \cdot b \cdot h^2$$

$$A_{s.min.1} := \frac{M_{cr} \cdot 10^6 - 0.4 f_{Ftu.m} \cdot b \cdot h^2}{f_{yk} \cdot z} = 95.73 \text{ mm}^2$$

$$A_{s.min.2} := \frac{0.2 k_h \cdot f_{ct.eff} \cdot A_c}{f_{yk}} = 129.3 \text{ mm}^2$$

$$A_{s.min} := \max(A_{s.min.1}, A_{s.min.2}) = 129.3 \text{ mm}^2$$

$$A_s \geq A_{s.min} \quad \rightarrow \text{OK}$$

Calculation of crack width:

Factor converting the mean crack width into a calculated crack width:

$$k_w := 1.3$$

Coefficient to account for the increase of crack width due to curvature:

$$a_{y,i} := c + \frac{\phi}{2} = 30 \text{ mm}$$

$$k_{1r} := \frac{h-x}{h-a_{y,i}-x} = 1.3 \quad (\text{one face in tension})$$

Tensile reinforcement ratio accounting for the different bond properties of reinforcing bars, referred to the effective concrete area:

$$h_{c,eff} := \min\left(c + 5\phi, 10\phi, 3.5c, h-x, \frac{h}{2}\right) = 75 \text{ mm} \quad (\text{single layer of bars})$$

$$b_{c,eff} := 4 \cdot 10\phi = 400 \text{ mm} \quad \text{Effective width (pr meter)}$$

$$A_{c,eff} := b_{c,eff} \cdot h_{c,eff} = 30000 \text{ mm}^2 \quad \text{Effective area (pr meter)}$$

$$\rho_{s,eff} := \frac{A_s}{A_{c,eff}} = 0.01$$

Mean crack spacing:

$$\text{For } s > 10\phi \quad s_{r,m,cal,F} := h-x = 131 \text{ mm}$$

The stress is equal to the design residual tensile strength for $CMOD_1$:

$$\sigma_s = 382.6 \text{ MPa}$$

$$k_t := 0.6 \quad (\text{Short term loading})$$

$$\alpha_e := \frac{E_s}{E_{cm}} = 7.36$$

Plates subjected to direct loads and stabilized cracking, where end restraint dominates, $\Delta\varepsilon$ may be determined as:

$$\Delta\varepsilon = \varepsilon_{sm} - \varepsilon_{cm}$$

$$\varepsilon_{dif,1} := \frac{\sigma_s - k_t \cdot \frac{f_{ct,eff}}{\rho_{s,eff}} \cdot (1 + \alpha_e \cdot \rho_{s,eff})}{E_s} = 0.00058 \quad \text{or} \quad \varepsilon_{dif,2} := (1 - k_t) \frac{\sigma_s}{E_s} = 0.00077$$

$$\Delta\varepsilon := \max(\varepsilon_{dif,1}, \varepsilon_{dif,2}) = 0.00077$$

Crack width:

$$w_{k.cal.F} := k_w \cdot k_{1r} \cdot s_{r.m.cal.F} \cdot \Delta\varepsilon = 0.169 \text{ mm}$$

Crack width limit:

$$\sigma_c = 10 \text{ MPa}$$

Stress for concrete

$$0.6 f_{ck} = 36.21 \text{ MPa}$$

$$\sigma_c \leq 0.6 f_{ck} \quad \rightarrow \text{OK}$$

F.5 Crack Width Calculation - NB38 - 250 kN loading

Calculation of crack width according to NB38

Element 11 - with 250 kN loading

Calculations of crack width only applies for elements with conventional reinforcement according to NB38

Dimensions:

$b := 1000 \text{ mm}$	One meter plate-strip
$l := 1300 \text{ mm}$	Plate length
$h := 150 \text{ mm}$	Plate thickness
$c := 25 \text{ mm}$	Cover

Conventional Reinforcement:

$f_{yk} := 500 \text{ MPa}$	
$n := 4$	Number of bars
$A_s := n \cdot 78.5 = 314 \text{ mm}^2$	Effective reinforcement area ($\phi 10cc250$)
$\phi := 10 \text{ mm}$	Bar diameter
$s := 250 \text{ mm}$	Spacing between bars
$E_s := 200000 \text{ MPa}$	Modulus of elasticity

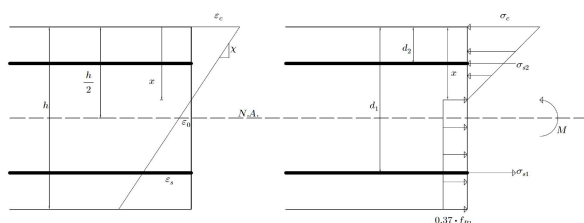
FRC properties:

$f_{ck} := 60.35 \text{ MPa}$	$f_{R.1m} := 4.48 \text{ MPa}$	$E_{cm} := 27189 \text{ MPa}$
$f_{ctm} := 4.31 \text{ MPa}$	$f_{R.3m} := 3.75 \text{ MPa}$	

Cross-section:

$$x := 52 \text{ mm} \quad \sigma_c := 6.8 \text{ MPa} \quad \sigma_s := 65.2 \text{ MPa}$$

$$d := h - c - \frac{\phi}{2} = 120 \text{ mm} \quad z := d - \frac{1}{3} x = 103 \text{ mm}$$



Factor accounting for variation in fibre orientation:

$$\kappa_0 := 1.0$$

Mean residual tensile strength:

$$f_{Fts.m} := \kappa_0 \cdot 0.45 \cdot f_{R.1m} = 2.02 \text{ MPa} \quad f_{Ftu.m} := \kappa_0 \cdot 0.37 \cdot f_{R.3m} = 1.39 \text{ MPa}$$

$f_{R.1m}$ and $f_{R.3m}$ replaces the $\frac{f_{R.1k}}{\gamma_{SF}}$ and $\frac{f_{R.3k}}{\gamma_{SF}}$ in design residual tensile strength

Uncracked cross-section:

$$A_c := b \cdot h = 150000 \text{ mm}^2$$

$$\eta := \frac{E_s}{E_{cm}} = 7.356$$

$$\alpha d := \frac{A_c \cdot 0.5 \cdot h + \eta \cdot A_s \cdot d}{A_c + \eta \cdot A_s} = 75.68 \text{ mm}$$

$$I_{cl} := \frac{b \cdot h^3}{12} + b \cdot h \cdot \left(\alpha d - \frac{h}{2} \right)^2 = 2.813 \cdot 10^8 \text{ mm}^2$$

$$I_{sl} := A_s \cdot (d - \alpha d)^2 = 6.167 \cdot 10^5 \text{ mm}^4$$

$$M_{cr} := \frac{I_{cl} + \eta \cdot I_{sl}}{h - \alpha d} \cdot f_{ctm} \cdot 10^{-6} = 16.58 \text{ kNm}$$

Minimum reinforcement:

$$k_h := 0.8 - 0.6 \cdot \frac{\min(b, h)}{1000} - 0.3 = 0.41 \quad \text{Use: } k_h := 0.5 \quad (\text{Requirements: } 0.5 - 0.8)$$

$$M_{R.min} \geq M_{cr}$$

$$M_{R.min} = f_{yk} \cdot A_{s.min} \cdot z + 0.4 f_{Ftu.m} \cdot b \cdot h^2$$

$$A_{s.min.1} := \frac{M_{cr} \cdot 10^6 - 0.4 f_{Ftu.m} \cdot b \cdot h^2}{f_{yk} \cdot z} = 79.69 \text{ mm}^2$$

Given that $\frac{f_{ctm}}{f_{yk}} = 0.009 \geq 0.005$:

$$A_{s.min.2.1} := 0.26 \cdot \frac{(f_{ctm} - 2.15 \cdot f_{Ftu.m})}{f_{yk}} \cdot b \cdot d = 82.8 \text{ mm}^2 \quad \text{or} \quad A_{s.min.2.2} := 0.13 \cdot \frac{f_{ctm}}{f_{yk}} \cdot b \cdot d = 134.47 \text{ mm}^2$$

$$A_{s.min.2} := \max(A_{s.min.2.1}, A_{s.min.2.2}) = 134.47 \text{ mm}^2$$

$$A_{s.min} := \max(A_{s.min.1}, A_{s.min.2}) = 134.47 \text{ mm}^2$$

$$A_s \geq A_{s.min} \quad \rightarrow \text{OK}$$

Calculation of crack width:

Factor to account for bond conditions:

$$k_b := 0.8 \quad (\text{Good bond conditions})$$

Tensile reinforcement ratio accounting for the different bond properties of reinforcing bars, referred to the effective concrete area:

$$h_{c,eff} := \min \left(c + 5 \phi, 10 \phi, 3.5 c, h - x, \frac{h}{2} \right) = 75 \text{ mm} \quad (\text{single layer of bars})$$

$$b_{c,eff} := 4 \cdot 10 \phi = 400 \text{ mm} \quad (\text{Effective width (pr meter)})$$

$$A_{c,eff} := b_{c,eff} \cdot h_{c,eff} = 30000 \text{ mm}^2 \quad (\text{Effective area (pr meter)})$$

$$\rho_{s,eff} := \frac{A_s}{A_{c,eff}} = 0.01$$

Mean crack spacing:

$$s_{r,max,cal.F} := 2 c + 0.35 k_b \cdot \frac{\phi}{\rho_{s,eff}} \cdot \left(1 - \frac{f_{Fts,m}}{f_{ctm}} \right) = 192.39 \text{ mm}$$

The stress is equal to the design residual tensile strength for $CMOD_1$:

$$\sigma_s = 65.2 \text{ MPa}$$

$$k_t := 0.6 \quad (\text{Short term loading})$$

$$\alpha_e := \frac{E_s}{E_{cm}} = 7.36$$

Plates subjected to direct loads and stabilized cracking, where end restraint dominates, $\Delta \varepsilon$ may be determined as:

$$\Delta \varepsilon = \varepsilon_{sm} - \varepsilon_{cm}$$

$$\varepsilon_{dif,1} := \frac{\sigma_s - k_t \cdot \frac{f_{ctm}}{\rho_{s,eff}} \cdot (1 + \alpha_e \cdot \rho_{s,eff})}{E_s} = -0.001 \quad \text{or} \quad \varepsilon_{dif,2} := (1 - k_t) \frac{\sigma_s}{E_s} = 0.00013$$

$$\Delta \varepsilon := \max(\varepsilon_{dif,1}, \varepsilon_{dif,2}) = 0.00013$$

Crack width:

$$w_{k,cal.F} := s_{r,max,cal.F} \cdot \Delta \varepsilon = 0.025 \text{ mm}$$

Crack width limit:

$$\sigma_c = 6.8 \text{ MPa}$$

Stress for concrete

$$0.6 f_{ck} = 36.21 \text{ MPa}$$

$$\sigma_c \leq 0.6 f_{ck} \quad \rightarrow \text{OK}$$

F.6 Crack Width Calculation - NB38 - 300 kN loading

Calculation of crack width according to NB38

Element 11 - with 300 kN loading

Calculations of crack width only applies for elements with conventional reinforcement according to NB38

Dimensions:

$b := 1000 \text{ mm}$	One meter plate-strip
$l := 1300 \text{ mm}$	Plate length
$h := 150 \text{ mm}$	Plate thickness
$c := 25 \text{ mm}$	Cover

Conventional Reinforcement:

$f_{yk} := 500 \text{ MPa}$	
$n := 4$	Number of bars
$A_s := n \cdot 78.5 = 314 \text{ mm}^2$	Effective reinforcement area ($\phi 10cc250$)
$\phi := 10 \text{ mm}$	Bar diameter
$s := 250 \text{ mm}$	Spacing between bars
$E_s := 200000 \text{ MPa}$	Modulus of elasticity

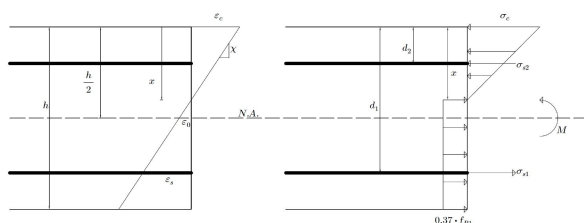
FRC properties:

$f_{ck} := 60.35 \text{ MPa}$	$f_{R.1m} := 4.48 \text{ MPa}$	$E_{cm} := 27189 \text{ MPa}$
$f_{ctm} := 4.31 \text{ MPa}$	$f_{R.3m} := 3.75 \text{ MPa}$	

Cross-section:

$$x := 39 \text{ mm} \quad \sigma_c := 9.2 \text{ MPa} \quad \sigma_s := 139.0 \text{ MPa}$$

$$d := h - c - \frac{\phi}{2} = 120 \text{ mm} \quad z := d - \frac{1}{3} x = 107 \text{ mm}$$



Factor accounting for variation in fibre orientation:

$$\kappa_0 := 1.0$$

Mean residual tensile strength:

$$f_{Fts.m} := \kappa_0 \cdot 0.45 \cdot f_{R.1m} = 2.02 \text{ MPa} \quad f_{Ftu.m} := \kappa_0 \cdot 0.37 \cdot f_{R.3m} = 1.39 \text{ MPa}$$

$f_{R.1m}$ and $f_{R.3m}$ replaces the $\frac{f_{R.1k}}{\gamma_{SF}}$ and $\frac{f_{R.3k}}{\gamma_{SF}}$ in design residual tensile strength

Uncracked cross-section:

$$A_c := b \cdot h = 150000 \text{ mm}^2$$

$$\eta := \frac{E_s}{E_{cm}} = 7.356$$

$$\alpha d := \frac{A_c \cdot 0.5 \cdot h + \eta \cdot A_s \cdot d}{A_c + \eta \cdot A_s} = 75.68 \text{ mm}$$

$$I_{cl} := \frac{b \cdot h^3}{12} + b \cdot h \cdot \left(\alpha d - \frac{h}{2} \right)^2 = 2.813 \cdot 10^8 \text{ mm}^2$$

$$I_{sl} := A_s \cdot (d - \alpha d)^2 = 6.167 \cdot 10^5 \text{ mm}^4$$

$$M_{cr} := \frac{I_{cl} + \eta \cdot I_{sl}}{h - \alpha d} \cdot f_{ctm} \cdot 10^{-6} = 16.58 \text{ kNm}$$

Minimum reinforcement:

$$k_h := 0.8 - 0.6 \cdot \frac{\min(b, h)}{1000} - 0.3 = 0.41 \quad \text{Use: } k_h := 0.5 \quad (\text{Requirements: } 0.5 - 0.8)$$

$$M_{R.min} \geq M_{cr}$$

$$M_{R.min} = f_{yk} \cdot A_{s.min} \cdot z + 0.4 f_{Ftu.m} \cdot b \cdot h^2$$

$$A_{s.min.1} := \frac{M_{cr} \cdot 10^6 - 0.4 f_{Ftu.m} \cdot b \cdot h^2}{f_{yk} \cdot z} = 76.46 \text{ mm}^2$$

Given that $\frac{f_{ctm}}{f_{yk}} = 0.009 \geq 0.005$:

$$A_{s.min.2.1} := 0.26 \cdot \frac{(f_{ctm} - 2.15 \cdot f_{Ftu.m})}{f_{yk}} \cdot b \cdot d = 82.8 \text{ mm}^2 \quad \text{or} \quad A_{s.min.2.2} := 0.13 \cdot \frac{f_{ctm}}{f_{yk}} \cdot b \cdot d = 134.47 \text{ mm}^2$$

$$A_{s.min.2} := \max(A_{s.min.2.1}, A_{s.min.2.2}) = 134.47 \text{ mm}^2$$

$$A_{s.min} := \max(A_{s.min.1}, A_{s.min.2}) = 134.47 \text{ mm}^2$$

$$A_s \geq A_{s.min} \quad \rightarrow \text{OK}$$

Calculation of crack width:

Factor to account for bond conditions:

$$k_b := 0.8 \quad (\text{Good bond conditions})$$

Tensile reinforcement ratio accounting for the different bond properties of reinforcing bars, referred to the effective concrete area:

$$h_{c,eff} := \min \left(c + 5 \phi, 10 \phi, 3.5 c, h - x, \frac{h}{2} \right) = 75 \text{ mm} \quad (\text{single layer of bars})$$

$$b_{c,eff} := 4 \cdot 10 \phi = 400 \text{ mm} \quad \text{Effective width (pr meter)}$$

$$A_{c,eff} := b_{c,eff} \cdot h_{c,eff} = 30000 \text{ mm}^2 \quad \text{Effective area (pr meter)}$$

$$\rho_{s,eff} := \frac{A_s}{A_{c,eff}} = 0.01$$

Mean crack spacing:

$$s_{r,max,cal.F} := 2 c + 0.35 k_b \cdot \frac{\phi}{\rho_{s,eff}} \cdot \left(1 - \frac{f_{Fts,m}}{f_{ctm}} \right) = 192.39 \text{ mm}$$

The stress is equal to the design residual tensile strength for $CMOD_1$:

$$\sigma_s = 139 \text{ MPa}$$

$$k_t := 0.6 \quad (\text{Short term loading})$$

$$\alpha_e := \frac{E_s}{E_{cm}} = 7.36$$

Plates subjected to direct loads and stabilized cracking, where end restraint dominates, $\Delta \varepsilon$ may be determined as:

$$\Delta \varepsilon = \varepsilon_{sm} - \varepsilon_{cm}$$

$$\varepsilon_{dif,1} := \frac{\sigma_s - k_t \cdot \frac{f_{ctm}}{\rho_{s,eff}} \cdot (1 + \alpha_e \cdot \rho_{s,eff})}{E_s} = -0.00064 \quad \text{or} \quad \varepsilon_{dif,2} := (1 - k_t) \frac{\sigma_s}{E_s} = 0.00028$$

$$\Delta \varepsilon := \max(\varepsilon_{dif,1}, \varepsilon_{dif,2}) = 0.00028$$

Crack width:

$$w_{k,cal.F} := s_{r,max,cal.F} \cdot \Delta \varepsilon = 0.053 \text{ mm}$$

Crack width limit:

$$\sigma_c = 9.2 \text{ MPa}$$

Stress for concrete

$$0.6 f_{ck} = 36.21 \text{ MPa}$$

$$\sigma_c \leq 0.6 f_{ck} \quad \rightarrow \text{OK}$$

F.7 Crack Width Calculation - NB38 - 350 kN loading

Calculation of crack width according to NB38

Element 11 - with 350 kN loading

Calculations of crack width only applies for elements with conventional reinforcement according to NB38

Dimensions:

$b := 1000 \text{ mm}$	One meter plate-strip
$l := 1300 \text{ mm}$	Plate length
$h := 150 \text{ mm}$	Plate thickness
$c := 25 \text{ mm}$	Cover

Conventional Reinforcement:

$f_{yk} := 500 \text{ MPa}$	
$n := 4$	Number of bars
$A_s := n \cdot 78.5 = 314 \text{ mm}^2$	Effective reinforcement area ($\phi 10cc250$)
$\phi := 10 \text{ mm}$	Bar diameter
$s := 250 \text{ mm}$	Spacing between bars
$E_s := 200000 \text{ MPa}$	Modulus of elasticity

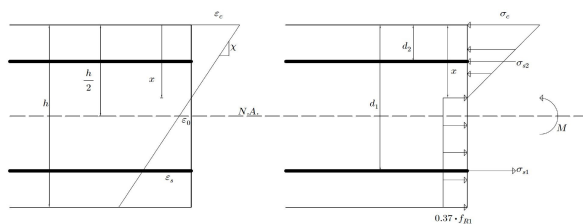
FRC properties:

$f_{ck} := 60.35 \text{ MPa}$	$f_{R.1m} := 4.48 \text{ MPa}$	$E_{cm} := 27189 \text{ MPa}$
$f_{ctm} := 4.31 \text{ MPa}$	$f_{R.3m} := 3.75 \text{ MPa}$	

Cross-section:

$$x := 31 \text{ mm} \quad \sigma_c := 10.8 \text{ MPa} \quad \sigma_s := 227.6 \text{ MPa}$$

$$d := h - c - \frac{\phi}{2} = 120 \text{ mm} \quad z := d - \frac{1}{3} x = 110 \text{ mm}$$



Factor accounting for variation in fibre orientation:

$$\kappa_0 := 1.0$$

Mean residual tensile strength:

$$f_{Fts.m} := \kappa_0 \cdot 0.45 \cdot f_{R.1m} = 2.02 \text{ MPa} \quad f_{Ftu.m} := \kappa_0 \cdot 0.37 \cdot f_{R.3m} = 1.39 \text{ MPa}$$

$f_{R.1m}$ and $f_{R.3m}$ replaces the $\frac{f_{R.1k}}{\gamma_{SF}}$ and $\frac{f_{R.3k}}{\gamma_{SF}}$ in design residual tensile strength

Uncracked cross-section:

$$A_c := b \cdot h = 150000 \text{ mm}^2$$

$$\eta := \frac{E_s}{E_{cm}} = 7.356$$

$$\alpha d := \frac{A_c \cdot 0.5 \cdot h + \eta \cdot A_s \cdot d}{A_c + \eta \cdot A_s} = 75.68 \text{ mm}$$

$$I_{cl} := \frac{b \cdot h^3}{12} + b \cdot h \cdot \left(\alpha d - \frac{h}{2} \right)^2 = 2.813 \cdot 10^8 \text{ mm}^2$$

$$I_{sl} := A_s \cdot (d - \alpha d)^2 = 6.167 \cdot 10^5 \text{ mm}^4$$

$$M_{cr} := \frac{I_{cl} + \eta \cdot I_{sl}}{h - \alpha d} \cdot f_{ctm} \cdot 10^{-6} = 16.58 \text{ kNm}$$

Minimum reinforcement:

$$k_h := 0.8 - 0.6 \cdot \frac{\min(b, h)}{1000} - 0.3 = 0.41 \quad \text{Use: } k_h := 0.5 \quad (\text{Requirements: } 0.5 - 0.8)$$

$$M_{R.min} \geq M_{cr}$$

$$M_{R.min} = f_{yk} \cdot A_{s.min} \cdot z + 0.4 f_{Ftu.m} \cdot b \cdot h^2$$

$$A_{s.min.1} := \frac{M_{cr} \cdot 10^6 - 0.4 f_{Ftu.m} \cdot b \cdot h^2}{f_{yk} \cdot z} = 74.6 \text{ mm}^2$$

Given that $\frac{f_{ctm}}{f_{yk}} = 0.009 \geq 0.005$:

$$A_{s.min.2.1} := 0.26 \cdot \frac{(f_{ctm} - 2.15 \cdot f_{Ftu.m})}{f_{yk}} \cdot b \cdot d = 82.8 \text{ mm}^2 \quad \text{or} \quad A_{s.min.2.2} := 0.13 \cdot \frac{f_{ctm}}{f_{yk}} \cdot b \cdot d = 134.47 \text{ mm}^2$$

$$A_{s.min.2} := \max(A_{s.min.2.1}, A_{s.min.2.2}) = 134.47 \text{ mm}^2$$

$$A_{s.min} := \max(A_{s.min.1}, A_{s.min.2}) = 134.47 \text{ mm}^2$$

$$A_s \geq A_{s.min} \quad \rightarrow \text{OK}$$

Calculation of crack width:

Factor to account for bond conditions:

$$k_b := 0.8 \quad (\text{Good bond conditions})$$

Tensile reinforcement ratio accounting for the different bond properties of reinforcing bars, referred to the effective concrete area:

$$h_{c,eff} := \min \left(c + 5 \phi, 10 \phi, 3.5 c, h - x, \frac{h}{2} \right) = 75 \text{ mm} \quad (\text{single layer of bars})$$

$$b_{c,eff} := 4 \cdot 10 \phi = 400 \text{ mm} \quad (\text{Effective width (pr meter)})$$

$$A_{c,eff} := b_{c,eff} \cdot h_{c,eff} = 30000 \text{ mm}^2 \quad (\text{Effective area (pr meter)})$$

$$\rho_{s,eff} := \frac{A_s}{A_{c,eff}} = 0.01$$

Mean crack spacing:

$$s_{r,max,cal.F} := 2 c + 0.35 k_b \cdot \frac{\phi}{\rho_{s,eff}} \cdot \left(1 - \frac{f_{Fts,m}}{f_{ctm}} \right) = 192.39 \text{ mm}$$

The stress is equal to the design residual tensile strength for $CMOD_1$:

$$\sigma_s = 227.6 \text{ MPa}$$

$$k_t := 0.6 \quad (\text{Short term loading})$$

$$\alpha_e := \frac{E_s}{E_{cm}} = 7.36$$

Plates subjected to direct loads and stabilized cracking, where end restraint dominates, $\Delta \varepsilon$ may be determined as:

$$\Delta \varepsilon = \varepsilon_{sm} - \varepsilon_{cm}$$

$$\varepsilon_{dif,1} := \frac{\sigma_s - k_t \cdot \frac{f_{ctm}}{\rho_{s,eff}} \cdot (1 + \alpha_e \cdot \rho_{s,eff})}{E_s} = -0.00019 \quad \text{or} \quad \varepsilon_{dif,2} := (1 - k_t) \frac{\sigma_s}{E_s} = 0.00046$$

$$\Delta \varepsilon := \max (\varepsilon_{dif,1}, \varepsilon_{dif,2}) = 0.00046$$

Crack width:

$$w_{k,cal.F} := s_{r,max,cal.F} \cdot \Delta \varepsilon = 0.088 \text{ mm}$$

Crack width limit:

$$\sigma_c = 10.8 \text{ MPa}$$

Stress for concrete

$$0.6 f_{ck} = 36.21 \text{ MPa}$$

$$\sigma_c \leq 0.6 f_{ck} \quad \rightarrow \text{OK}$$

F.8 Crack Width Calculation - NB38 - 400 kN loading

Calculation of crack width according to NB38

Element 11 - with 400 kN loading

Calculations of crack width only applies for elements with conventional reinforcement according to NB38

Dimensions:

$b := 1000 \text{ mm}$	One meter plate-strip
$l := 1300 \text{ mm}$	Plate length
$h := 150 \text{ mm}$	Plate thickness
$c := 25 \text{ mm}$	Cover

Conventional Reinforcement:

$f_{yk} := 500 \text{ MPa}$	
$n := 4$	Number of bars
$A_s := n \cdot 78.5 = 314 \text{ mm}^2$	Effective reinforcement area ($\phi 10cc250$)
$\phi := 10 \text{ mm}$	Bar diameter
$s := 250 \text{ mm}$	Spacing between bars
$E_s := 200000 \text{ MPa}$	Modulus of elasticity

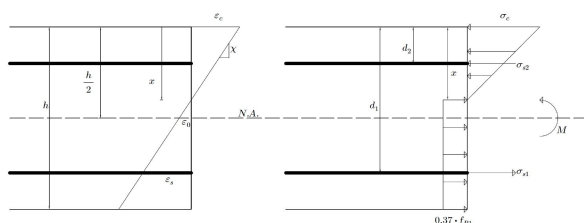
FRC properties:

$f_{ck} := 60.35 \text{ MPa}$	$f_{R.1m} := 4.48 \text{ MPa}$	$E_{cm} := 27189 \text{ MPa}$
$f_{ctm} := 4.31 \text{ MPa}$	$f_{R.3m} := 3.75 \text{ MPa}$	

Cross-section:

$$x := 26 \text{ mm} \quad \sigma_c := 11.7 \text{ MPa} \quad \sigma_s := 315.6 \text{ MPa}$$

$$d := h - c - \frac{\phi}{2} = 120 \text{ mm} \quad z := d - \frac{1}{3} x = 111 \text{ mm}$$



Factor accounting for variation in fibre orientation:

$$\kappa_0 := 1.0$$

Mean residual tensile strength:

$$f_{Fts.m} := \kappa_0 \cdot 0.45 \cdot f_{R.1m} = 2.02 \text{ MPa} \quad f_{Ftu.m} := \kappa_0 \cdot 0.37 \cdot f_{R.3m} = 1.39 \text{ MPa}$$

$f_{R.1m}$ and $f_{R.3m}$ replaces the $\frac{f_{R.1k}}{\gamma_{SF}}$ and $\frac{f_{R.3k}}{\gamma_{SF}}$ in design residual tensile strength

Uncracked cross-section:

$$A_c := b \cdot h = 150000 \text{ mm}^2$$

$$\eta := \frac{E_s}{E_{cm}} = 7.356$$

$$\alpha d := \frac{A_c \cdot 0.5 \cdot h + \eta \cdot A_s \cdot d}{A_c + \eta \cdot A_s} = 75.68 \text{ mm}$$

$$I_{cl} := \frac{b \cdot h^3}{12} + b \cdot h \cdot \left(\alpha d - \frac{h}{2} \right)^2 = 2.813 \cdot 10^8 \text{ mm}^2$$

$$I_{sl} := A_s \cdot (d - \alpha d)^2 = 6.167 \cdot 10^5 \text{ mm}^4$$

$$M_{cr} := \frac{I_{cl} + \eta \cdot I_{sl}}{h - \alpha d} \cdot f_{ctm} \cdot 10^{-6} = 16.58 \text{ kNm}$$

Minimum reinforcement:

$$k_h := 0.8 - 0.6 \cdot \frac{\min(b, h)}{1000} - 0.3 = 0.41 \quad \text{Use: } k_h := 0.5 \quad (\text{Requirements: } 0.5 - 0.8)$$

$$M_{R.min} \geq M_{cr}$$

$$M_{R.min} = f_{yk} \cdot A_{s.min} \cdot z + 0.4 f_{Ftu.m} \cdot b \cdot h^2$$

$$A_{s.min.1} := \frac{M_{cr} \cdot 10^6 - 0.4 f_{Ftu.m} \cdot b \cdot h^2}{f_{yk} \cdot z} = 73.48 \text{ mm}^2$$

Given that $\frac{f_{ctm}}{f_{yk}} = 0.009 \geq 0.005$:

$$A_{s.min.2.1} := 0.26 \cdot \frac{(f_{ctm} - 2.15 \cdot f_{Ftu.m})}{f_{yk}} \cdot b \cdot d = 82.8 \text{ mm}^2 \quad \text{or} \quad A_{s.min.2.2} := 0.13 \cdot \frac{f_{ctm}}{f_{yk}} \cdot b \cdot d = 134.47 \text{ mm}^2$$

$$A_{s.min.2} := \max(A_{s.min.2.1}, A_{s.min.2.2}) = 134.47 \text{ mm}^2$$

$$A_{s.min} := \max(A_{s.min.1}, A_{s.min.2}) = 134.47 \text{ mm}^2$$

$$A_s \geq A_{s.min} \quad \rightarrow \text{OK}$$

Calculation of crack width:

Factor to account for bond conditions:

$$k_b := 0.8 \quad (\text{Good bond conditions})$$

Tensile reinforcement ratio accounting for the different bond properties of reinforcing bars, referred to the effective concrete area:

$$h_{c,eff} := \min \left(c + 5 \phi, 10 \phi, 3.5 c, h - x, \frac{h}{2} \right) = 75 \text{ mm} \quad (\text{single layer of bars})$$

$$b_{c,eff} := 4 \cdot 10 \phi = 400 \text{ mm} \quad \text{Effective width (pr meter)}$$

$$A_{c,eff} := b_{c,eff} \cdot h_{c,eff} = 30000 \text{ mm}^2 \quad \text{Effective area (pr meter)}$$

$$\rho_{s,eff} := \frac{A_s}{A_{c,eff}} = 0.01$$

Mean crack spacing:

$$s_{r,max,cal.F} := 2 c + 0.35 k_b \cdot \frac{\phi}{\rho_{s,eff}} \cdot \left(1 - \frac{f_{Fts,m}}{f_{ctm}} \right) = 192.39 \text{ mm}$$

The stress is equal to the design residual tensile strength for $CMOD_1$:

$$\sigma_s = 315.6 \text{ MPa}$$

$$k_t := 0.6 \quad (\text{Short term loading})$$

$$\alpha_e := \frac{E_s}{E_{cm}} = 7.36$$

Plates subjected to direct loads and stabilized cracking, where end restraint dominates, $\Delta \varepsilon$ may be determined as:

$$\Delta \varepsilon = \varepsilon_{sm} - \varepsilon_{cm}$$

$$\varepsilon_{dif,1} := \frac{\sigma_s - k_t \cdot \frac{f_{ctm}}{\rho_{s,eff}} \cdot (1 + \alpha_e \cdot \rho_{s,eff})}{E_s} = 0.00025 \quad \text{or} \quad \varepsilon_{dif,2} := (1 - k_t) \frac{\sigma_s}{E_s} = 0.00063$$

$$\Delta \varepsilon := \max (\varepsilon_{dif,1}, \varepsilon_{dif,2}) = 0.00063$$

Crack width:

$$w_{k,cal.F} := s_{r,max,cal.F} \cdot \Delta \varepsilon = 0.121 \text{ mm}$$

Crack width limit:

$$\sigma_c = 11.7 \text{ MPa}$$

Stress for concrete

$$0.6 f_{ck} = 36.21 \text{ MPa}$$

$$\sigma_c \leq 0.6 f_{ck} \quad \rightarrow \text{OK}$$

G Inductive test

G.1 Fibre orientation in cubes

Cube	L_y	L_x	L_z
B1-1(1)	2.50	6.00	3.40
B1-1(2)	2.90	5.90	4.30
B1-6(1)	2.00	7.50	4.60
B1-6(2)	1.80	6.10	4.00
B2-1(1)	2.00	5.70	2.60
B2-1(2)	1.50	5.80	2.70
B2-7(1)	1.80	6.60	2.70
B2-7(2)	1.60	4.80	2.10
B5-1D(1)	3.10	6.30	2.70
B5-1D(2)	2.20	5.60	3.60
B5-6D(1)	1.70	7.40	2.50
B5-6D(2)	2.20	6.10	3.00
B5-1S(1)	3.00	9.00	6.60
B5-1S(2)	3.20	7.10	6.10
B5-2S(1)	2.90	6.80	6.10
B5-2S(2)	3.90	8.80	7.10

Cube	L_y / B_v	L_x / B_v	L_z / B_v	SUM	C_f	n_y	n_x	n_z	C_y	C_x	C_z
B1-1(1)	0.00107	0.00256	0.00145	0.00508	34.12	0.350	0.651	0.443	24.2 %	45.1 %	30.7 %
Avg					35.92				24.6 %	43.3 %	32.1 %
B1-1(2)	0.00124	0.00252	0.00184	0.00559	37.71	0.365	0.605	0.489	25.0 %	41.5 %	33.5 %
B1-6(1)	0.00085	0.00320	0.00196	0.00602	40.71	0.244	0.673	0.487	17.4 %	47.9 %	34.7 %
Avg					37.41				17.9 %	47.2 %	34.9 %
B1-6(2)	0.00077	0.00260	0.00171	0.00508	34.12	0.261	0.658	0.498	18.4 %	46.4 %	35.1 %
B2-1(1)	0.00085	0.00243	0.00111	0.00440	29.32	0.327	0.690	0.404	23.0 %	48.5 %	28.4 %
Avg					28.87				20.8 %	49.7 %	29.5 %
B2-1(2)	0.00064	0.00248	0.00115	0.00427	28.42	0.258	0.710	0.425	18.5 %	51.0 %	30.5 %
B2-7(1)	0.00077	0.00282	0.00115	0.00474	31.72	0.248	0.589	0.320	21.4 %	50.9 %	27.7 %
Avg					27.82				21.2 %	50.7 %	28.1 %
B2-7(2)	0.00068	0.00205	0.00090	0.00363	23.92	0.352	0.848	0.478	21.0 %	50.5 %	28.5 %
B5-1D(1)	0.00132	0.00269	0.00115	0.00517	34.72	0.226	0.557	0.297	21.0 %	51.6 %	27.5 %
Avg					33.67				24.7 %	48.7 %	26.5 %
B5-1D(2)	0.00094	0.00239	0.00154	0.00487	32.62	0.427	0.689	0.385	28.5 %	45.9 %	25.6 %
B5-6D(1)	0.00073	0.00316	0.00107	0.00495	33.22	0.321	0.633	0.470	22.5 %	44.4 %	33.0 %
Avg					32.77				20.6 %	49.8 %	29.6 %
B5-6D(2)	0.00094	0.00260	0.00128	0.00482	32.32	0.259	0.765	0.365	18.7 %	55.1 %	26.3 %
B5-1S(1)	0.00128	0.00384	0.00282	0.00794	54.20	0.199	0.489	0.277	20.6 %	50.7 %	28.7 %
Avg					50.90				20.3 %	47.3 %	32.4 %
B5-1S(2)	0.00137	0.00303	0.00260	0.00700	47.61	0.311	0.686	0.562	19.9 %	44.0 %	36.1 %
B5-2S(1)	0.00124	0.00290	0.00260	0.00675	45.81	0.339	0.604	0.547	22.8 %	40.5 %	36.7 %
Avg					51.80				21.7 %	40.9 %	37.4 %
B5-2S(2)	0.00167	0.00376	0.00303	0.00845	57.80	0.252	0.505	0.468	20.6 %	41.2 %	38.2 %

G.2 Fibre orientation in cylinders

Core	L_z	L_0	L_{45}	L_{90}
P1-1	0.9	3.0	4.2	3.3
P1-2	1.1	4.6	4.2	3.7
P1-3	0.9	3.2	3.2	4.3
P1-4	1.4	6.0	1.8	2.3
P1-5	0.8	2.8	3.1	2.6
P5-1	3.5	3.6	2.5	5.2
P5-2	1.3	5.5	3.8	1.0
P5-3	2.3	5.2	5.0	3.1
P5-4	1.1	5.9	6.1	2.0
P9-2	1.2	5.4	4.5	1.9
P9-3	1.5	1.7	3.8	5.8
P9-4	1.5	6.4	4.5	2.7
P9-5	1.5	1.5	2.6	3.7
P13-1	3.1	2.6	4.1	7.7
P13-2	2.5	3.7	4.6	3.6
P13-3	1.8	3.9	6.4	5.0
P13-4	1.3	1.9	2.0	4.2
P13-5	1.7	2.6	3.1	2.9
P13-6	2.0	2.3	3.9	4.0
P14-1	1.9	3.7	4.9	3.1
P14-2	1.9	3.6	5.1	3.4
P14-3	4.8	5.6	6.1	5.2
P14-4	2.2	2.2	2.8	5.1
P14-5	1.5	3.8	5.4	3.2

	L_e	n_z	n_0	n_{90}	sum	C_l	C_z	C_0	C_{90}	L_{ani}	L_{iso}	θ_{max}	θ_{min}	L_{max}	L_{min}	n_{max}	n_{min}	iso fac
P1-1	0.0040	0.225	0.591	0.628	1.444	26.66	16 %	41 %	43 %	2.233	1.978	-49.1	-139.1	4.211	2.089	0.730	0.464	0.636
P1-2	0.0052	0.209	0.654	0.569	1.433	35.29	15 %	46 %	40 %	0.953	3.650	-3.2	-93.2	4.603	3.697	0.654	0.569	0.870
P1-3	0.0047	0.188	0.557	0.672	1.418	31.37	13 %	39 %	47 %	1.638	2.890	67.5	-22.5	4.528	2.972	0.694	0.531	0.765
P1-4	0.0054	0.261	0.755	0.401	1.417	36.45	18 %	53 %	28 %	6.296	0.844	25.9	-64.1	7.141	1.159	0.837	0.217	0.259
P1-5	0.0035	0.233	0.622	0.593	1.448	22.74	16 %	43 %	41 %	0.868	2.244	-38.0	-128.0	3.112	2.288	0.664	0.546	0.822
P5-1	0.0069	0.454	0.467	0.597	1.519	46.56	30 %	31 %	39 %	4.340	2.121	56.4	-33.6	6.462	2.338	0.684	0.337	0.493
P5-2	0.0044	0.298	0.816	0.234	1.349	29.00	22 %	61 %	17 %	4.876	0.690	-6.9	-96.9	5.566	0.934	0.822	0.217	0.265
P5-3	0.0059	0.371	0.655	0.467	1.494	39.94	25 %	44 %	31 %	2.844	2.657	-19.5	-109.5	5.501	2.799	0.679	0.434	0.639
P5-4	0.0050	0.220	0.781	0.381	1.382	33.72	16 %	57 %	28 %	6.111	0.742	-23.9	-113.9	6.853	1.047	0.853	0.210	0.247
P9-2	0.0047	0.255	0.767	0.383	1.406	31.75	18 %	55 %	27 %	4.096	1.500	-13.0	-103.0	5.596	1.704	0.783	0.352	0.449
P9-3	0.0050	0.298	0.335	0.774	1.407	33.70	21 %	24 %	55 %	4.317	1.484	-89.3	-179.3	5.801	1.699	0.774	0.335	0.433
P9-4	0.0059	0.256	0.744	0.422	1.422	39.98	18 %	52 %	30 %	3.896	2.505	0.8	-89.2	6.401	2.699	0.744	0.422	0.568
P9-5	0.0037	0.381	0.384	0.705	1.470	24.67	26 %	26 %	48 %	2.316	1.384	90.0	0.0	3.700	1.500	0.705	0.384	0.544
P13-1	0.0075	0.390	0.343	0.722	1.456	50.90	27 %	24 %	50 %	5.806	2.102	78.8	-11.2	7.908	2.392	0.734	0.320	0.436
P13-2	0.0055	0.420	0.555	0.545	1.519	36.79	28 %	37 %	36 %	2.003	2.599	-43.5	-133.5	4.601	2.699	0.638	0.447	0.701
P13-3	0.0060	0.301	0.542	0.636	1.478	40.36	20 %	37 %	43 %	4.265	2.211	-52.9	-142.9	6.476	2.424	0.745	0.387	0.520
P13-4	0.0041	0.312	0.425	0.717	1.454	27.43	21 %	29 %	49 %	3.278	1.329	68.8	-21.2	4.607	1.493	0.758	0.354	0.467
P13-5	0.0040	0.396	0.539	0.579	1.514	26.63	26 %	36 %	38 %	0.802	2.329	-56.6	-146.6	3.131	2.369	0.608	0.506	0.833
P13-6	0.0046	0.403	0.449	0.648	1.500	30.93	27 %	30 %	43 %	2.386	1.897	-69.3	-159.3	4.284	2.016	0.676	0.408	0.604
P14-1	0.0049	0.373	0.599	0.534	1.506	32.50	25 %	40 %	35 %	3.220	1.709	-39.3	-129.3	4.930	1.870	0.716	0.372	0.519
P14-2	0.0050	0.367	0.580	0.559	1.506	33.29	24 %	39 %	37 %	3.375	1.728	-43.2	-133.2	5.103	1.897	0.721	0.370	0.512
P14-3	0.0087	0.480	0.537	0.511	1.528	59.46	31 %	35 %	33 %	1.533	4.595	-37.0	-127.0	6.128	4.672	0.569	0.475	0.834
P14-4	0.0053	0.391	0.394	0.693	1.478	35.63	26 %	27 %	47 %	3.538	1.792	74.8	-15.2	5.331	1.969	0.712	0.362	0.508
P14-5	0.0047	0.314	0.618	0.553	1.485	31.74	21 %	42 %	37 %	4.050	1.374	-40.5	-130.5	5.424	1.576	0.769	0.330	0.429



 **NTNU**

Norwegian University of
Science and Technology